Università degli Studi di Ferrara

DOCTORAL COURSE IN
"Biomedical and Biotechnological Science"

CYCLE XXXIV

COORDINATOR Prof. Paolo Pinton

"Study of factors involved in the calcific aortic valve disease"

Scientific/Disciplinary Sector BIO/13

Candidate
Dr. Luisa Marracino

Supervisor
Prof. Paola Rizzo

Years 2018/2021

TABLE OF CONTENTS

1. INTRODUCTION

1.1. Aortic Valve Structure and Function

The aortic valve is the valve that separates the aorta from the left ventricle of the heart, responsible for pumping oxygenated blood to the rest of the body. Therefore, its function is essential to sustain human life. The aortic valve is composed of three layers: the fibrosa, which consists mainly of collagen; the spongiosa, consisting primarily of glycosaminoglycans; and the ventricularis which contains elastin. Aortic valve interstitial cells (AVICs) populate these layers and become activated to remodel the extracellular matrix (ECM) of the valve when necessary. Aortic valve endothelial cells (VECs) line the valve and provide a barrier from the blood. They prevent clotting, mediate infiltration of lipids and nutrients, and modulate extravasation of inflammatory cells. The interaction between AVICs and VECs is essential for proper development and maintenance of the aortic valve. The ECM composition of the valve and cellular composition maintenance ensure that it remains flexible, strong, and compliant, making it durable for a human lifetime. In calcific aortic valve disease (CAVD), the aortic valve undergoes pathological matrix-remodeling which lead to valve thickening and formation of calcium nodules that compromise the correct functionality of aortic valve. While CAVD was initially viewed as a degenerative process, different studies in the field have found that the progression of CAVD is not simply a degenerative process, but a mechanobiological manifestation controlled by key cellular regulators of inflammatory and osteogenesis factors [1, 2].

1.2. Calcific Aortic Valve Disease (CAVD): prevalence, diagnosis, prognosis, and risk factors

Among cardiovascular diseases, CAVD is a notable cause of illness and death with a high global prevalence of about 12.6 million cases, and an estimated 102.700 of these cases resulted in death [3]. It is a complex, multifaced disease characterized by alterations such as fibrosis, lipid, and calcium accumulation in the valve leaflets which can be asymptomatic (aortic sclerosis), or it can lead to remodeling of valve tissue sufficiently severe to result in hemodynamic changes at the aortic valve (aortic stenosis, AS). In

particular, the narrowing of the aortic valve opening and the consequent left ventricular outflow obstruction is responsible for the development of symptoms and following events that characterize the later stages of the disease [4].

Currently, aortic sclerosis affects 25% of the population over the age of 65 with aortic stenosis occurring in nearly 2%. Echocardiography helps to make the diagnosis of CAVD but is not able to predict its evolution and therefore is unable to give the opportunity to intervene at the early stages of the disease [5].

There are no approved pharmacological treatments available to stop the progression or treat CAVD and, at present, surgical valve replacement or transcatheter aortic valve transplantation (TAVR) are the standard treatment options for severe, symptomatic aortic stenosis with no guarantee of long- term success. It has been shown that the use of statins, even if they counteract calcification in vitro, are not effective in large randomized clinical trials [6]. Similarly, the effectiveness of Angiotensin-converting enzyme inhibitors (ACE) in preventing the progression of AS in clinical practice is still uncertain [7].

The underlying etiology of CAVD is poorly understood, but several clinical risk factors have been identified, many of these are common to other cardiovascular disorders including atherosclerosis. Elevated total cholesterol, low-density lipoprotein (LDL) triglycerides, decreased high-density lipoproteins, male sex, tobacco use, hypertension, and diabetes mellitus have been reported to increase the incidence of aortic stenosis [8].

In addition to these factors, there are genetic factors which play a significant role in the progression of the disease. A single nucleotide polymorphism (SNP) in the Lipoprotein(A) (LPA) locus (rs10455872) is associated with aortic valve calcification as detected by CT scans [9]. The same study demonstrated that genetically determined Lp(a) levels were associated with aortic valve calcification, indicating that high Lp(a) levels causally increases the risk for CAVD. Recently, it was reported that genetically determined low Lp(a) levels reduced the risk of CAVD by 37%. [10]. Notch1 mutations are associated with severe calcification of the aortic valve [11] and studies in animal models of this disease have shown that dysregulation of Notch in endothelial cells [12] or interstitial cells of the aortic valve [13] promotes calcification of the valve. Though only a handful of genes mutations have been established as disease-causing, it is possible that the availability of new technologies will lead to the detection of additional genes implicated in human valvular disease [14].

It is predicted that by 2050 CAVD patients will undergo 80000 surgical valve replacement per year [15]. It has also been known that after onset of symptoms, survival declines rapidly due to angina, syncope, and heart failure [16]. The lack of specific diagnostic tools for early-stage aortic stenosis, before irreversible cardiac damage occurs, poses a challenge for the development of effective therapies. Therefore, there is a need for the development of novel diagnostics and therapeutics intervention for CAVD and the investigation of signaling pathways involved in CAVD development and progression is the only approach that will make this possible.

1.3. The role of Cyclooxygenases-2 (COX-2) in CAVD

Inflammation-caused endothelial dysfunction characterized by several impaired functions, including decrease of nitric oxide (NO) availability, plays a key role in the early stages of aortic valve disease [17, 18]. Several studies support the hypothesis that impairment of NO may be a mechanism underlying AS, such as the increased expression of thioredoxin-interacting protein (TXNIP), a marker of reactive oxygen species (ROS)-induced oxidative stress, which is suppressed by NO, in a rabbit model of mild aortic stenosis [19] and the increased levels of myeloperoxidase (MPO), a NO scavenger, in stenotic valves [20]. Therefore, anti-inflammatory therapy has been considered as a possible strategy to interfere with CAVD progression [21].

During disease progression, AVICs from mineralized valves show activation of different pathway associated to myofibroblasts or osteoblasts differentiation, both contributing to the formation of calcific nodules [22]. In vitro and in vivo findings have shown that several inflammatory mediators, such as Cyclooxygenases -2 (COX-2), promote trans-differentiation of AVICs and thus promote calcifying degeneration [23]. Cyclooxygenases are a family of oxidoreductase enzymes, main mediators of inflammation by catalyzing the first step of arachidonic acid (AA) metabolism and prostaglandin synthesis. Three isoforms of COXs have been described so far, COX-1, COX-2 and COX-3 [24, 25]. COX-1, the first COX isoform discovered, is constitutively expressed in almost all tissues and its metabolites play an important role in maintaining the physiological conditions of the organism, ensuring the homeostasis or maintenance of prostaglandins levels (PGs), which in turn regulate vasodilatation and blood flow hemodynamics [26]. COX-2, the inducible

isoform, is expressed only at some stages of cell differentiation. In addition, the expression of COX-2 has been observed in pathological processes such as inflammation and angiogenesis, among others [27]. COX-1 and COX-2 catalyze the conversion of AA into prostaglandins through a two-step reaction. First, two molecules of oxygen are added to AA, giving rise to prostaglandin G2 (PGG2); after this reaction, PGG2 is reduced, generating PGH2, which gives rise to the remaining prostaglandins, tromboxan A2 and prostacyclins [28]. COX-3 has similar structural and catalytic properties to COX-1 and COX-2 but has only 20% of the activity of COX-1 and COX-2. Nevertheless, this isoform has not yet been isolated in humans [24]. COX-2 is a suitable target for drugs against inflammatory diseases and tumorigenesis, as this is enzyme that contributes most to prostanoid synthesis in inflammatory processes and its expression is upregulated by inflammatory mediators, but also by hypoxic conditions and in many types of cancer [29]. Interestingly, the cyclooxygenase pathway has been shown to modulate nitric oxide synthase (NOS) activity and vice versa. Mechanisms by which nitric oxide can modulate prostaglandin synthesis include direct S-nitrosylation of COX and inactivation of prostaglandin I synthase by peroxynitrite, the product of the reaction of superoxide with nitric oxide. Conversely, prostaglandins can promote an increased association of dynein light chain (DLC) (also known as protein inhibitor of neuronal nitric oxide synthase) with NOS1, thereby reducing its activity [30].

COX-2 is implicated in bone formation. Kreke et al., demonstrated that induction of COX-2, along with activation of mitogen-activated protein kinases (MAPKs) ERK and p38 and expression of other genes, is an early event which occurs in shear stress-induced osteogenesis and may contribute to osteoblastic differentiation [31].

In the context of CAVD, high COX-2 expression was first observed in AVICs in calcified nodules of Klotho mice, a model of premature ageing and aortic valve calcification. In these mice, celecoxib, a selective COX-2 inhibitor, reduced aortic valve calcification (AV) [32]. However, in contrast with these results, a recent retrospective clinical study found an association between AS and celecoxib use [33]. The same study demonstrated the pro-calcifying effect of COX-2 inhibition in porcine AVICs [33]. The role of COX-2 in AS has mainly been studied in non-human models, and it remains uncertain whether inhibition of COX-2 delays or promotes CAVD in humans.

1.4. The role of the Notch pathway in CAVD

1.4.1. The Notch pathway

The Notch pathway is a highly conserved pathway that plays a pivotal role in several cellular processes, such as proliferation, stem cells maintenance, and differentiation during embryonic development and post-natally [34]. It is a short-range communication system between two adjacent cells, based on a ligand-activated receptor. Notch receptors and ligands are both transmembrane proteins located on the surface of cells. Mammals possess four different Notch receptors, referred to as NOTCH1, NOTCH2, NOTCH3, and NOTCH4 [35]. Notch receptors are synthesized as single-chain precursors and cleaved into an extracellular and a trans-membrane subunit in the Golgi apparatus. These two subunits are held together on the cell membrane by non-covalent bonds. The Notch ligands are members of the DSL (Delta/Serrate/LAG-2) family of proteins named Delta-like and Jagged. In mammals there are multiple Delta-like and Jagged ligands (Delta-like 1, 3, 4, and Jagged 1, 2). Ligand binding allows the first proteolytic cut of Notch trans-membrane domain by a surface protease, A Disintegrin And Metalloproteas (ADAM), which removes the extracellular portion of Notch and creates a membrane tethered intermediate that is a substrate for γ-secretase, an intramembranous aspartyl-protease complex. This last cut releases the active form of Notch (Notch intracellular domain, NICD) which translocates into the nucleus where it binds the transcriptional factor CBF-1/Suppressor of hairless/ Lag-1 (CSL), also known as recombination signal sequence binding protein J-kappa (RBP-Jk or RBPJ). NICD binding displaces a co-repressor complex (Co-R) and promotes the transcription of Notch target genes such as Hairy/enhancer of split (Hes) and Hes-related proteins (Hey1 and 2). These factors regulate further downstream genes involved in the regulation of cell cycle [36], apoptosis [37] and stemness [38] (Figure 1). This is commonly defined *canonical* Notch signaling pathway. During the past years data have been accumulating on the *non-canonical* Notch signaling, which is independent of CSL, and it involves the interaction with Phosphoinositide 3-kinases (PI3Ks), Wnt/β-catenin, mTORC2/Akt, nuclear factor kappa-light-chain-enhancer of activated B cells (NF-κB), YY1, or HIF-1α pathways at both the cytoplasmic and/or nuclear levels (Figure 1).

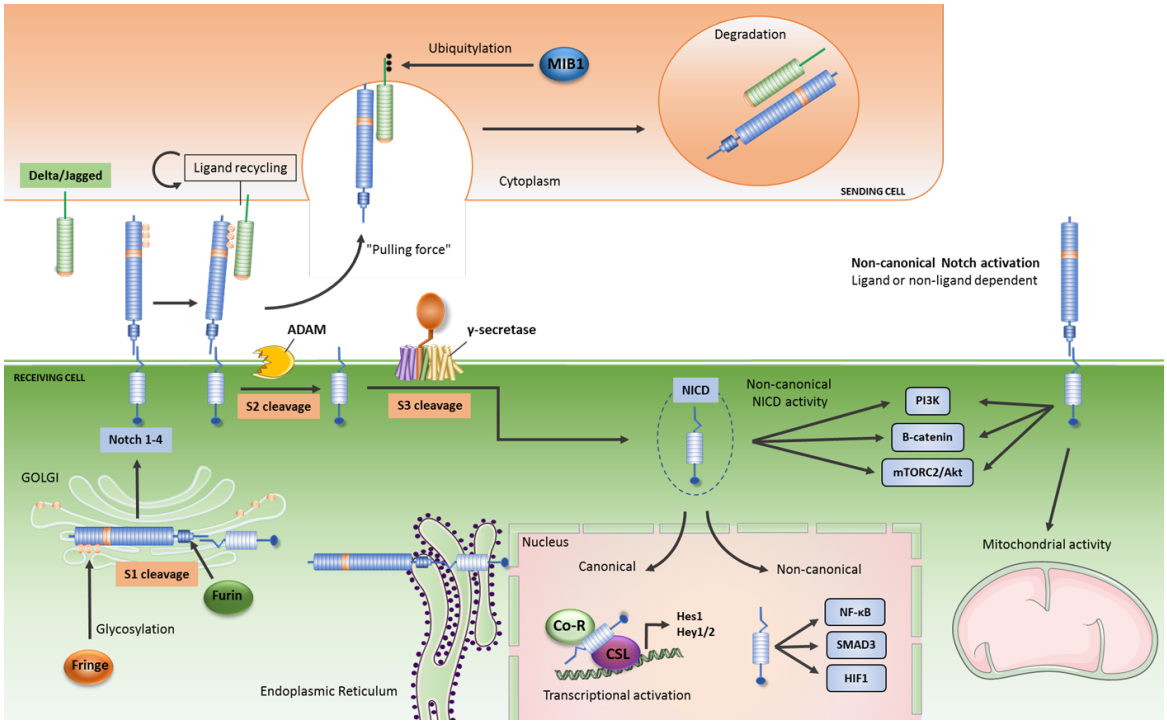

Figure 1. Canonical and noncanonical Notch signaling pathway. In the canonical Notch pathway, precursor of Notch receptors undergoes Furin-mediated cleavage (S1) in the Golgi apparatus, which is necessary to form the functional heterodimeric receptor. Upon Notch glycosylation by the Fringe family of glycosyltransferases, the Notch receptor translocates to the plasma membrane, where it interacts with a Delta/Jagged ligand, present on the surface of an adjacent cell. Notch signaling is activated when the ligand, bound to the receptor, is ubiquitylated by MIB1, an event that generates the mechanical force necessary for exposing the second cleavage site of Notch receptors. This event leads ADAM to perform the second cleavage (S2). The third cleavage (S3), by the γ-secretase complex, promotes the release of the intracellular domain of the receptor (NICD). NICD translocates into the nucleus where it promotes the transcription of canonical Notch target genes, such as Hey1 and 2 and HES1. The noncanonical Notch signaling pathway may be γ-secretase dependent or independent. This later may also occur either in the presence or in the absence of its ligand. Noncanonical Notch signaling is also independent of CSL, and it is mediated by the interaction with PI3K, mTORC2, AKT, Wnt, NF-κB, YY1, or HIF-1α pathways at either the cytoplasmic and/or nuclear levels [39].

Depending on the cellular context, the Notch signaling plays different, even opposite, roles and differential Notch receptor-ligand interactions can trigger different responses [40, 41]. In vascular smooth muscle cells (VSMCs), Jagged1- mediated activation of Notch pathway induces contractile phenotype [42]. In macrophages induction of Notch signaling by the

ligand Dll4 promotes their proinflammatory activation, both in vitro and in vivo [43, 44]. In our previous study we found that atherosclerotic plaques from peripheral artery disease (PAD) patients were characterized by “stable” or “inflamed” gene expression profiles associated to Notch activation by ligand Jagged1 or Dll4, respectively [45]. Of interest, it has been shown that in mice, endothelial deletion of Jagged1 leads to valve calcification and congenital heart defects [46]. These data suggest that the ligand-specific activation of this pathway has an important impact on disease characteristics and progression. Thus, therapeutic strategies could be implemented to interfere with disease progression by targeted modulation of Notch signaling components, including the ligands Jagged1 and Dll4.

In the context of cancer, activation of the Notch pathway is generally associated with cancer progression by promoting cancer cell survival [47]. Therefore, several clinical trials have been conducted in cancer patients and more are underway targeting Notch. One approach is to use γ-secretase inhibitors, small molecules that prevent the release of the active form of Notch by inhibiting the proteolytic activity of the γ-secretase complex. These clinical trials have shown tolerable toxicity but also low efficacy of γ-secretase inhibitors, in part because of off-target effects and the dose of administration, which must be nontoxic but at the same time capable of completely blocking the signaling pathway (for a more in-depth discussion on Notch inhibition in cancer the reader is referred to [48-51]). Other approaches which have been used to inhibit Notch both in vitro and in vivo, included the use of: ADAM inhibitors, and/or monoclonal antibodies (mAbs) that specifically target Notch receptors and/or ligands. Delivery of both γ-secretase inhibitors and Dll4 mAb by specific binding of solid lipid nanoparticles to death receptors (DR)-5 on triple negative breast cancer cells is currently under investigation [52]. Interesting, Zheng et al. developed a fully human monoclonal antibody to Jagged1, 15D11, which inhibits Jagged1 in breast cancer cells and, in combination with chemotherapy, synergistically reduces bone metastasis in a mouse model of breast cancer [53]. In animal models of pathologies with a recognized underlying inflammatory state, such as chronic obstructive pulmonary disease (COPD), arthritis and metabolic syndrome [54-56], the use of γ-secretase inhibitors or mAb to inhibit the Notch pathway has been shown to be efficient in reducing the inflammatory response, but to date, no clinical trials have tested the efficacy of Notch inhibition in this context.

In contrast to cancer, activation of Notch in the cardiovascular system is required for prevention of cardiomyocytes [57] and endothelial cells apoptosis [58] caused by various proinflammatory stimuli. Thus, activation of Notch in the heart [59] and endothelium [47] may represent a new therapeutic approach to combat diseases such as coronary artery disease (CAD) and heart failure (HF), which remain the leading cause of death worldwide.
One of the challenges in the activation of Notch in CVDs is the need to specifically target Notch activators to cardiomyocytes and endothelial cells to avoid cell transformation in other tissues and/or the induction of a dysregulated inflammation. These are major challenges to overcome and may explain why activation of Notch to affect the progression of heart disease and atherosclerosis has only been attempted in animal models [59]. Therefore, novel approaches are needed to investigate the feasibility and efficacy of Notch-based diagnostic tests and therapies for CVD in humans. One potential approach to specifically activate Notch in cardiomyocytes and endothelium could be the use of Notch-regulating microRNAs (miRNAs) [60].

1.4.2. Dysregulation of Notch in CAVD

The involvement of the Notch pathway in aortic valve calcification is certain, as inherited Notch1-inactivating mutations are associated with severe aortic valve calcification [11]. Furthermore, clinical studies [61] and findings in animal models have shown that deregulation of Notch pathway both in endothelial [12] and interstitial cells [13] is associated with pathological mineralisation of valvular cells. Specifically, the profile of Notch-related gene expression in the interstitial cells of the aortic valve of patients differs from that in cells of healthy individuals. This difference is related to dysregulated Notch-dependent events in patients' cells, such as NICD-dependent induction of EMT and calcification [61]. Of interest, calcified aortic valve disease has been associated with higher expression of the lncRNA H19, which impairs NOTCH1 expression [62].
Active Notch in ECs seems to be required to prevent calcification. In 2012, Hofmann et al. demonstrated that deletion of Jagged1 in murine endothelial cells leads to aortic valve calcification [46]. Later, Theodoris et al. showed that heterozygous nonsense mutations in NOTCH1 cause aortic valve calcification in human induced pluripotent stem cells (iPSCs)

-derived endothelial cells by inducing transcription of genes involved in oxidative stress, inflammation, and osteogenesis [12].

Some studies support the concept that activation of Notch1 prevent osteogenic differentiation in AVICs. Nigam et al. showed that Notch1 suppresses Bmp2 in aortic valve cells and prevents the progression of osteo-genic calcification [63]. Likewise, Acharya et al. demonstrated that inhibition of Notch1 promotes the development of calcification, whereas activation of Notch attenuated the calcification process [64]. In contrast with these results, Zeng et al. have shown that Notch1 induces osteogenic differentiation in human AVICs [13]. Furthermore, in AVICs derived from CAVD patients, activation of Notch1 contributes to pro-osteogenic differentiation [61].

Whether the activation of Notch in AVICs is pro- or anti-osteogenic is unclear. It is possible that the discrepancies described are due to different in vitro and in vivo experimental conditions in different laboratories. Furthermore, only Notch1 has been investigated in this context, for the understanding of the role of Notch the other receptors (Notch2, Notch 3, and 4) and ligands (Dll4 and Jagged) should be investigated. Additionally, interaction between VECs and AVICs is essential to ensure the proper development and maintenance of the aortic valve [65, 66]. An in vitro co-culture study of endothelial cells (ECs) with aortic smooth muscle cells (SMCs) show that ECs have an osteoinductive effect on SMCs and that this effect depends on activation of Notch signalling in ECs [67]. Thus, to fully understand the role of Notch signalling in CAVD, the possible miscommunication between VECs and AVICs in this disease should be investigated.

1.4.3. Crosstalk between the Notch pathway and COX-2

Different studies reported the crosstalk between COX-2 and the Notch pathway [68-70]. It has been shown that Jagged1/Notch signaling inhibition has been linked to COX-2 induction in VSMCs [71] and Dll4-mediated Notch signaling in macrophages activates NF-k B [44, 56], which, in turn, induces VCAM1 and COX-2 transcription. Furthermore, as previously discussed, our data in atherosclerotic plaques from PAD patients showed that the activation of Notch signalling depends on the type of ligands since COX-2 correlated positively with Dll4 and negatively with Jagged1. Additionally, patients follow up showed that Dll4 ligand-associated signature could have unfavourable effects on the progression of

the disease [45]. The cross-talk between COX-2 and the Notch pathway in CAVD has not been investigated.

1.5. Clonal Hematopoiesis of Indeterminate Potential (CHIP) and cardiovascular disease

Random mutations, which accumulate during life, can confer a selective advantage to hematopoietic stem cell in which they occur and give rise to clones of mutant cells. When this occurs in hematopoietic stem cells, a relevant proportion of differentiated cells with mutations may be found in the blood. Although the presence of mutant cells increases the risk of developing leukaemia, most people who carry mutant clones never develop symptomatic blood diseases. The condition characterized by the presence of mutant clones without overt blood pathology is defined clonal hematopoiesis of indeterminate potential (CHIP) [72]. Conventionally, CHIP carriers were defined as individuals carrying clonal somatic mutations in genes linked to hematologic malignancy with a variant allele fraction (VAF) of at least 2%, but without a known hematologic malignancy or other clonal disorder. This condition is common among older persons and, unexpectedly, in recent years, it has emerged that CHIP carriers have an increased risk of developing cardiovascular disease such as myocardial infarction, atherosclerosis, and coronary-artery calcification [73]. The most frequently mutated CHIP genes are those encoding epigenetic factors such as DNA methyltransferase 3A (DNMT3A), Tet methylcytosine dioxygenase 2 (TET2) and ASXL transcriptional regulator 1 (ASXL1) or signaling proteins such as Janus kinase 2 (JAK2) [74, 75]. TET2, DNMT3A and JAK2 mutations are associated with increased cardiovascular risk in epidemiological studies and are causally implicated in cardiovascular diseases in animal models [76]. JAK2 mutations are associated with thrombosis in CHIP patients [77] and their causal role in thrombosis has been demonstrated in an animal model of myeloproliferative neoplasm (MPN) [78]. DNMT3A and TET2 are also associated with adverse heart failure progression in patients with ischemic and non-ischemic heart disease [79] and, increased death or HF re-hospitalization during a median follow-up of 4.4 years [80]. Consistently, studies in animal model confirmed the casual relationship between Tet2-mutation and the development of HF [81]. In the context of aortic stenosis there is one study which reported that TET2 and DNMT3A mutations were enriched in patients aortic valve stenosis [82], and this is linked to an

increase of the inflammatory signature of circulating monocytes [83] and to alterations in the number of circulating pro-inflammatory T cells [82], but causality has not been established yet (Figure 2). The mechanisms linking CHIP to cardiovascular disease are only partially known. Findings in animal models suggest that CHIP-related mutations increase inflammatory responses and demonstrated the causal role of CHIP mutations in promoting atherosclerosis and heart failure [73, 84, 85]. It is thought that CHIP promotes cardiovascular disease by increasing the inflammatory potential of immune cells carrying mutations, as evidenced by elevated or circulating inflammatory markers [86] or specific inflammatory cell subsets [82]. Increased inflammatory potential of CHIP has also been experimentally confirmed in cell lines with mutations in TET2 or DNMT3A [87, 88]. More recently, single-cell RNA sequencing of human peripheral blood cells has elegantly confirmed that the presence of CHIP mutations promotes an inflammatory phenotype in both monocytes and T cells [83]. Although it is now clear that CHIP mutations can induce immune cells to respond excessively, the precise cellular and molecular mechanisms by which CHIP -induced inflammation promotes human cardiovascular disease remain unknown.

Of interest, even if not in the context of CVDs, Notch1 mutations have been identified in Tet2-/- T-cell tumors and contribute to the initiation/progression of T-cell malignancy [89]. Furthermore, it has been shown that DNA hypomethylation of COX-2 promoter region could contribute to the transcriptional regulation of COX-2 expression and elicit a pro-inflammatory response in an animal model of ketamine-induced ulcerative cystitis (KIC) [90]. This highlights the importance of epigenetic mechanisms, and thus a possible role for Tet2 in the transcriptional modulation of COX-2.

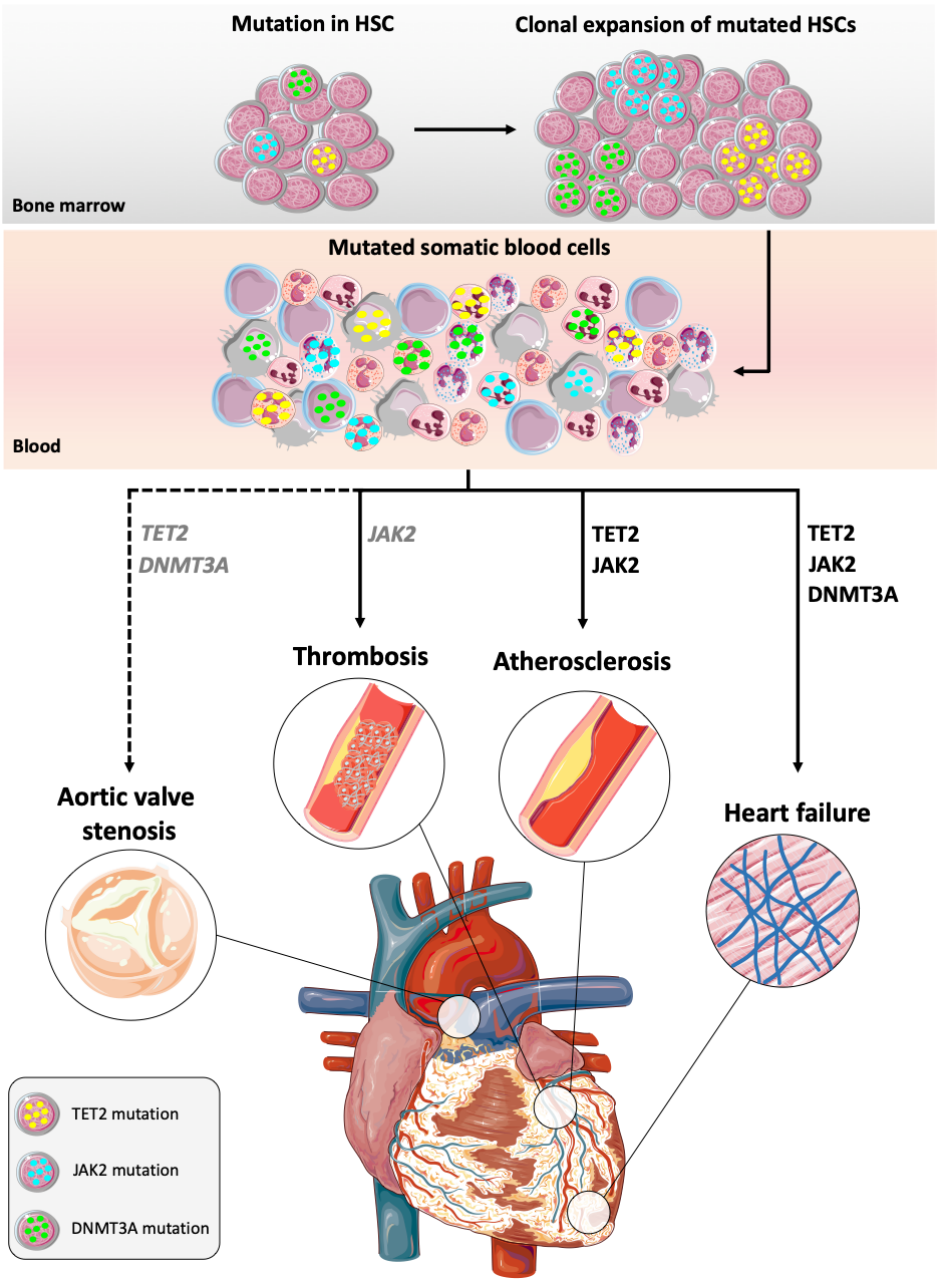

Figure 2. Clonal hematopoiesis of indeterminate potential (CHIP) causes cardiovascular disease. Mutations can confer a selective advantage to a hematopoietic stem cell (HSC) which can give rise to a significant proportion of mutated somatic blood cells. TET2 and JAK2 mutations preferentially involve myeloid cells. DNTM3A mutations are present in somatic blood cells of both myeloid and lymphoid origin. Mutations in the genes TET2, DNMT3A and JAK2 (in black) are associated with increased cardiovascular risk in epidemiological studies, and they have been causally implicated in cardiovascular disease in animal model. TET2 and DNMT3A mutations (in grey italic) are enriched in aortic valve stenosis, but causality has not been established yet (indicated with dashed lines). JAK2 (in grey italic)

hyperactivation is associated with thrombosis in CHIP patients; causality between JAK2 mutations and thrombotic diseases has been established in an animal model of myeloproliferative neoplasm (MPN) [76].

Based on the evidence that CHIP mutations trigger inflammatory responses, and that pro-inflammatory state confers a fitness advantage to cells carrying CHIP mutations [84, 87, 91] one of the possible approaches to reducing both clonal expansion and CHIP -dependent inflammation could be targeting inflammation.

Cai and coworkers showed that in mice, loss of TET2 causes increased expression of IL-1β and IL-6, which in turn activates the Shp2/STAT-3 signaling, leading to inflammatory response. In these mice, inhibition of the IL -6 downstream effectors SHP2-STAT3 reduced both IL -6 production and clonal expansion of Tet2- KO HSPC [92]. Monoclonal antibodies against specific cytokines such as IL -1β (canakinumab) and IL -6 (tocilizumab and clazakizumab) are already used in clinical practice or tested in clinical trials to treat diseases in which cytokines are abnormally released [93-95]. Similarly, targeting inflammatory pathways mediated by IL -1β and IL -6 could mitigate the effect of a CHIP-mediated inflammation response.

The mutagenic event leading to hyperactivation of JAK2, is associated with thromboembolic events, also by activating β1 and β2 integrins in leukocytes. Similarly, selective inhibition of Jak2 with ruxolitinib or fedratinib [96, 97] already tested in animal model, or anti-integrin inhibitors may attenuate atherothrombotic complications. At present, no interventions to reduce the cardiovascular risk associated with CHIP have been attempted in the clinical setting.

2. AIM OF THE STUDY

Due to the incomplete understanding of the pathogenies of CAVD, no effective medical treatment can prevent or slow the progression of this disease and aortic valve replacement remains the only clinical treatment for severe, symptomatic aortic stenosis.

Inflammation plays a major role in CAVD and thus, the identification of the major players involved could help to identify a precise, tailored therapeutic approach.

COX-2 and Notch pathway, both involved in inflammation, play a role in CAVD but, their precise role and their cross-talk in this context are still partially unknown. Furthermore, a new player has recently emerged, CHIP, which seems to be involved in CAVD and other cardiovascular disease with mechanisms still unknown, which could also involve Notch and, possibly COX-2.

COX-2 is the target of a widely used drug. Agents able to inhibit Notch are in the clinic trial for cancer patients. Several agents able to interfere with CHIP are available. It is therefore imperative understand how these pathways, together or independently could lead to a “precise” therapeutic approach to CAVD.

Based on these premises, the aims of this study were:

AIM1

To investigate the hypothesis that CAVD is a consequence of deregulated interaction between VECs and AVICs caused by altered expression levels of Notch ligands. In Aim1 we will also characterize the cross-talk between Notch signaling and COX-2.

AIM2

To provide further evidence that CHIP is involved in CAVD and uncover the molecular mechanism by which these mutations in blood cells could affect the aortic valve environment.

3. Materials and Methods

3.1. Study population

For the first aim we studied 83 patients undergoing cardiac surgery: 61 patients who had valve replacement for calcific severe aortic stenosis (group 1) and 22 patients without AV calcification (control group 2). For the second aim we enrolled 168 patients undergoing valve replacement for severe calcific aortic stenosis. Of these, 112 patients had cardiac surgery and 56 patients had TAVI. In addition, 5 patients without calcific aortic stenosis were included as a control group. In both cohorts control group underwent valve replacement for one of the following conditions: 1) severe aortic insufficiency; 2) aortic root aneurysm. All patients were enrolled at Maria Cecilia Hospital, Cotignola (RA), Italy. The study was approved by Ethics Committee of "Romagna" (approval code: 590/2017) and was conducted according to the Declaration of Helsinki. All patients gave written informed consent.

3.2. Biological samples collection

Aortic valve leaflets removed during surgery were immediately immersed in RNA later (Thermo Fisher Scientific, Waltham, Massachusetts, USA). Blood samplings were performed from an antecubital vein using a 21-gauge needle or from the central venous line. Blood was collected in the early morning at least 12 hours after the last administration of anticoagulant drugs. The first 2 to 4 mL of blood were discarded, and the remaining was collected in EDTA tubes, aliquoted, and immediately stored at -80 °C.

3.3. Gene Expression

Aortic valves leaflets preserved in RNAlater (ThermoFisher Scientific, Waltham, MA, USA) were disrupted and homogenized with the TissueRuptor® (Qiagen, Hilden, Germany). Total RNA was extracted with RNeasy® Fibrous Tissue Mini Kit (Qiagen, Hilden, Germany) according to the manufacturer's instructions. RNA concentration and purity were evaluated by Nanodrop 2000 spectrophotometer (ThermoFisher Scientific). 100 ng of RNA were reverse transcribed in a volume of 25 µl using 250 units of

SuperScript III reverse transcriptase and 50 ng of random hexamers on SimpliAmpTM Thermal Cycler (ThermoFisher Scientific). 2 µl of the cDNA mixture were used 4 for real-time PCR experiments. Real-time PCR reactions were conducted on StepOnePlusTM Real-Time PCR System (ThermoFisher Scientific), using PerfeCta SYBR Green SuperMix with ROX kit (Quanta Biosciences, Beverly, MA, USA) according to the manufacturer's protocol. Primers concentration was 500 nM. Primers sequences used are: RPL13: forward 5′-GGAGGTGCAGGTCCTGGTGCTT-3′, reverse 5′-CGTACGACCACCACCTTCCGG-3′; PTGS2 (COX2): forward 5′-CAAATTGCTGGCAGGGTTGC-3′, reverse 5′-AGGGCTTCAGCATAAAGCGT-3′; ACTA-2 (α-SMA): forward 5′- CCGACCGAATGCAGAAG-3′, reverse 5′-ACAGAGTATTTGCGCTCCGAA-3′; JAGGED-1: forward 5'-GACTCATCAGCCGTGTCTCA-3', reverse 5'-TGGGGAACACTCACACTCAA-3'; Dll4: forward 5'- GCGAGAAGAAAGTGGACAGG-3', reverse-ATTCTCCAGGTCATGGCAAG-3'. 3 non-calcific samples were not used for α-SMA expression due to limited amount of RNA and/or cDNA. Gene expression levels were expressed as relative copy number calculated with $2^{-\Delta Ct}$ formula using RPL13 as reference gene.

3.4. AVICs Isolation and Cell Culture

Leaflets were incubated with 600 U/mL collagenase II (ThermoFisher Scientific) for 10 minutes at 37°C then were gently scraped to remove aortic valve endothelial cells. Leaflets were then rinsed with HBSS and then diced before incubation with 200 U/mL collagenase II for 4 hours to disaggregate the tissue. Next, the cell suspension was repeatedly pipetted, and filtered through a 100 µm cell strainer to remove residual chunks and spun at 400 g to obtain a cell pellet that was washed with HBSS. Finally, cells were plated and grown in M199 medium (ThermoFisher Scientific) containing 2% FBS (ThermoFisher Scientific) and 1% 70 penicillin/streptomycin (ThermoFisher Scientific). To minimize AVICs trans-differentiation to myofibroblasts which may occur during culturing, we added to the medium 10 ng/ml of Fibroblast Growth Factor (FGF) 2 and 50 ng/ml insulin (Sigma Aldrich) (Porras et al. 2017; Latif et al. 2015). To induce AVICs calcification cells were grown in M199 medium supplemented with 10% FBS, 50 µM ascorbic acid, 0.1 µM

dexamethasone and 10 mM β-glycerophosphate (Sigma Aldrich) for 14 days. AVICs were used between passages 3 and 5.

3.5. Histology and Immunohistochemistry (AIM1)

For histological and immunofluorescence analysis, aortic valves removed during surgery were immediately fixed in 10% neutral buffered formalin for 24h and then embedded in paraffin. For histology and immunostaining, 5 μm sections were cut using a microtome (SLEE medial, Mainz, Germany) and placed on polylysine glass slides. For histology, sections were re-hydrated and stained with Movat's pentachrome stain (Abcam, Cambridge, UK) according to manufacturer's instructions. For immunofluorescence analysis, sections were re-hydrated and antigen retrieval was performed in 10mM citrate buffer at 95 °C for 13 minutes. Sections were washed with PBS for 20 minutes and then blocked and permeabilized with 10% BSA solution with 0.3% Triton-X 100 for 1 hour. After blocking, sections were washed 3 times with PBS 1X and then incubated at 4 °C overnight with rabbit anti-COX2 and mouse α-SMA antibodies diluted in 1% bovine serum albumin (BSA). Unbound antibody was removed washing 3 times with PBS and sections were incubated for 1 hour at room temperature in the dark with anti-rabbit antibody conjugated with Alexa Fluor 488 and anti-mouse antibody conjugated to and Alexa Fluor 647 (ThermoFisher Scientific) diluted in 1% BSA. After 3 washes in PBS 1X, slides were mounted with aqueous mounting solution containing DAPI Prolong (ThermoFisher Scientific). Images were taken with a confocal microscope (Nikon A1 system) using 10X or 20X objectives.

3.6. Histology and immunostaining (AIM2)

Valves, 8-μm sections were cut using a microtome (SLEE medial, Mainz, Germany). Russell-Movat pentachrome stain (Abcam, Cambridge, UK) was performed according to the manufacturer's instructions. For immunohistochemistry analysis, after antigen retrieval with EDTA buffer (Sigma-Aldrich, St. Louis, MO, Stati Uniti), slices were incubated overnight with an anti-BAFF-R or CD138 antibodies (Abcam, Cambridge, UK) diluted 1:250 or 1:8000, respectively. Slides were stained with HRP/DAB detection kit (Abcam,

Cambridge, UK) and counterstained with hematoxylin to visualize cell nuclei. Images of entire aortic valve cusps were composed using NIS-Elements Microscope Imaging Software (Nikon, Tokyo, Japan) from a series of adjacent pictures taken with a 4x objective taken with a Nikon Eclipse Ni microscope (Nikon, Tokyo, Japan). Immunostaining images were taken with a 20x objective with a Nikon Eclipse Ni microscope (Nikon, Tokyo, Japan).

3.7. Western Blotting

AVICs were collected by scraping and lysed on ice for 30 min in RIPA buffer (Thermo Fisher Scientific) containing freshly added phenylmethylsulfonyl fluoride (PMSF) (Sigma Aldrich, St. Louis, MO, USA), protease inhibitors mix M (SERVA, Heidelberg, Germany), and phosphorylase inhibitors mix phosSTOP (Sigma Aldrich, St. Louis, MO, USA). Protein concentration of each lysate was quantified by using DC protein assay (Biorad). Protein samples were denatured at 100 °C for 5 min in sample buffer (Thermo Fisher Scientific) containing 0.5 M dithiothreitol (DTT). Proteins (10 µg) were separated on Mini-PROTEAN® TGX™ (Biorad) and transferred to nitrocellulose membranes with Trans-Blot® Turbo (Biorad). Nonspecific binding was blocked by incubating membranes with Tris-buffered saline (TBS)/Tween 0.1% and pH 7.6 and containing 5% nonfat dry milk or 5% bovine serum albumin (BSA) for 1 h at room temperature. Nitrocellulose membranes were incubated overnight at 4 °C with primary antibodies as indicated below, washed 3 times in TBS/Tween 0.1%, and incubated for 1 h at room temperature with secondary peroxidase-conjugated antibodies in TBS/Tween 0.1% and containing 5% nonfat dry milk or 5% BSA. Membranes were washed 3 times in TBS/Tween 0.1% and developed using Clarity or Clarity Max Western ECL blotting substrates (Biorad). Images of the blots were obtained with ChemiDoc camera (Biorad). The antibody to COX-2 was from Abcam (Cambridge, UK), peroxidase-conjugate secondary antibodies, were from ThermoFisher Scientific (Waltham, MA, USA), the mouse monoclonalantibody to -SMA and Œ≤-actin (AC-15) were purchased from Sigma Aldrich (St. Louis, MO, USA).

3.8. Nodule Formation Assay

AVICs were plated onto plates or Petri dishes at a density of 75,000 cells/cm^2 in M199 medium supplemented with 1% FBS, with or without 5 ng/mL recombinant human transforming growth factor (TGF)-β1 (Sigma Aldrich, St. Louis, MO, USA) [19679827] and with or without 5 μM celecoxib (Sigma Aldrich). After 4 days, cells were fixed for 10 min in 4% paraformaldehyde (PFA, Sigma Aldrich). Finally, cells were rinsed with deionized water, incubated with 14 mM Alizarin Red Stain (Sigma Aldrich) for 10 min. Cells were washed 2 times with PBS to remove excess of Alizarin Red. Round/oval and red-stained nodules with a diameter of 50–100 μm (estimated from 5-cell diameter) [19679827]. Red-stained nodules were manually counted under an inverted microscope (Nikon). Alizarin Red was also quantified from the stained cells by acetic acid extraction followed by neutralization with ammonium hydroxide to enable colorimetric detection at 405 nm using microplate photometer (Multiskan, ThermoFisher Scientific).

3.9. Apoptosis

Apoptosis was evaluated with the Annexin V/ Propidium Iodide (PI) binding assay. After treatments, AVICs were stained with Annexin V-FITC and PI (ThermoFisher Scientific) in a binding buffer (10 mM Hepes, 5 mM KCl, 150 mm NaCl, 1.8 mM $CaCl_2$, 1 mM $MgCl_2$, pH 7.4), left in the dark at room temperature for 20 min. Annexin V-FITC and PI positive cells were quantified by flow cytometry (Attune Nxt Flow cytometer, ThermoFisher Scientific). The data were analyzed with Attune Nxt Software (ThermoFisher Scientific). Annexin V-positive cells were considered apoptotic, and apoptosis was expressed as percentage of Annexin V-positive cells on total cells.

3.10. Construction of Lentiviral vectors

Lentiviral production was performed as described previously [98]. In brief, 100-mm dishes of subconfluent 293T cells were cotransfected with 15 μg of vector carrying the sequences of Dll4 and Jagged1, as well as their antagonists – shDll4 and shJagged1. 5.27 μg pMD2.G, and 9.73 μg pCMV-dR8.74psPAX2 packaging with PEI reagent by calcium-phosphate method. The following day the medium was changed to fresh, and the cells were

incubated for 24 hours to obtain high-titer virus production. Produced lentivirus was concentrated from supernatant by ultracentrifugation, resuspended in 1% BSA/PBS and frozen in aliquots at -80°C. The virus titer was defined by GFP-expressing virus. The short hairpins to Dll4 and Jagged1 mRNAs were synthesized as two oligos followed by annealing, resulting double-strand sh sequence was cloned in pLKO.1 - TRC cloning vector (Addgene plasmid # 10878; http://n2t.net/addgene:10878; RRID: Addgene_10878) [39].

3.11. Isolation and induction of osteogenic differentiation in AVICs transfected with Lentiviruses

We obtained aortic valves from two patients with CAVD diseases. Valve leaflets were washed in PBS and incubated for 10 minutes at 37°C in 0.2% collagenase solution (Collagenase type IV, Worthington Biochemical Corporation, USA). The valve was vortexed for one minute to remove VECs. To isolate AVICs the remaining valve tissue was incubated with 0.2% collagenase solution for 24 hours at 37°C. Then the tissue was pipetted repeatedly to break up the tissue mass and spun at 300 g for five minutes. The pellet containing AVICs were resuspended in DMEM (Gibco) supplemented with 15% FBS, 2mM L-glutamine, and 100units/ml penicillin/streptomycin, and plated on T75 flask. AVICs were cultured by enzymatic tissue dissociation and then osteogenic differentiation was induced. The cells were seeded at a density of 10^4 cells / cm2. The next day, the medium was replaced with a differentiation medium (DMEM containing 10% of bovine fetal serum (HyClone, USA), 1% of L-glutamine (Gibco, USA), a mixture of Penicillin (100 U/ml) and streptomycin (100 µg/ml) (Gibco, USA), osteogenic factors: 50 µM ascorbic acid, 1 µM dexamethasone, and 10 mM beta-glycerol phosphate (Sigma, USA). Differentiation was assessed within 21 days by Alizarine Red staining: cells were washed with PBS, fixed in 70% ethanol for 60 min, washed twice with distillated water and stained using Alizarin Red solution (Sigma). The images of calcium phosphate deposition were analyzed for the ratio of differentiated and undifferentiated cell areas with MosaiX software (Carl Zeiss microsystems, Germany).

3.12. Detection of CHIP

DNA was extracted from whole blood samples with DNeasy Blood & Tissue Kit (Qiagen, Hilden, Germany), according to the manufacturer's instructions. After genomic DNA (gDNA) extraction, gDNA concentration was assessed using the Qubit dsDNA BR Assay Kit (ThermoFisher Scientific, Waltham, MA, USA) on a Qubit 2.0 Fluorometer (ThermoFisher Scientific, Waltham, MA, USA); the DNA Integrity Number was determined at Agilent 2200 TapeStation System (Agilent Technologies, Santa Clara, CA, USA) using the DNA genomic assay; the 260/230 and 260/280 ratios were determined by the NanoDrop spectrophotometer to exclude the presence of organic compounds and protein contamination, respectively. Libraries were prepared using SureSelectXT Low Input Target Enrichment System for Illumina Paired-End Multiplexed Sequencing Library protocol (Agilent Technologies, Santa Clara, CA, USA), starting from 200 ng of gDNA and according to manufacturer's instructions. Hybridization capture of DNA libraries was performed through a custom RNA probes panel designed to enrich the 9 genes commonly mutated in CHIP. To improve the identification of low allele frequency variants and exclude PCR duplicates, 10-bp unique molecular identifiers (UMIs) were incorporated into each DNA fragment during library preparation. Libraries' quality and size distribution were assessed on Agilent 2200 TapeStation System (Agilent Technologies, Santa Clara, CA, USA) with the DNA1000 Kit. Before sequencing, the pooled libraries were diluted at a final concentration of 2nM and denatured according to the NextSeq System Denature and Dilute Libraries Guide (Illumina, San Diego, CA, USA); 1% of PhiX DNA was also added to the mix. The pool was sequenced at a loading concentration of 1,8 pM on Illumina NextSeq-500 System in a 2x150 bp paired-end reads format, obtaining an average coverage of 646X. Paired-end demultiplexed reads were produced using bcl2fastq and the quality control was performed using FastQC. The reads were trimmed from the adapters using Trimmomatic [99] (v0.39) with a minimum length of 30 bp, and a leading and trailing of 10 bp. The UMI were extracted using UMITools [100] and the resulting reads were mapped on the human genome (hg38) using BWA MEM (v0.7.17) [99]. Sorting and indexing were performed using SAMtools (v1.10) [101], while the BAM correction and the metrics collections were obtained using Picard (v2.20.3). Mutect2 from GATK [102] (v4.1.2.0) was used for the variant calling of the somatic variants using the *af-only-gnomad.hg38.vcf* as germline-resource. Only the variants that were annotated as "PASS"

by FilterMutectCalls were considered as somatic variants. The filtered variants were annotated using wANNOVAR [103]. We considered CHIP-associated variants the ones with Variant Allele Frequency (VAF) more than 0.02 [72] and less than 0.35 to exclude germinal mutations.
This protocol was performed by Genomix4Life S.r.l., spin-off of University of Salerno.

3.13. RNA sequencing of aortic valves

Aortic valves leaflets preserved in RNAlater (ThermoFisher Scientific, Waltham, MA, USA) were disrupted and homogenized with the TissueRuptor® (Qiagen, Hilden, Germany). Total RNA was extracted with RNeasy® Fibrous Tissue Mini Kit (Qiagen, Hilden, Germany) according to the manufacturer's instructions. The RNA concentration was measured using the Qubit RNA HS Assay Kit (ThermoFisher Scientific, Waltham, MA, USA) on a Qubit 2.0 Fluorometer (ThermoFisher Scientific, Waltham, MA, USA) while RIN (RNA Integrity Number) was determined at Agilent 2200 TapeStation System (Agilent Technologies, Santa Clara, CA, USA) using the RNA assay. The 260/230 and 260/280 ratios were determined at the NanoDrop spectrophotometer to exclude the presence of organic compounds and protein contamination, respectively. Indexed libraries were prepared starting from 150 ng of purified RNA with TruSeq Stranded Total RNA Library Prep Kit (Illumina, San Diego, CA, USA) according to the manufacturer's instructions. Libraries' size distribution was assessed using the Agilent 2200 TapeStation System (Agilent Technologies, Santa Clara, CA, USA) and pooled in equimolar amounts, with a final concentration of 1,5 nM. The pooled samples were sequenced on NovaSeq 6000 System (Illumina, San Diego, CA, USA) in a 2x100 paired-end format at a final concentration of 250 pM. Paired-end demultiplexed reads were produced using bcl2fastq and the quality control was performed using FastQC. The reads were trimmed from the adapters using Cutadapt [104] (v3.3) with a minimum length of 20 bp. The produced reads were mapped on the human genome (Gencode v37 primary assembly annotation) using STAR [105] (v2.7.8a). The raw counts were obtained using featureCounts on Rsubread (v2.0.1) [106]. Normalization and Differential Expression analysis were performed on R (v4.0.2) using DeSeq2 (v1.28.1) [107]. Functional analyses of differentially expressed genes were generated through the use of Ingenuity Pathway Analysis [108] and only the

significant pathways with a p-value < 0.05 were considered. This protocol was performed by Genomix4Life S.r.l., spin-off of University of Salerno.

3.14. Statistics

Normality was assessed before further analyses. Student t test for independent measures was employed to test statistical significance in the mean differences of gene expression levels in two groups. ANOVA applying appropriate post-test for multiple comparisons were used to compare groups of in vitro experiments. Correlations were calculated by Spearman's rank methods and expressed as R Spearman coefficient. CIBERSORTx [109] was used in absolute mode with 1000 permutations to impute gene expression data and provide an estimation of the cell type's abundances in the samples. Student's T and Mann-Whitney U tests were used, respectively, to assess statistical differences of normal continuous distributed and not normally distributed data. A Chi-squared test was used to determine the presence of significant differences between the expected frequencies and the observed ones for discrete variables. Principal Component Analysis (PCA) plots of previously normalized and log transformed data were created using plotPCA function from DESeq2 [107]. p-values ≤ 0.05 were considered statistically significant. All calculations, statistical analyses, and survival curves were produced on R (v4.0.2) or with GraphPad Prism version 8.0 (GraphPad software Inc., San Diego, CA, USA).

4. RESULTS

4.1. Expression of COX-2 and Notch ligands in Calcific Human Aortic Valves

4.1.1. COX-2 expression is decreased in Calcific Human Aortic Valves

mRNA level of COX-2 was quantified by qRT-PCR from total RNA obtained from whole aortic valves of patients with (group 1) and without CAVD (group 2). The clinical characteristics of the patients are shown in Table 1. We found that COX-2 mRNA

expression was higher in non-calcified than in calcified AVs (0.013 ± 0.002 vs. 0.006 ± 0.0004 relative copy number; $p < 0.0001$) (Figure 3A).

Since activated fibroblasts, which arise from trans-differentiation of AVICs, are characterized by high levels of α-smooth muscle actin (α-SMA) [110] and play a key role in CAVD, to further explore the link between COX-2 and CAVD progression we also compared the levels of COX-2 with the levels of α-SMA in CAVD and control AVs. Consistent with the presence of myofibroblasts in CAVD, we found that α-SMA expression was higher in calcific valves than in non-calcific samples (0.034 ± 0.004 vs. 0.059 ± 0.005 relative copy number; $p = 0.0005$). To investigate whether differences between calcified and non-calcified AVs in COX-2 mRNA were related to the different expression of COX-2 in AVICs, we isolated AVICs from a subset of 4 calcific and 4 non calcific AVs and we measured the levels of COX-2 protein. We found that AVICs from calcific samples showed lower level of COX-2, compared to non-calcific samples (Figure 3B). Furthermore, AVICs from calcific AVs had higher levels of α-SMA compared to cells isolated from non-calcific AVs (Figure 3B), in agreement with other studies [111]. Consistently, immunohistochemistry staining highlighted that non-calcified valves contain cells both expressing COX-2 and α-SMA in an area including spongiosa and fibrosa identified by Movat's pentachrome staining. The corresponding area of calcified samples is heavily thickened and populated by a few COX-2 positive cells and a few α- SMA positive cells (Figure 3C). Limited co-localisation of COX -2 and α- SMA is present in the controls, while the few COX-2 positive cells in the CAVD samples also express α- SMA, as shown by the presence of double positive (yellow/orange) cells (Figure 3C). Correlation analyses showed a negative association between α-SMA and COX-2 levels both in AVICs ($R = -0.762$; $p = 0.02$) and in AVs ($R = -0.187$; $p = 0.05$). Additionally, COX-2 expression levels correlated inversely with the presence of CAVD ($R = -0.858$; $p < 0.01$). Taken together these results suggest that COX-2 reduction may play a role in CAVD by promoting the AVICs activation.

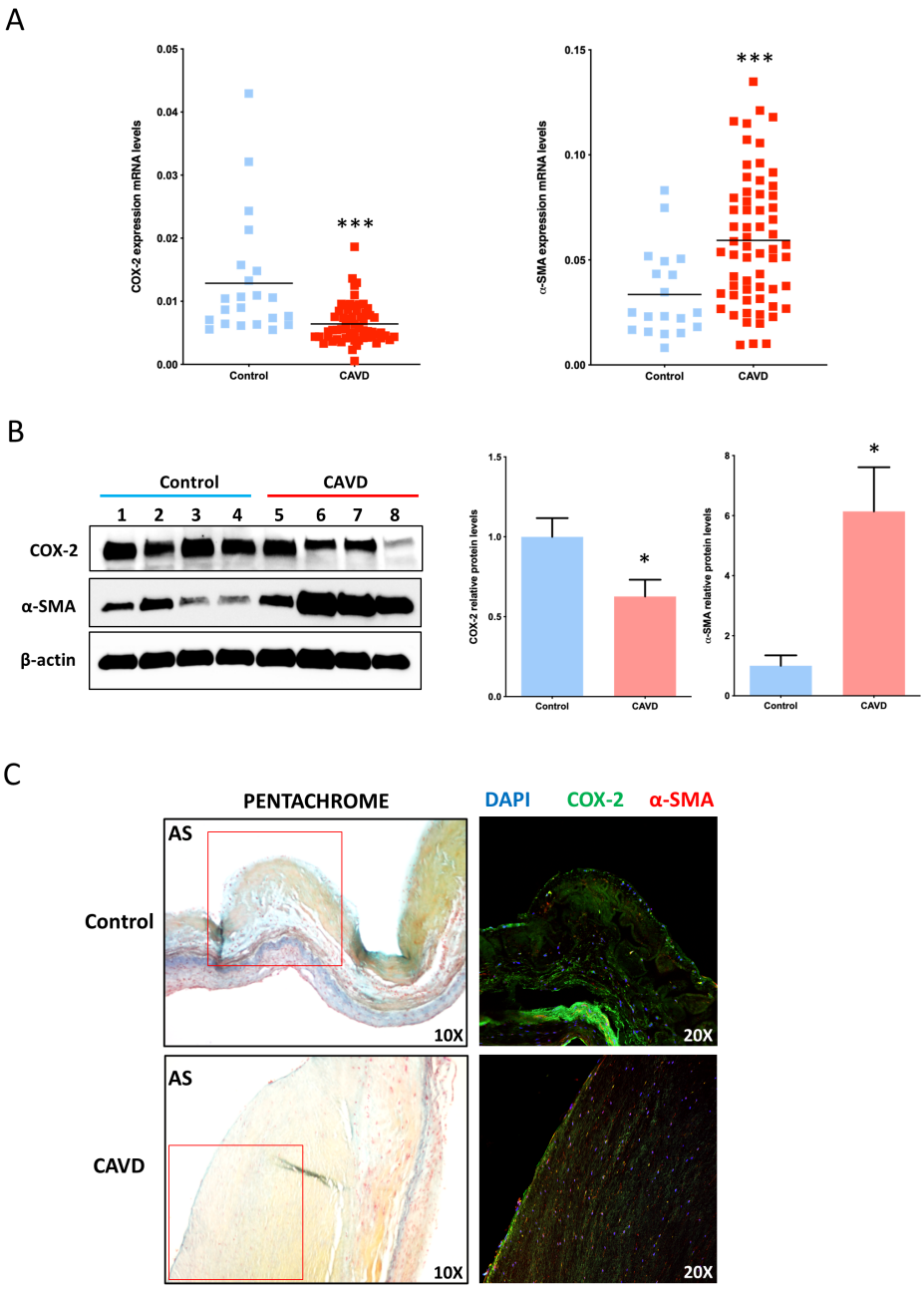

Figure 3. COX-2 expression is decreased in human calcific aortic valves. (A) Cyclooxygenase 2 (COX-2) and α-smooth muscle actin (SMA) mRNA levels in non-diseased aortic valves (n = 22) and in calcific aortic valve disease (CAVD) (n = 61); *** $p < 0.001$ (B) Western blots of COX-2 and α-SMA in aortic valve interstitial cells (AVICs) isolated from non-calcific aortic valves (AVs) (n = 4) or

calcified AVs (n = 4) and densitometric analysis of the levels of COX-2 and α-SMA of AVIC isolated from non-calcific AVs (n = 4) or calcified AVs (n = 4). Data were normalized for corresponding β-actin level. * $p < 0.05$ (C). Modified Movat's pentachrome stain and immunohistochemistry staining of COX-2 (green) and α-SMA (red) in control or calcific AVs. DAPI (blue) highlights cell nuclei. Images in the right panel show the corresponding areas indicated by red frames on the left panel. AS: Aortic Side.

Table 1. Clinical characteristics

	CAVD (*n* = 61)	**Control (*n* = 22)**	***p***
Age (years)	78 (73–81)	71 (64–78)	0.002
Male sex	33 (54)	15 (68)	0.251
BMI (kg/m^2)	27 (24–29)	28 (25–30)	0.274
Bicuspid	4 (6.5)	2 (11.0)	0.653

Table 1. Clinical characteristics. Continuous variables are presented as median (interquartile range), categorical variables are presented as count (percentage). BMI, body mass index. Comparisons between groups were performed with independent sample *t*-test, Mann–Whitney U-test, Pearson's Chi-squared test, or Fisher's exact test, as appropriate.

4.1.2. Celecoxib increases number of calcific nodules in Human Aortic Interstitial Cells

To investigate the effect of COX-2 inhibition in CAVD, we induced the calcification of human AVICs isolated from non-calcific aortic valves by 4 days treatment with TGF-β1 [112] in the presence or absence of celecoxib and assessed the number of calcific nodules (CNs). It is well known that the initial step of valve calcification is characterized by TGF-β1- induced activation of myofibroblast phenotype [110]. As expected, treatment with TGF-β1 increased the number of CNs detected by Alizarin Red staining (Figure 4A, B).

Importantly, in AVICs treated with celecoxib we observed an increased number of CNs, both in the presence of TGF-β1 and at basal condition (Figure 4A, B). Furthermore, treatment with TGF-β1 increased α-SMA protein levels in AVICs and celecoxib- only treatment induced α-SMA to an extent like that of TGF-β1 (Figure 4E). The treatment with celecoxib did not further increase the level of α-SMA in comparison to treatment with TGF-β1 only. These results demonstrated that celecoxib induces AVICs activation, accelerating dystrophic calcification even in absence of TGF-β1. We also explored the effect of COX-2 inhibition in AVICs grown in osteogenic medium for 14 days. Under these conditions, AVICs display calcific accumulation as showed by Alizarin Red staining (Figure 4C, D). The addition of celecoxib to the osteogenic medium, causes an increase in calcium deposition, on the contrary when added to standard medium celecoxib alone did not increase calcification (Figure 4C, D). Finally, since apoptosis induced by different stimuli including TGF-β, plays a key role in dystrophic calcification, we measured apoptosis levels in AVICs following treatment with celecoxib and TGF-β1 for 4 days and observed that both TGF-β1 and celecoxib induce apoptosis in AVICs, and co-treatment with TGF-β1 and celecoxib has an additive effect on apoptosis (Figure 4F).

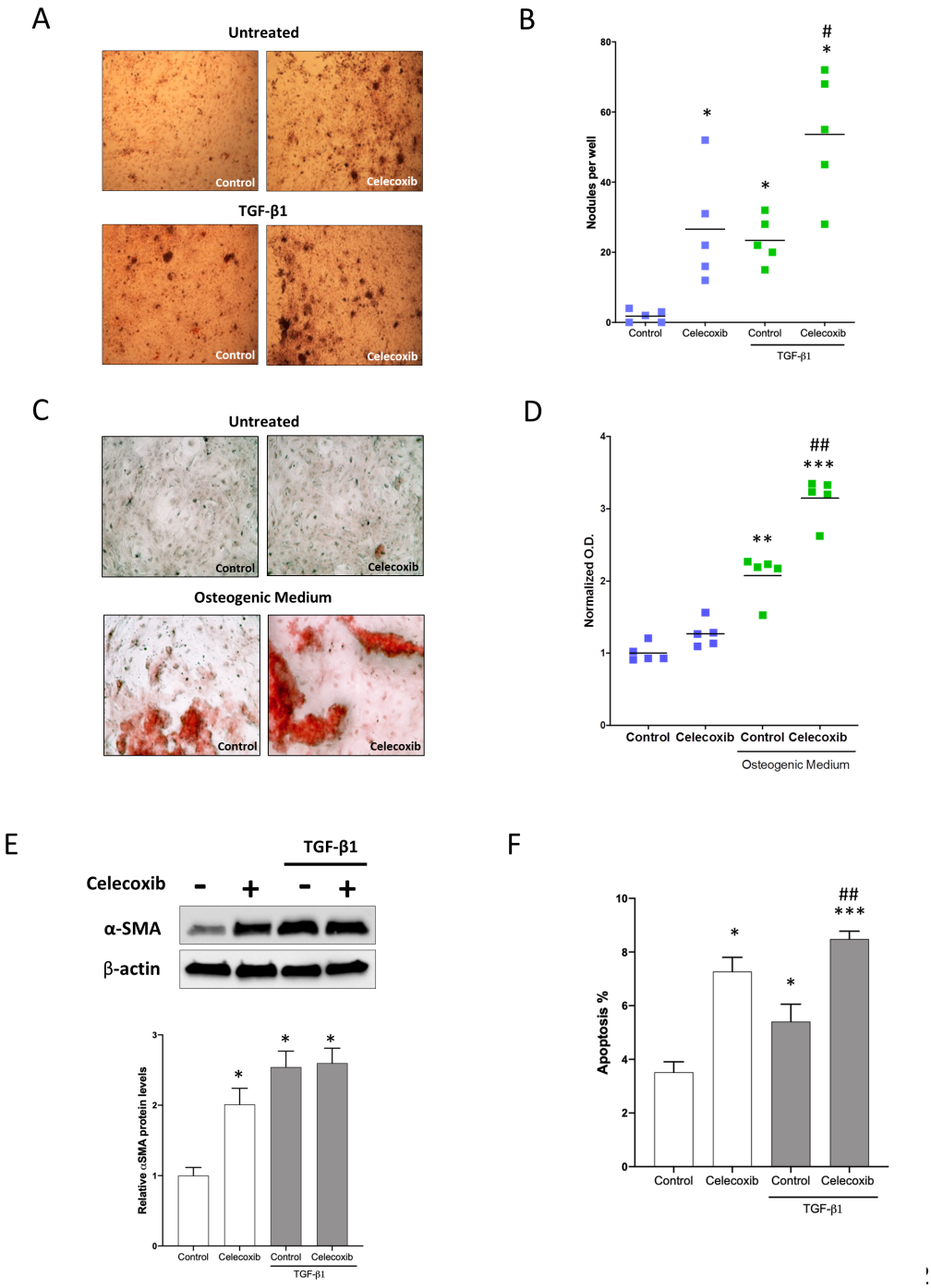

Figure 4. Celecoxib promotes myofibroblast induction, apoptosis and calcification in human AVICs. (A) In AVICs isolated from non-calcific AVs, TGF-β1 10 nM or celecoxib 5 μM induces the formation of calcium nodules (CN) identified by Alizarin Red staining. Images were taken using a 10× objective. (B) The experiments were performed with AVICs isolated from 5 non-calcific AVs. * $p < 0.05$ in comparison to control; # $p < 0.05$ in comparison to control with TGF-β1. (C) In AVICs isolated

from non-calcific AVs and grown in osteogenic medium, celecoxib 5 μM induces the formation of calcium nodules identified by Alizarin Red staining Images were taken using a 20× objective. (D) Alizarin Red stain was quantified by acetic acid extraction followed by neutralization with ammonium hydroxide to enable colorimetric detection at 405 nm. The experiments were performed with AVICs isolated from 5 non-calcific AVs. ** $p < 0.01$, *** $p < 0.001$ in comparison to control; ## $p < 0.01$ in comparison to control with TGF-β1. (E) Representative Western blot and densitometric analysis showing that TGF-β1 10 nM or celecoxib 5 μM induces the expression of α-SMA in human AVICs isolated from non-calcific AVs after 4 days. The experiments were performed with AVICs isolated from 3 non-calcific AVs. * $p < 0.05$ in comparison to control. (F) In AVICs isolated from non-calcific AVs, TGF-β1 10 nM or celecoxib 5 μM induces apoptosis. * $p < 0.05$, *** $p < 0.001$ in comparison to control; ## $p < 0.001$ in comparison to control with TGF β1.

4.1.3. Jagged1 and Dll4 expression is dysregulated in Calcific Human Aortic Valves and correlates directly or inversely, respectively, with COX -2

To investigate the expression of Notch ligands in CAVD, we quantified Jagged1 and Dll4 mRNA levels in total RNA extracted from whole cusps of aortic valves from patients with CAVD and without CAVD. We found that Jagged1 expression was higher in non-calcific compared to CAVD samples (0.23 vs 0.17; $p = 0.0004$). Conversely, Dll4 expression was lower in non-calcific vs CAVD samples (0.021 vs 0.091; $p = 0.005$) (Figure 5A). Additionally, to further dissect the link between COX-2 and Notch ligands in the pathophysiology of CAVD, we performed correlation analyses between COX-2, Jagged1 and Dll4 expression in CAVD patients. We found that COX-2 expression correlated, directly with Jagged1 ($R = +0.416$, $p < 0.001$) or inversely with Dll4 levels ($R = -0.394$, $p < 0.01$) (Figure 5B). These data show that the transition from Jagged1 to Dll4 expression during valve calcification goes in parallel with COX-2 downregulation.

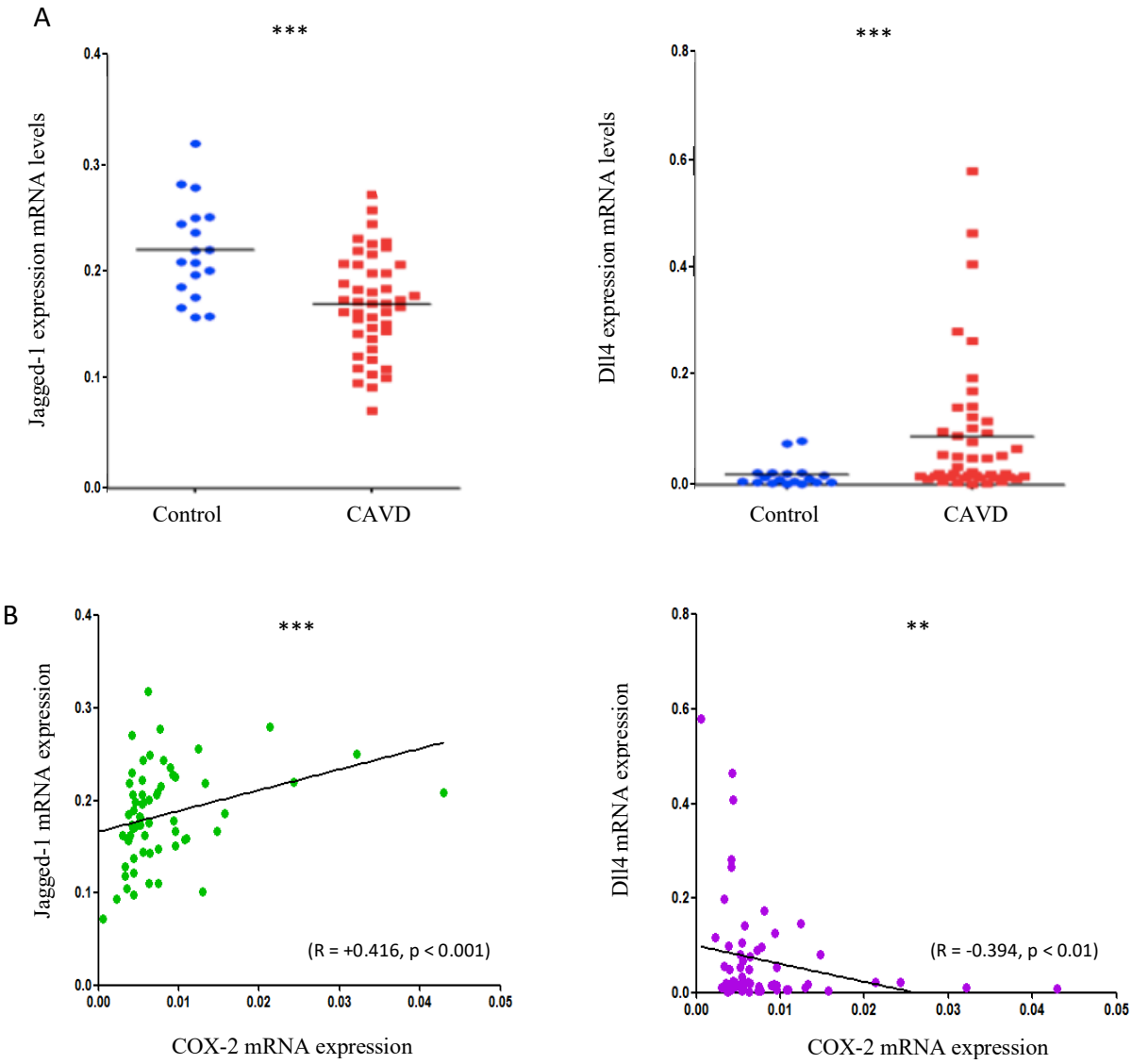

Figure 3. Jagged1 and Dll4 expression is dysregulated in calcific aortic valves and correlates directly or inversely, respectively, with COX-2. A) Jagged1 and Dll4 mRNA levels in non-diseased aortic valves (CTRL) (n = 22) and in calcific aortic valve disease (CAVD) (n = 61); *** $p < 0.001$. B) Correlation analyses between COX-2 and the Notch ligands Jagged1 and Dll4 mRNA levels. Correlations between the two variables were tested by Spearman's correlation coefficient. ** $p < 0.01$; *** $p < 0.001$.

4.1.4. Jagged1 and Dll4 have opposite effects in calcification of AVICs isolated from CAVD patients

To better investigate the hypothesis of a dysregulation of Notch ligands in CAVD we transduced AVICs derived from two CAVD patients, with lentiviruses carrying Jagged1 or Dll4 sequences, and shJagged1 or shDll4 sequences to inhibit endogenous Dll4 and Jagged1, in presence of osteogenic medium (OM). Twenty-one days after stimulation with osteogenic medium, calcification occurred as shown by strong Alizarin Red staining in AVICs grown in OM and control vector (TRC) compared to AVICs (CTRL) grown in standard medium (Figure 6). In AVICs from the first patient, treatment with shDll4 strongly increased calcium deposition, compared to AVICs treated only with osteogenic medium or TRC. We did not observe difference in calcium deposition between AVIC transfected with Dll4 and TRC. In AVICs treated with Jagged1 we observed similar Alizarin Red staining, compared to untreated cells. Addition of shJagged1 led to less calcium deposition, compared to AVICs treated only with osteogenic medium or TRC. We observe the same trend in the second patient even though less evident.

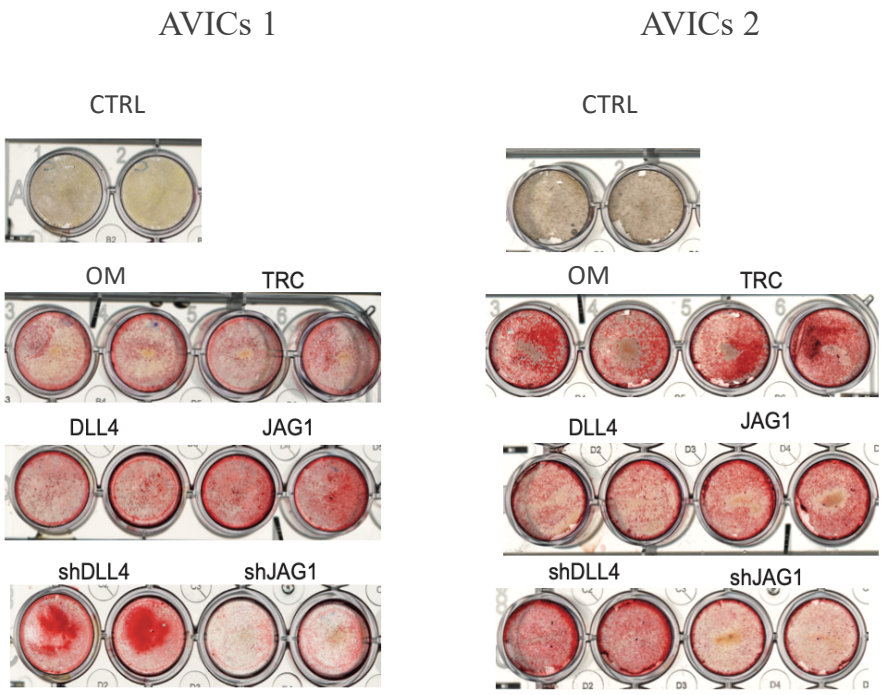

Figure 6. Inhibition of Jagged1 and Dll4 reduces and increased, respectively, calcium deposition in vitro. AVICs isolated from calcific AVs were grown in osteogenic medium (OM) and treated with

control vector - TRC, lentivirus bearing Dll4, Jagged1 and their inhibitors, shDll4 and shJagged1. Calcium deposition was identified by Alizarin Red staining after 21 days. The images of calcium phosphate deposition were analyzed for the ratio of differentiated and undifferentiated cell areas with MosaiX software (Carl Zeiss microsystems, Germany). These are the results of a single experiment that need to be validated with more experiments.

4.2. Investigation of involvement of CHIP in Calcific Human Aortic Valves

4.2.1. Detection of CHIP in blood cells of patients with calcific aortic stenosis

DNA extracted from blood cells from a cohort of 168 patients affected by severe AS was analyzed by targeted sequencing using a custom panel of 9 genes, selected among those more frequently mutated in CHIP, namely: DNMT3A, TET2, ASXL1, JAK2, NOTCH1, TP53, KDM6A, CBL, and NF1. An average of 15 million reads per sample were generated, covering the regions of interest at 99.89% with at least 10X coverage and approximately 98% with 50X coverage and with an average depth of 350X. 306 somatic variants distributed among the 9 genes were found. After filtering for variants not synonymous and with a variant allele frequency (VAF) higher than 0.02, 75 mutations associated with CHIP were found. In agreement with the literature [73] the most frequently mutated genes were TET2 (24) and DNMT3A (29), accounting for 32% and 38.6% of the total CHIP-related mutations identified (Supplementary Table1).

Overall, we identified 51 out of 168 subjects with CHIP (30.3%), defined as the presence of at least one mutation with VAF >2. Respectively, 45% and 37% of all the patients with CHIP have at least one mutation in DNMT3A or TET2, while only 10% have one mutation in ASXL1, JAK2, TP53, KDM6A, NF1, NOTCH1, or NF1. No mutations in CBL were observed in our cohort. Interestingly, most ASXL1 and TET2 mutations are frameshift deletions, while for all other genes most are missense mutations (Figure 7A, Supplementary Table1). Moreover, 50.6% of the detected variants associated with CHIP were classified as pathogenic by VarSome [113], 34.6% as likely pathogenic, 10.6% as Variant of Unknown Significance (VUS), and only 4% as benign (Figure 7B and Supplementary Table1).

The frequency of CHIP in the whole cohort was 30.3%. Importantly, in comparison to published results on unselected populations cohorts [74, 75] the frequency of CHIP among severe aortic valve stenosis patients was higher in all age groups and similar to that previously reported for this disease [82].

4.2.2. Clinical characteristics and prognosis after valve replacement

The clinical and echocardiographic and laboratories characteristics of the patients are summarized in Supplementary Table 2. There were no significant differences (threshold P-value < 0.05) between the CHIP and no-CHIP groups, except for the age, which was higher in the CHIP group (80.9 vs 78.4). Neither risk factors nor the presence of clinically manifest atherosclerotic vascular disease were different. Likewise, hematological and laboratory values did not differ between the two groups except for hemoglobin that was slightly lower in CHIP carriers (12.5 vs 13.1 g/dL). Patients carrying CHIP mutations experienced a significantly worse survival within 12 months from valve replacement (Figure 7C).

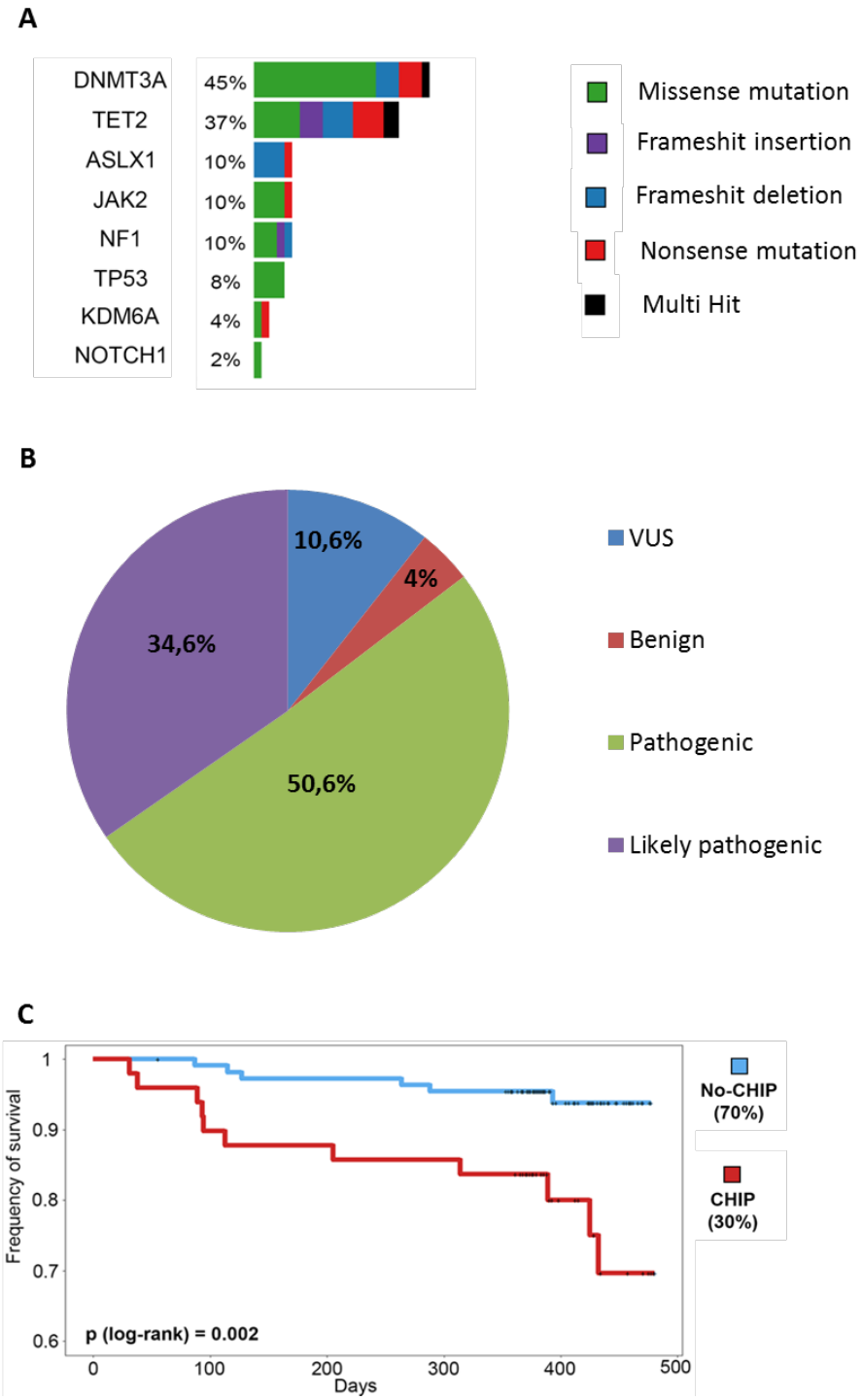

Figure7. A) Mutations landscape in the 9 genes with the percentage of per-gene mutations and the type of mutations. B) Pie chart of variants clinical annotation from VarSome. C) Kaplan-Meier curve of CHIP (red) vs No-CHIP (blue).

4.2.3. Transcriptome profiling of calcific aortic valves

To gain insights into the molecular mechanism of CAVD in CHIP patients, we performed RNA-seq in a subset of aortic valves removed during valve replacement surgery from: patients with aortic stenosis carrying DNMT3A and TET2 CHIP mutations (n = 11); patients with aortic stenosis without CHIP (n = 7); non-calcified aortic valves from patients without CHIP (n = 5), which we used as non-calcific valve reference (Supplementary Table 3). To minimize confounding factors, we included only samples from patients carrying TET2 or DNMT3A mutations, as previous studies demonstrated that monocytes from cardiovascular patients harboring mutations in DNMT3A or TET2 exhibit a highly inflamed transcriptome [83]. Among CHIP carriers, 4 patients had TET2 mutation, 5 had DNMT3A mutations, and 1 had both TET2 and DNMT3A mutations. VAF ranged from 2% to 31%. CHIP and no-CHIP patients were similar for age, as well as co-morbidities and severity of stenosis as shown in Supplementary Table 4. Principal component analysis (PCA) analysis partially clustered non-calcific versus calcific samples but did not clearly differentiate CHIP from non-CHIP samples. PCA has also highlighted a remarkable heterogeneity in the transcriptomic profile of the calcific samples, particularly of those from patients with CHIP (Figure 8). Comparison of samples from no-CHIP carriers versus non-calcified controls revealed 859 differentially expressed genes (DEGs) (Supplementary Table 5), including several genes regulating biological processes implicated in aortic valve calcification such as immune and inflammatory responses, ossification, and chondrogenic differentiation. Among the top 50 DEGs, many have already been observed in previous RNA-seq studies using similar samples [114, 115], including genes related to inflammatory responses such as CCL8, VCAM1, SLAMF8, or related to alterations of extracellular matrix, mineralization, and osteo-chondrogenic differentiation such as PRG4, TNC, FN1, COL11A1, RUNX1, AXIN2, and ACAN.

Comparison of the valves from CHIP patients with normal controls identified 266 DEGs (Supplementary Table 6). Most of these genes are related to adaptive immune responses based on Gene Ontology (GO) functional annotation, with 67 genes related to B cells activation and immunoglobulins production, accounting for roughly 25% of the DEGs. Strikingly, of the top 50 DEGs, nearly half (23 genes) are involved in adaptive immune responses, with 17 of them being involved in the humoral response. These genes include

those that encode antibodies components, comprising constant and variable regions, light and heavy chains of both IgG and IgA such as IGKC, IGHA1, IGHG1, and IGHG2. Among DEGs not related to humoral immunity many overlap with those already implicated in aortic valve calcification, these include TNC, PRG4, COL11A1, SMOC2, FN1, and OGN.

When directly comparing the transcriptome of calcific samples of patients with or without CHIP, only 5 differentially expressed genes (DEGs) satisfied the criterion of $p < 0.05$ adjusted for the false discovery rate (FDR) (Supplementary Table 7), this is probably due to the high heterogeneity in gene expression of calcific samples. Noteworthy, among these genes, immunoglobulin κ constant (IGKC) and IGKV1-12 are involved in antigenic responses, AXIN2 plays a well-known role in vascular calcification, and COL12A1 has been implicated in aortic stenosis and osteo-chondrogenic differentiation [12, 116, 117].

Pathways analysis revealed that valves from patients without CHIP, in comparison to non-calcific controls, show disruption in multiple pathways including, Th1, Th2, and NK cells signaling, leukocytes extravasation, phagosome activation, atherosclerosis signaling, and inhibition of matrix metalloproteases (Figure 9A). CHIP carriers, in comparison to controls, display alterations that partly overlap those of non-CHIP carriers, such as phagosome activation, atherosclerosis signaling, and inhibition of matrix metalloproteases. In addition, in CHIP carriers, pathways such as IL-15 signaling, B cell receptor signaling, lupus in B cells signaling, and rheumatoid arthritis pathways were dysregulated in comparison to control (Figure 9B). Interestingly, the direct comparison of CHIP and non-CHIP samples, although based only on 5 DEGs, returned alteration of pathways related to IL-15 signaling, B cells development, and lupus in B cells signaling (Figure 9C).

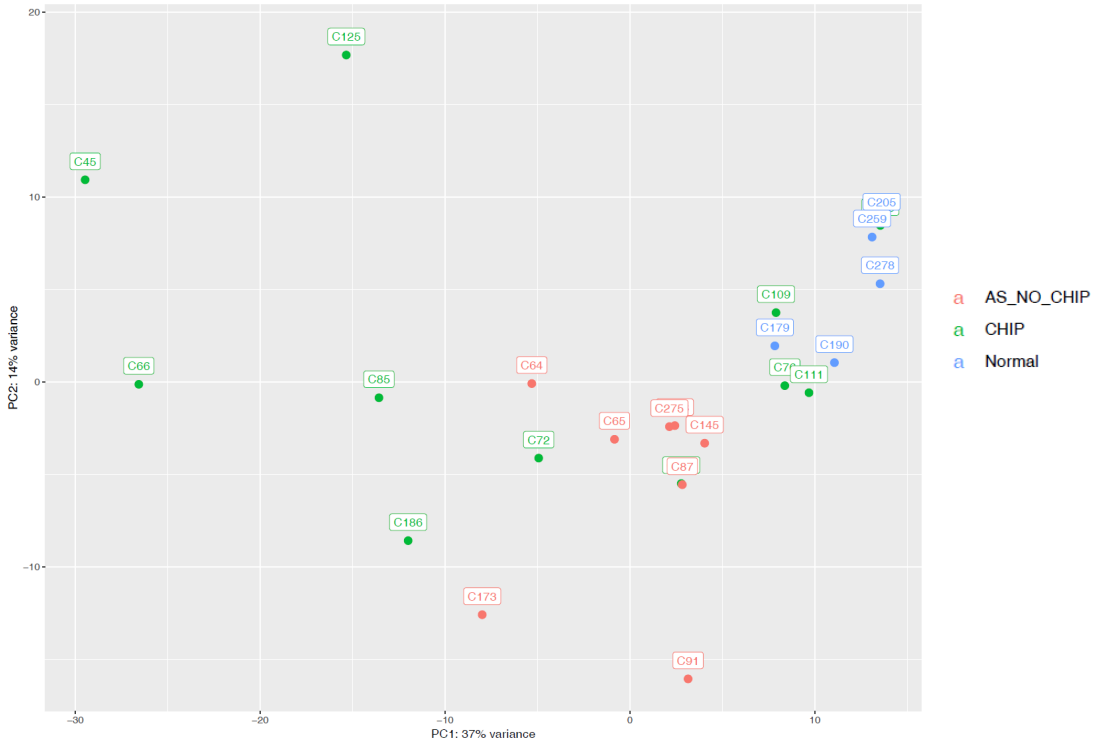

Figure 8. PCA plot of the first two components of the RNA-Seq data. Each group is colored differently.

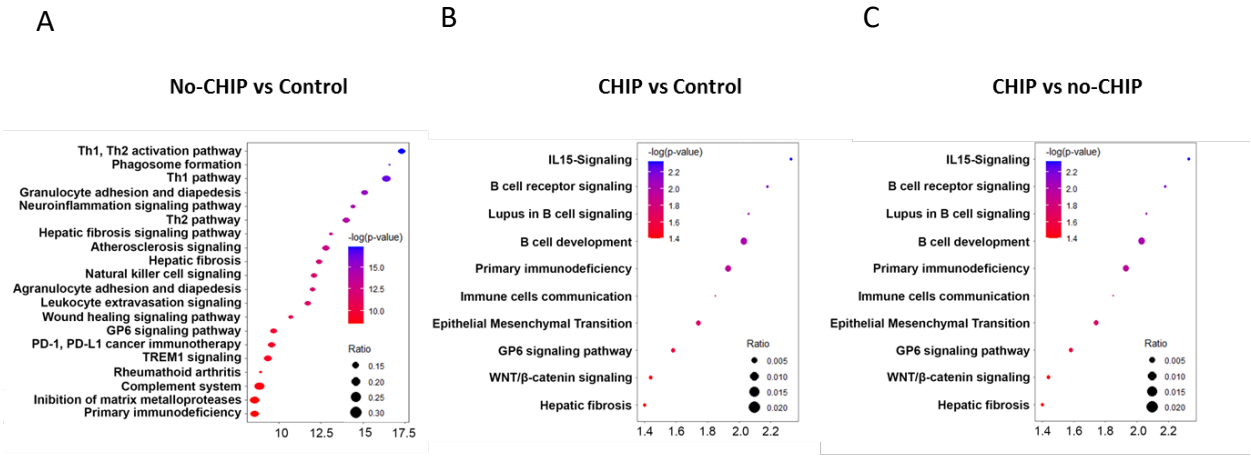

Figure 9. Dot plot of the IPA canonical pathways analysis, showing the ratio (bigger dot size is related to bigger ratio) of each gene set and the -log p-value (ranging from red to blue), of No-CHIP vs Control (A), CHIP vs Control (B) and CHIP vs No-CHIP (C).

4.2.4. Immune cells and immunoglobulins in calcific aortic valves

To characterize the immune cell presents in aortic valve samples we used CIBERSORTx, a deconvolution algorithm that estimates the abundance of 22 immune cell subpopulations starting from bulk RNA-seq data. The immune cells relative amounts in the aortic valves of CHIP and non-CHIP CAVD patients, and non-calcific controls, are shown in Figure 10. We observed that the calcified samples, from both CHIP and non-CHIP carriers contain more immune cells, in comparison to controls.

When comparing CAVD samples, with or without CHIP, the CHIP- valves contain more naïve B cells and plasma cells, even if the difference is slightly above the limit of significance ($p = 0.055$). Importantly, the amount of infiltrated B cells varies considerably among valves with some samples containing virtually no B cells and others with relatively high levels of cells of the B lineage. Although the presence of B cells was not restricted to CHIP samples, high levels of B cells infiltrate (defined as those exceeding the median of calcific samples) are more prevalent in valves of CHIP patients (7/11) in comparison to non-CHIP (2/8) or controls (1/5).

A

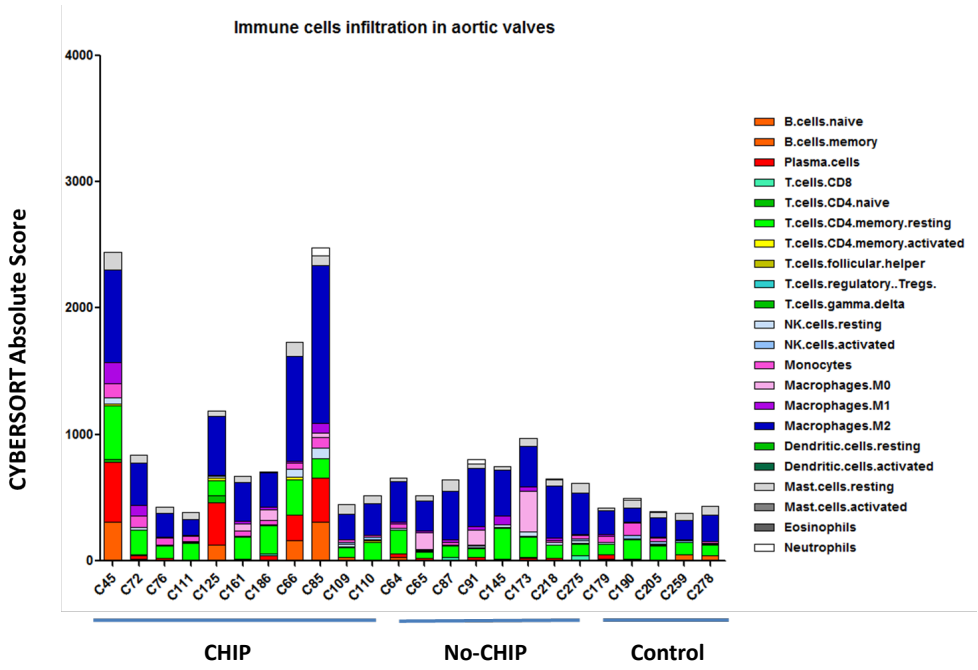

B

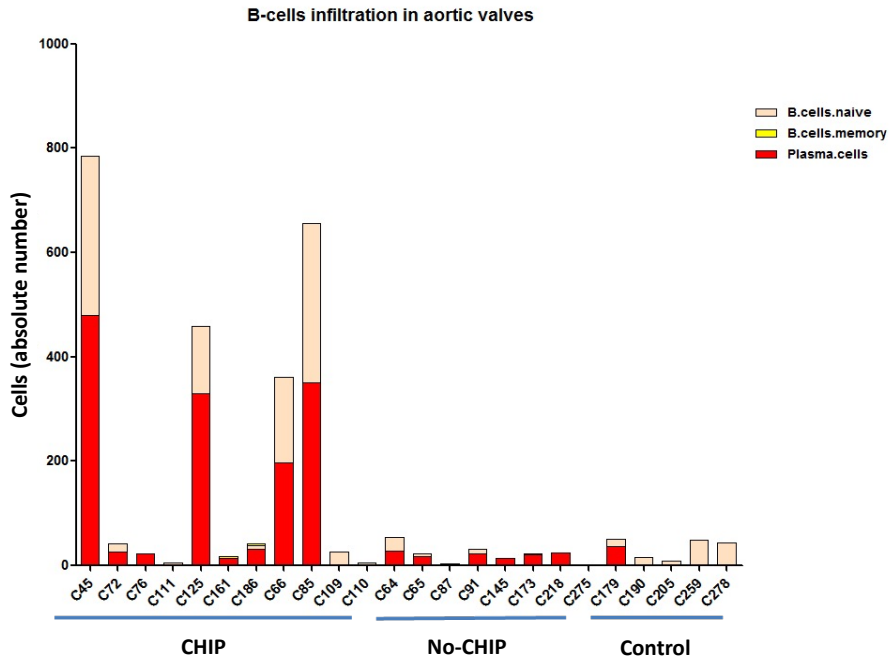

Figure 10. A) Content of immune cells profile in aortic valve samples obtained by RNA-Seq data. B) Content of naïve B cells, B cells memory and plasma cells in aortic valve samples obtained by RNA-Seq data.

We have also estimated the content of immunoglobulin-related transcripts in aortic valve samples. As expected, data mirrored those of plasma cells calculated by deconvolution confirming that samples with high B cells infiltration also contain more transcripts encoding antibodies (Figure 11A).

To confirm the presence of antibody-producing cells we performed immunohistochemistry of aortic valve - formalin-fixed samples, matching those used for RNA-seq. We used BAFF-R or CD138 (Syndecan-1) as markers of activated B cells or plasma cells, respectively [118]. As shown in Figure 11B, we confirmed that samples containing high levels of immunoglobulins transcripts display obvious B cells/plasma cells infiltration. In contrast, we found only sporadic or no B cells in samples containing little or no immunoglobulins transcripts. Interestingly, in the valves expressing high levels of immunoglobulins, BAFF-R positive cells were found in clusters containing also CD138-positive cells often localized near the calcific lesions (Figure 11B).

Interestingly, among CHIP carriers, those with high levels of immunoglobulins (first quartile) had worse survival (4 death out of 7) compared to those of the first three quartiles (1 death out of 20). Unfortunately, given the relatively low number of patients with CHIP in the AVR group, it was not possible to perform a survival analysis (i.e. Cox regression).

A

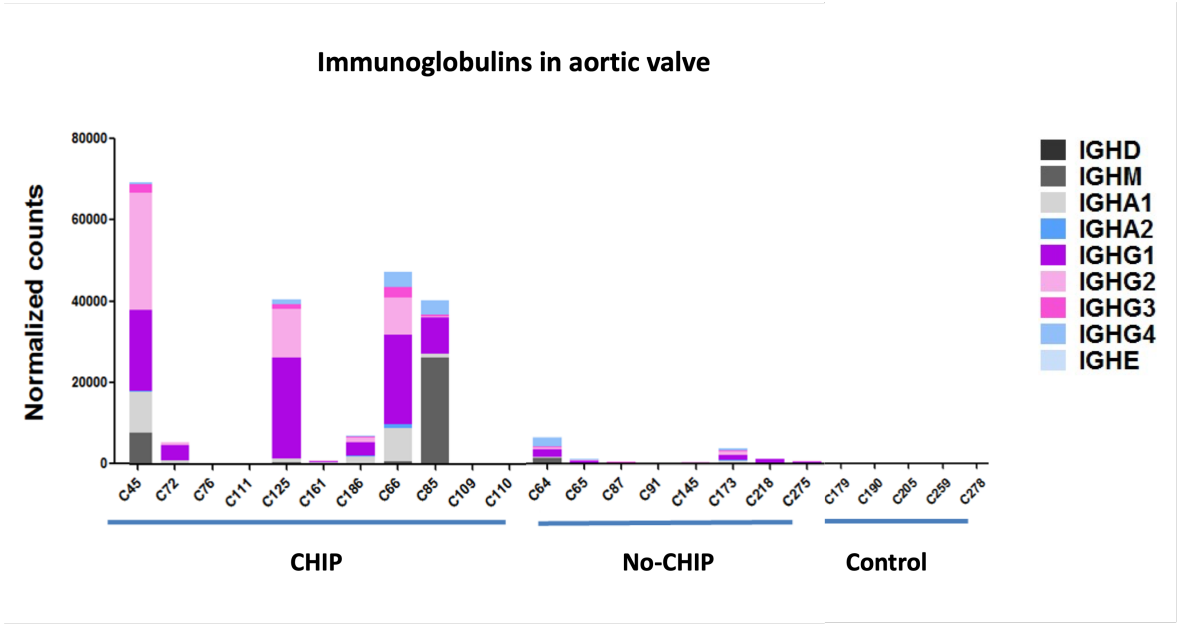

B

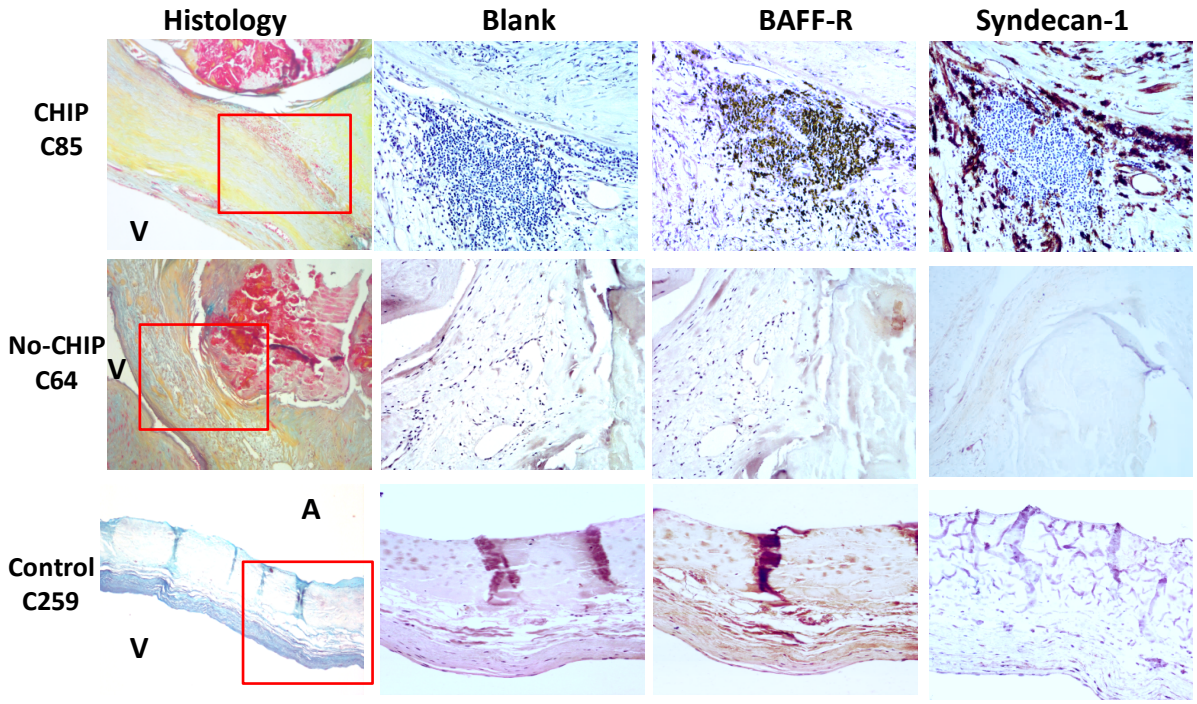

Figure 11.A) Content of immunoglobulins- related transcripts in aortic valve samples. B) Immunohistochemistry of B cells in aortic valves. Representative images of aortic valves of controls, No-CHIP, CHIP samples. Histological staining shows the cusp after Russell-Movat pentachrome staining identifying elastin fibers as black, collagens as yellow, proteoglycans as blue, muscle as red, and cell nuclei as purple. Red squares indicate the areas corresponding to immunohistochemistry images. BAFF-R or CD138 (Syndecan-1) antibodies were used to stain activated B cells or plasma cells, respectively. Negative control sections (Blank) underwent the same procedure except for the primary antibody which was omitted. A. aortic Side. V: Ventricular Side.

5. DISCUSSION

CAVD, a common pathology in elderly, remains the third leading cause of heart disease worldwide and its incidence is expected to continue to rise due to the increasing ageing of the population. As the only standard treatment is surgical valve replacement, with no guarantee of long-term success, there is an urgent need to help patients globally through the identifications of novel biomarkers able to improve the prevention, early diagnosis, and treatment of this disease. This study aimed to elucidate the molecular mechanisms underlying CAVD progression by investigating Notch, COX-2 and CHIP.

We found that AVs from AS patients were characterized by lower levels of COX-2 and increased levels of α-SMA compared to non-calcific samples. Furthermore, we confirmed this inverse correlation between COX-2 and α -SMA in AVICs isolated from AVs of CAVD patients and non-calcific AVs. Overall, our results support the hypothesis of a mechanistic model of CAVD progression based on the transdifferentiation of AVICs into α- SMA expressing myofibroblasts and show that these cells express less COX-2 compared with non-activated AVICs. In contrast to our findings, C. Wirrig et al. reported that human calcific AVs, express higher level of COX-2 compared to non-calcific samples [32]. This difference might be related to the different methodology used to quantify COX-2 expression. Unlike Wirring et al., who measured the number of COX-2 expressing cells near the area of the calcification, we measured the total amount of COX-2 in aortic valve. Of note, the cells expressing COX-2 in Wirring's study are not activated cells with a myofibroblasts-like phenotype and did not express α- SMA. Thus, it is possible to speculate that COX-2 induction is an early event in the process of calcification and that

during trans-differentiation of AVICs into myofibroblasts could be a transition from COX-2 to α- SMA expression, leading to calcification. Consistently with this hypothesis it has been observed that interleukin (IL)-1 differently regulated the expression of COX-2, with an initial mild increase at 2–4 hours followed by a more dramatic decrease below basal level by 24 hours [119]. In addition, Kreke et al., showed that induction of COX-2 occurs is an early phase of shear stress-induced osteogenesis [31]. To confirm the involvement of COX-2 downregulation in osteogenic differentiation, we treated AVICs isolated from non-calcific samples with celecoxib, a selective inhibitor of COX-2, and we found that COX-2 inhibition promotes transdifferentiation of AVICs toward a myofibroblastic phenotype and formation of calcific nodules, even in the absence of TGF-β1, a cytokine involved in collagen deposition and calcification of the AV [120]. In addition, in AVICs grown in the presence of osteogenic medium, celecoxib increased calcium deposition as shown by Alizarin Red staining. These results are in agreement with a recent study which reported that in porcine AVICs celecoxib is associated to dystrophic calcification [33].

It is well known that apoptosis induced by different stimuli such as TGF-β, plays a crucial role in dystrophic calcification [121]. In this study, we found that celecoxib increased apoptosis of AVICs, both in the presence or absence of TGF-β1.

Overall, our results show that reduced COX-2 expression is a characteristic of calcified aortic valves and inhibition of COX-2 with celecoxib promotes a pro-calcific phenotype in AVICs isolated from human AV as previously shown in porcine AVICs [33].

Dysregulation of the Notch pathway in aortic valve interstitial cells (AVICs) and valve endothelial cells (VECs) is involved in the pathogenesis of CAVD but the exact role of Notch components pathway in this context is still unclear. There is accumulating evidence that VECs and AVICs interact to ensure the proper development and maintenance of the aortic valve [65, 66]. Probably a disruption of this interaction could contribute to valve pathology and subsequent calcification. It is well known that activation of Notch by different ligands can trigger different, even opposite responses [40, 41]. Our previous study showed that atherosclerotic plaques from PAD patients are characterized by a “stable” or “inflamed” gene expression profiles associated to Notch activation by the ligand Jagged1 or Dll4, respectively. Furthermore, in the same study clinical follow up suggests that Dll4 ligand-associated signature could have unfavourable effects on the progression of the

disease [45]. Based on this evidence, we speculated that the molecular mechanisms underlying CAVD could be the dysregulation of the levels of Notch ligands, Dll4 and Jagged1. We found that calcific aortic valve isolated from CAVD patients express higher level of Dll4 and lower level of Jagged1 compared to non- calcific aortic valve. In addition, we found that COX-2 expression correlated, directly or inversely with Jagged1 and Dll4 levels, respectively. Our data suggest that a transition from Jagged1 to Dll4 may occurs in CAVD leading to COX-2 downregulation and subsequent calcification. In agreement with our conclusions, crosstalk between Notch pathway and COX-2 have been demonstrated by different studies [68-70].

Since these analyses derived from total RNA extracted from aortic valve, and since Notch has different role depending on cellular context, to strengthen our conclusions, we investigated the role of Notch ligands in aortic valve interstitial cells isolated from two CAVD patients using lentiviral vectors carrying Notch ligand Jagged1 and Dll4 sequences or their inhibitors, shJagged1 and shDll4. We found that inhibition of Dll4 strongly increases calcium deposition, compared to AVICs treated only with osteogenic medium or control vector-TRC. On the contrary, inhibition of Jagged1 display opposite effect. These data suggest an anti-calcific role of Dll4 and pro-calcific for Jagged1. Of relevance, different studies have shown that Jagged1 induces the calcification [122-124]. In AVICs treated with Jagged1 we observed faint Alizarin Red staining, compared to untreated cells. We did not observe difference in calcium deposition between AVICs transfected with Dll4 and untreated cells. Our in vitro data are in apparent contrast with the data for explanted valves in which we found a downregulation of Dll4. More studies are needed but it is important to consider that the data from the valves are the contribution of different cell types not just AVICs. The next steps will be to confirm the preliminary results that we obtained and to better investigate the effects arising from overexpression and suppression of these ligands during osteogenic differentiation.

Recently a new risk factors has emerged in the context of cardiovascular disease, which is CHIP or clonal hematopoiesis of indeterminate potential. Some evidence suggest that CHIP is also involved in CAVD but with mechanisms still unknown [76].

In our population, 51 out of 168 CAVD patients has CHIP mutations (30.3%) with the most frequently mutated CHIP genes in DNMT3Aand TET2, according to the literature

[72]. Analyzing the transcriptome of aortic valves from CAVD patients, as expected, we found that CHIP and non-CHIP patients shared altered expression of several genes previously associated with CAVD and related to the extracellular matrix and osteochondrocyte transition, such as TNC, PRG4, COL11A1, SMOC2, FN1, OGN. If we focused on valves derived from patients with CHIP, RNAseq examination revealed more profound involvement of humoral immunity, as indicated by higher levels of transcripts related to B cells and immunoglobulin production, compared with noncalcified valves or valves without CHIP. Furthermore, the comparison of the transcriptomes of AVs from CHIP patients with those without CHIP or with noncalcified samples revealed alteration of several signalling pathways related to B-cell function and to autoimmune diseases such as lupus systemic lupus erythematosus and rheumatoid arthritis.In addition, IL-15 signaling was altered in the AVs of CHIP carriers. In agreement with previous reports indicating that CHIP-associated mutations affect circulating immune cells, including monocytes, neutrophils, and T cells [76], we found that end-stage aortic valves of CHIP patients contained more monocytes, B cells, and plasma cells than non-CHIP carriers. We also observed a trend suggesting that CHIP carriers also have more T cells and macrophages, although the difference was not statistically significant, likely due to the relatively small number of samples.

Overall, our results suggest that aortic valve calcification in CHIP carriers occurs through the typical valvular changes of the disease and that the involvement of adaptive immune activation is enhanced in CHIP carriers and often involves humoral responses. Our results are consistent with recent data showing that in the context of CHIP, the interaction of innate and adaptive responses leads to an abnormal inflammatory response [83] and that subtypes of immune cells cooperate in the inflammatory response within calcified aortic valves [125].

Calcification of the aortic valve is a multistep disease that occurs within years, which means that the valves are already profoundly altered at the time of surgery. The phenotype of end-stage calcified aortic valves is the result of multiple layers of inflammatory damage that have occurred during the way leading to the symptomatic disease. In this context, it seems plausible that the increase in the activity of monocytes and T cells in CHIP carriers [126] favors a chronic inflammatory state in the valve that can then attract humoral immunity. However, CHIP mutations also occur in B cells [72, 127] and a more direct role

of CHIP mutations in B cells seems possible [86]. B cells are not normally present in healthy heart valves but can accumulate in calcified aortic valve tissue ([118, 128]. B cells can be activated by TLR signaling or cytokines secreted by macrophages, such as B cell-activating factor (BAFF), which promotes their proliferation. On this basis, it has been proposed that B cell accumulation may underlie a progressive cycle of pro- inflammatory antigen presentation and production of pro-inflammatory markers linking B cells to CAVD. Thus, it might be hypothesized that increasing number of B cells within aortic valves could accelerate inflammation and increase the progression of aortic valve disease [118]. Our data are consistent with this model. Of interest, a very recent study has discovered that two antibodies naturally present in humans, in particular antibodies against the xenoantigens galactose-α1,3-galactose (αGal) and N-glycolylneuraminic acid (Neu5Gc), are responsible for triggering the immune response that causes the calcification and deterioration of heart implants of animal origin. These antibodies recognize molecules from the animal tissue of the valve as foreign and initiate an inflammatory response that ends up damaging the valve [129]. It would be of interest to investigate the epitope(s) against which are directed the immunoglobulins observed in the valves.

This is the first study which hints to the existence of a causal relationship between activation of B cells with pathological calcification. However, future work will be needed to assess whether the enhanced activation of humoral immunity reflects only increased inflammation in individuals with CHIP or whether there is a causal relationship with pathological calcification. In our study, calcific aortic valves removed by surgery display a remarkable heterogeneity. This is not unexpected, as several studies have pointed out that the phenotype of stenotic valve can vastly vary [130], as well as the features of immune infiltration [115]. In our study, while higher immunoglobulin levels were found more frequently in CHIP carriers, a relevant fraction of CHIP carriers showed immunoglobulin's levels comparable to non-CHIP. It must be considered that the presence of immunoglobulins in CAVD is not a peculiar feature of CHIP, as we have found that the calcific valves of non-CHIP carriers can also contain humoral immunity cells. Many reasons explain this scenario. One of the possible reasons could be that the activation of humoral immunity could be associated to other conditions, not necessarily with CHIP. Of interest, in this study we found also that survival after 12 months was lower in CHIP-

compared to non-CHIP carriers as. Prior to our study, another work reported the presence of CHIP in CAVD patients at the time of valve replacement determines a poor prognosis after successful TAVI [82] and that B cells in AV are associated to the gravity of the disease [118].

6. CONCLUSIONS AND FUTURE PERSPECTIVE

One of the challenges of the future of life sciences will be the revolution of medicine, now predominantly "curative" into P4 medicine: predictive, preventive, personalized and participatory. The medicine of the next decade will hopefully be revolutionized by the ability to "personalize" the health response, inextricably linked to omic approaches (proteomics, metabolomics, predictive genomics) related to disease susceptibility and to the study of individual response to therapeutic treatments (pharmacogenomics). This information will make disease care radically more cost effective by personalizing care to each person's unique biology and by treating the causes rather than the symptoms of disease. This project draws its basic reasons from these premises and focused on the identification of novels predictive markers aortic valve stenosis (AS).

In this study we identified COX-2, the Notch pathway and CHIP as players in the progression of the disease.

We found that COX-2 downregulation is associated to dystrophic calcification. It has been shown that most selective COX-2 inhibitors had adverse cardiovascular effects. Association between aspirin and aortic valve calcification has been reported [131] and there is evidence that warfarin accelerates calcification by affecting matrix GLA protein activation [132]. Of note, aortic stenosis is associated with gastrointestinal bleeding [133]; in principle, COX-2 inhibitors may be useful, as they have been developed for limiting gastrointestinal side effects, but they should be avoided if they exacerbate AV calcification. If additional studies will confirm the link between celecoxib use and the development or progression of CAVD, this could influence prescribing patterns for medications that relieve inflammatory pain and may be helpful to improve medical prescriptions.

We found that deregulation of Notch ligands could be present in AVICs of CAVD patients and suggest that the inhibition of Jagged1 may reduce calcification. In this scenario, targeting Notch ligands such as Jagged1 or Dll4, could offers the opportunity to selectively block specific components of the pathway important in disease progression. Our results, if confirmed in a larger study, could be translationally relevant since pharmacological Dll4 or Jagged1 inhibitors have been developed and are entering clinical trials for solid tumor [52 - 53].

Finally, the discovery of the possible involvement of chronic inflammation and humoral immunity in a relevant fraction of CHIP patients with CAVD may open new perspective for these patients. This inflammatory response resembles those involved in auto-immune diseases such as rheumatoid arthritis and lupus. For these pathologies anti-B cells drugs such as Inebilizumab, Ocrelizumab, Ofatumumab, Belimumab are used in clinical practice, while several others are under assessment in clinical trials [134]. Immunotherapy has already revolutionized the treatment of cancer and autoimmunity, and following the success of CANTOS, inflammation targeting has become a realistic goal in the treatment of CVD. Advances in the understanding the consequence of CHIP in CAVD, along with the advent of high-throughput genome sequencing approaches [135] are paving the way for a clinical use of CHIP in the evaluation of individual risk that in near future may lead to personalized immunotherapy for this disease.

Funding

Part of results of this work were supported by University of Ferrara through a grant “BANDO 2019 rivolto a giovani ricercatori dell’Università degli studi di Ferrara per il finanziamento di progetti di ricerca e mobilità internazionale (fondi 5 x 1000 2017)”.

Acknowledgements

I wish to gratefully acknowledge my academic Tutor Prof. Paola Rizzo for her invaluable supervision, support and tutelage during the course of my PhD degree and Prof. Antonio Pannuti, Dr. Francesco Vieceli Dalla Sega and Dr. Francesca Fortini for their mentorship and treasured support. My gratitude extends to the spin-off Genomix4Life S.r.l., of University of Salerno for helpful discussion and for performing Next Generation Sequencing analysis for CHIP investigation and RNA sequencing analyses. I also thank Prof. Anna Malashicheva, group Leader of Laboratory of Calcification Mechanisms, and the research team of Almazov National Medical Research Centre (Saint Petersubrg, Russia) for making possible to realize part of the results of this work.

Supplementary Table1: CHIP related variants characteristics

Sample	Chr	Start	End	Gene	Variant type	DNA change	Protein change	dbSNP ID	VarSome	VAF	DEPTH
ID80	chr17	7674212	7674212	TP53	nonsynonymous SNV	c.A751T	p.I251F	.	Likely Pathogenic	0.025	929
ID54	chr17	7674229	7674229	TP53	nonsynonymous SNV	c.G734A	p.G245D	rs121912656	Likely Pathogenic	0.021	430
ID113	chr17	7674962	7674962	TP53	nonsynonymous SNV	c.C569T	p.P190L	.	Likely Pathogenic	0.101	990
ID151	chr17	7675160	7675160	TP53	nonsynonymous SNV	c.C452G	p.P151R	.	Likely Pathogenic	0.044	291
ID18	chr17	31182783	31182783	NF1	nonsynonymous SNV	c.G586T	p.D196Y	rs2952999	Benign	0.327	99
ID44	chr17	31182783	31182783	NF1	nonsynonymous SNV	c.G586T	p.D196Y	rs2952999	Benign	0.344	193
ID130	chr17	31226459	31226459	NF1	frameshift insertion	c.2027dupC	p.I679Dfs*20	rs780157990	Pathogenic	0.331	80
ID55	chr17	31229457	31229457	NF1	nonsynonymous SNV	c.C2842A	p.Q948K	.	Uncertain Significance	0.02	333
ID158	chr17	31349207	31349207	NF1	frameshift deletion	c.7277delG	p.C2426Lfs*5	.	Pathogenic	0.145	361
ID111	chr2	25234323	25234323	DNMT3A	frameshift deletion	c.2695delC	p.R899Afs*6	.	Pathogenic	0.259	665
ID125	chr2	25234322	25234322	DNMT3A	nonsynonymous SNV	c.G2696A	p.R899H	.	Likely Pathogenic	0.065	894
ID160	chr2	25234373	25234373	DNMT3A	nonsynonymous SNV	c.G2645A	p.R882H	rs147001633	Pathogenic	0.021	335
ID61	chr2	25234373	25234373	DNMT3A	nonsynonymous SNV	c.G2645A	p.R882H	rs147001633	Pathogenic	0.188	488
ID19	chr2	25234374	25234374	DNMT3A	nonsynonymous SNV	c.C2644T	p.R882C	rs377577594	Pathogenic	0.201	685
ID56	chr2	25234374	25234374	DNMT3A	nonsynonymous SNV	c.C2644T	p.R882C	rs377577594	Pathogenic	0.049	734
ID76	chr2	25234374	25234374	DNMT3A	nonsynonymous SNV	c.C2644T	p.R882C	rs377577594	Pathogenic	0.2	431
ID20	chr2	25234386	25234386	DNMT3A	nonsynonymous SNV	c.T2632C	p.S878P	.	Likely Pathogenic	0.02	711
ID109	chr2	25235795	25235795	DNMT3A	frameshift deletion	c.2509delT	p.S837Qfs*3	.	Pathogenic	0.02	432
ID72	chr2	25236937	25236937	DNMT3A	nonsynonymous SNV	c.A2477G	p.K826R	rs770079872	Pathogenic	0.038	507
ID98	chr2	25236937	25236937	DNMT3A	nonsynonymous SNV	c.A2477C	p.K826T	.	Pathogenic	0.091	666
ID7	chr2	25239199	25239199	DNMT3A	nonsynonymous SNV	c.T2339C	p.I780T	rs370751539	Likely Pathogenic	0.232	505
ID98	chr2	25240306	25240306	DNMT3A	nonsynonymous SNV	c.T2318G	p.L773R	rs764303486	Likely Pathogenic	0.042	1026
ID76	chr2	25240397	25240397	DNMT3A	nonsynonymous SNV	c.C2227T	p.P743S	.	Likely Pathogenic	0.025	452
ID56	chr2	25240418	25240418	DNMT3A	nonsynonymous SNV	c.C2206T	p.R736C	rs761934754	Likely Pathogenic	0.038	889
ID148	chr2	25240420	25240420	DNMT3A	nonsynonymous SNV	c.A2204G	p.Y735C	rs147828672	Likely Pathogenic	0.06	262
ID18	chr2	25240431	25240431	DNMT3A	nonsynonymous SNV	c.C2193G	p.F731L	.	Likely Pathogenic	0.261	405
ID82	chr2	25241687	25241687	DNMT3A	nonsynonymous SNV	c.T1957G	p.L653V	.	Likely Pathogenic	0.346	848
ID161	chr2	25243933	25243933	DNMT3A	nonsynonymous SNV	c.T1901C	p.I634T	.	Likely Pathogenic	0.111	443
ID105	chr2	25243965	25243965	DNMT3A	stopgain	c.C1869G	p.Y623X	.	Pathogenic	0.127	853
ID42	chr2	25244338	25244338	DNMT3A	nonsynonymous SNV	c.G1668T	p.R556S	.	Pathogenic	0.046	428
ID111	chr2	25244580	25244580	DNMT3A	nonsynonymous SNV	c.G1627T	p.G543C	rs752222356	Likely Pathogenic	0.051	690
ID178	chr2	25244612	25244612	DNMT3A	nonsynonymous SNV	c.G1595A	p.G532D	.	Likely Pathogenic	0.192	881
ID178	chr2	25245290	25245290	DNMT3A	nonsynonymous SNV	c.A1517G	p.H506R	.	Likely Pathogenic	0.18	987
ID45	chr2	25246176	25246176	DNMT3A	frameshift deletion	c.1413delT	p.I471Mfs*179	.	Pathogenic	0.096	581
ID186	chr2	25246270	25246270	DNMT3A	stopgain	c.G1319A	p.W440X	rs773260349	Pathogenic	0.02	330
ID147	chr2	25247110	25247110	DNMT3A	frameshift deletion	c.1063delC	p.H355Tfs*51	.	Pathogenic	0.047	212

ID72	chr2	25247629	25247629	DNMT3A	nonsynonymous SNV	c.C976T	p.R326C	rs747448117	Uncertain Significance	0.161	547
ID15	chr2	25247715	25247715	DNMT3A	stopgain	c.G890A	p.W297X	.	Likely Pathogenic	0.042	397
ID133	chr20	32433542	32433558	ASXL1	frameshift deletion	c.1329_1345del	p.Y444fs*0	.	Uncertain Significance	0.048	650
ID116	chr20	32434435	32434435	ASXL1	stopgain	c.C1708T	p.Q570X	rs747847938	Pathogenic	0.027	807
ID10	chr20	32434600	32434622	ASXL1	frameshift deletion	c.1873_1895del	p.E630Rfs*13	rs766433101	Pathogenic	0.044	671
ID169	chr20	32434600	32434622	ASXL1	frameshift deletion	c.1873_1895del	p.E630Rfs*13	rs766433101	Pathogenic	0.032	616
ID96	chr20	32435579	32435579	ASXL1	frameshift deletion	c.2852delT	p.T952Lfs*26	.	Likely Pathogenic	0.08	1160
ID109	chr4	105234654	105234654	TET2	frameshift insertion	c.713dupT	p.S239Ffs*14	.	Pathogenic	0.046	556
ID110	chr4	105234654	105234654	TET2	frameshift insertion	c.713dupT	p.S239Ffs*14	.	Pathogenic	0.045	1106
ID18	chr4	105235163	105235163	TET2	frameshift insertion	c.1222dupC	p.P410Sfs*32	.	Likely Pathogenic	0.051	351
ID44	chr4	105235626	105235626	TET2	frameshift deletion	c.1684delC	p.P562Qfs*5	.	Pathogenic	0.02	664
ID77	chr4	105235713	105235713	TET2	stopgain	c.C1771T	p.Q591X	.	Pathogenic	0.219	746
ID166	chr4	105236095	105236095	TET2	frameshift deletion	c.2153delT	p.L719Cfs*31	.	Pathogenic	0.149	517
ID108	chr4	105236166	105236166	TET2	stopgain	c.C2224T	p.Q742X	.	Pathogenic	0.024	461
ID18	chr4	105236464	105236464	TET2	frameshift deletion	c.2522delT	p.S842Qfs*30	.	Likely Pathogenic	0.043	308
ID18	chr4	105236568	105236568	TET2	stopgain	c.C2626T	p.Q876X	rs781668759	Pathogenic	0.045	694
ID164	chr4	105237290	105237290	TET2	frameshift deletion	c.3348delA	p.N1118Ifs*18	.	Pathogenic	0.058	744
ID11	chr4	105242912	105242912	TET2	stopgain	c.T3579A	p.C1193X	.	Pathogenic	0.1	288
ID22	chr4	105242914	105242914	TET2	nonsynonymous SNV	c.C3581G	p.P1194R	.	Likely Pathogenic	0.145	415
ID61	chr4	105243714	105243714	TET2	stopgain	c.G3739T	p.E1247X	.	Pathogenic	0.026	506
ID98	chr4	105259626	105259626	TET2	frameshift insertion	c.3812dupG	p.C1271Wfs*28	rs755283040	Pathogenic	0.107	949
ID95	chr4	105259665	105259665	TET2	nonsynonymous SNV	c.T3850G	p.S1284A	.	Uncertain Significance	0.058	961
ID95	chr4	105259669	105259669	TET2	nonsynonymous SNV	c.T3854C	p.F1285S	.	Uncertain Significance	0.056	956
ID66	chr4	105259723	105259723	TET2	nonsynonymous SNV	c.G3908T	p.S1303I	.	Likely Pathogenic	0.032	922
ID85	chr4	105261774	105261775	TET2	frameshift deletion	c.3970_3971del	p.H1325Ffs*11	.	Pathogenic	0.028	412
ID113	chr4	105272571	105272571	TET2	nonsynonymous SNV	c.C4190T	p.T1397I	.	Likely Pathogenic	0.02	689
ID166	chr4	105272597	105272597	TET2	frameshift deletion	c.4216delT	p.F1406Lfs*41	.	Pathogenic	0.049	435
ID81	chr4	105272811	105272811	TET2	frameshift deletion	c.4430delA	p.K1478Sfs*92	.	Pathogenic	0.098	488
ID94	chr4	105275347	105275347	TET2	nonsynonymous SNV	c.A4837G	p.N1613D	.	Likely Pathogenic	0.025	1047
ID166	chr4	105276064	105276064	TET2	stopgain	c.C5554T	p.Q1852X	rs549395077	Uncertain Significance	0.083	627
ID21	chr4	105276203	105276203	TET2	nonsynonymous SNV	c.C5693T	p.S1898F	rs767475870	Likely Pathogenic	0.028	852
ID11	chr9	5069037	5069037	JAK2	stopgain	c.G1342T	p.E448X	.	Pathogenic	0.022	221
ID107	chr9	5073770	5073770	JAK2	nonsynonymous SNV	c.G1849T	p.V617F	rs77375493	Pathogenic	0.042	327
ID165	chr9	5073770	5073770	JAK2	nonsynonymous SNV	c.G1849T	p.V617F	rs77375493	Pathogenic	0.029	382
ID166	chr9	5073770	5073770	JAK2	nonsynonymous SNV	c.G1849T	p.V617F	rs77375493	Pathogenic	0.021	418
ID98	chr9	5073770	5073770	JAK2	nonsynonymous SNV	c.G1849T	p.V617F	rs77375493	Pathogenic	0.146	591
ID82	chr9	136500721	136500721	NOTCH1	nonsynonymous SNV	c.A5765G	p.N1922S	rs765708087	Benign	0.025	885
ID11	chrX	45062653	45062653	KDM6A	stopgain	c.G1432T	p.E478X	.	Uncertain Significance	0.021	331
ID22	chrX	45090729	45090729	KDM6A	nonsynonymous SNV	c.A3743G	p.Q1248R	.	Uncertain Significance	0.028	446

Supplementary Table1: CHIP related variants characteristics. For each variant, from left to right, the sample name, the genomic coordinate (chromosome, start, end and gene name), the variant type, the substitution effect (on DNA and on protein), the dbSNP ID (when available), the VarSome clinical classification, the Variant Allele Frequency, and the coverage are reported.

Supplementary Table 2: Baseline characteristics, echocardiographic and laboratory parameters in patients with and without CHIP							
	TOTAL MEAN	**TOTAL SD**	**No-CHIP MEAN (117)**	**No-CHIP SD**	**CHIP MEAN (51)**	**CHIP SD**	**P-value**
Age (168)	79.18	5.21	78.44	5.33	80.86	4.54	**0.007**
Weight kg (168)	72.49	12.02	72.91	12.15	71.55	11.78	0.485
Height cm (168)	163.98	8.47	164.31	8.20	163.24	9.11	0.382
BMI kg m2 (168)	26.92	3.87	26.96	3.87	26.84	3.90	0.687
SEX (F-M) (168)	87 (51.7%)-81		57 (48.7%)-60		30 (58.8%)-21		0.246
AVR Type (SAVR-TAVR) (168)	112 (72.6%)-56		83 (70.9%)-34		29 (56.8%)-22		0.101
Hypertension (YES-NO) (168)	139 (82.7%)-29		97 (82.9%)-20		42 (82.3%)-9		1
Dyslipidemia (YES-NO) (168)	117 (69.6%)-51		77 (65.8%)-40		40 (78.4%)-11		0.147
Type 2 Diabetes mellitus (YES-NO) (165)	43 (26%)-122		31 (26.9%)-84		12 (24%)-38		0.692
Atrial fibrillation (YES-NO) (168)	42 (25%)-126		30 (25.6%)-87		12 (23.5%)-39		0.853
Peripheral artery disease (YES-NO) (167)	34 (20.3%)-133		20 (17.2%)-96		14 (27.4%)-37		0.143
COPD (YES-NO) (168)	22 (13%)-146		13 (11.1%)-104		9 (17.6%)-42		0.338
Prior MI (YES-NO) (167)	19 (11.3%)-148		14 (11.9%)-103		5 (10%)-45		0.791
Smoking history (YES-NO) (168)	46 (27.3%)-122		33 (28.2%)-84		13 (25.4%)-38		0.864
Coronary Artery Disease (YES-NO) (168)	72 (42.8%)-96		47 (40.1%)-70		25 (49%)-26		0.312
ANGINA CLASS (>3 YES-NO) (152)	11 (7.2%)-141		6 (5.6%)-100		5 (10.8%)-41		0.304
NYHA III+IV (YES-NO) (151)	44 (29.1%)-107		28 (26.4%)-78		16 (35.5%)-29		0.330
Echocardiographic characteristics							
LV EF (167)	59.15	10.85	59.41	10.90	58.57	10.81	0.414
LV mass g (106)	131.67	111.68	119.36	110.23	165.94	110.46	0.066

Mean aortic gradient mmHg (167)	45.94	12.69	45.75	12.10	46.38	14.10	0.842
Functional AVA cm2 (127)	0.74	0.21	0.75	0.22	0.72	0.17	0.607
Mitral regurgitation (>3+ YES-NO) (164)	16 (9.7%)-148		8 (7%)-106		8 (16%)-42		0.088
Tricuspid regurgitation (>3+ YES-NO) (123)	5 (4%)-118		3 (3.5%)-82		2 (5.2%)-36		1
Aortic regurgitation (>3+ YES-NO) (166)	15 (9%)-151		10 (8.7%)-105		5 (9.8%)-46		1
Laboratory							
White blood count (167)	7.66	2.30	7.54	2.29	7.91	2.33	0.160
Neutrophils (167)	5.68	5.78	5.19	2.23	6.80	9.87	0.165
Lymphocytes (167)	1.65	1.26	1.55	0.56	1.89	2.11	0.745
Monocytes (167)	0.66	0.65	0.61	0.22	0.78	1.13	0.924
Eosinophils (167)	0.17	0.18	0.16	0.18	0.18	0.19	0.508
Basophils (167)	0.03	0.05	0.02	0.04	0.05	0.07	0.064
Hemoglobin g dl (168)	12.84	1.58	13.01	1.48	12.46	1.73	**0.014**
Platelets (168)	216.45	71.87	220.84	70.01	206.37	75.72	0.168
Creatinine mg dl (168)	1.07	0.41	1.05	0.43	1.12	0.37	0.100
Crockoft-gault eGFR ml min (>60 YES-NO) (168)	86 (51.2%)-82		66 (56.4%)-51		20 (39.2%)-31		0.060
Total cholesterol mg dl (165)	163.16	34.10	166.28	35.13	155.56	30.47	0.054
Triglycerides mg dl (165)	113.21	52.45	116.88	56.73	104.25	39.24	0.300
HDL mg dl (163)	51.05	14.55	52.16	15.55	48.40	11.53	0.172
Albumin g dl (158)	4.03	0.36	4.06	0.37	3.96	0.35	0.116
LDL (162)	89.90	27.69	91.41	29.03	86.32	24.11	0.427

Supplementary Table 2: Baseline characteristics, echocardiographic and laboratory parameters in patients with and without CHIP. Each column displays the mean or the standard deviation (SD) for the continuous variables of both groups (Total), the No-CHIP or the CHIP samples. For dichotomous variables, the total number of each variable and the percentage of the first one are reported. In the last column, the resulting p-value for each No-CHIP vs CHIP test is shown and the significant ones are written in bold.

Supplementary Table 3: RNA-Seq sequencing statistics			
Sample	**Group**	**Mapped reads**	**Percentage of aligned reads**
ID45	CHIP	22263482	85.65%
ID72	CHIP	4588989	73.61%
ID76	CHIP	9612871	78.23%
ID111	CHIP	13853335	80.12%
ID125	CHIP	9749336	82.60%

ID161	CHIP	6485491	79.55%
ID186	CHIP	8934923	82.52%
ID66	CHIP	6572496	67.85%
ID85	CHIP	11921087	78.98%
ID109	CHIP	8357765	82.28%
ID110	CHIP	12731921	84.57%
ID64	No-CHIP	9704635	79.41%
ID65	No-CHIP	8105644	80.96%
ID87	No-CHIP	11159153	83.91%
ID91	No-CHIP	9247704	74.47%
ID145	No-CHIP	20625906	83.86%
ID173	No-CHIP	6849705	79.44%
ID218	No-CHIP	9828418	86.24%
ID275	No-CHIP	11616654	84.52%
ID179	Control	7447958	87.39%
ID190	Control	6894232	78.60%
ID205	Control	18096943	85.88%
ID259	Control	8220733	84.32%
ID278	Control	11419798	85.84%

Supplementary Table 3: RNA-Seq sequencing statistics. The number of mapped reads and percentage of aligned reads are shown for each sample in each group.

Supplementary Table 4: Baseline characteristics, echocardiographic and laboratory parameters in patients with and without CHIP for RNA-Seq analysis

	TOTAL MEAN	**TOTAL SD**	**No-CHIP MEAN (8)**	**No-CHIP SD**	**CHIP MEAN (11)**	**CHIP SD**	**P-value**
Age (19)	78.16	3.92	76.50	4.11	79.36	3.47	0.097
Weight kg (19)	69.32	9.68	65.88	9.91	71.82	9.15	0.246
Height cm (19)	163.89	6.93	161.88	8.20	165.36	5.80	0.262
BMI kg m2 (19)	25.79	3.40	25.06	2.90	26.33	3.76	0.386
SEX (F-M) (19)	11 (57.8%)-8		6 (75%)-2		5 (45.4%)-6		0.340
AVR Type (SAVR-TAVR) (19)	19 (100%)-		8 (100%)-		11 (100%)-		NaN
Hypertension (YES-NO) (19)	17 (89.4%)-2		8 (100%)-		9 (81.8%)-2		NaN
Dyslipidemia (YES-NO) (19)	14 (73.6%)-5		6 (75%)-2		8 (72.7%)-3		1
Type 2 Diabetes mellitus (YES-NO) (19)	3 (15.7%)-16		1 (12.5%)-7		2 (18.1%)-9		1
Atrial fibrillation (YES-NO) (19)	1 (5.2%)-18		1 (12.5%)-7		-11 (100%)		NaN
Peripheral artery disease (YES-NO) (19)	3 (15.7%)-16		1 (12.5%)-7		2 (18.1%)-9		1
COPD (YES-NO) (19)	-19 (100%)		-8 (100%)		-11 (100%)		NaN

Prior MI (YES-NO) (18)	2 (11.1%)-16		1 (12.5%)-7		1 (10%)-9		1
Smoking history (YES-NO) (19)	7 (36.8%)-12		3 (37.5%)-5		4 (36.3%)-7		1
Coronary Artery Disease (YES-NO) (19)	6 (31.5%)-13		2 (25%)-6		4 (36.3%)-7		0.640
ANGINA CLASS (>3 YES-NO) (19)	1 (5.2%)-18		-8 (100%)		1 (9%)-10		NaN
NYHA III+IV (YES-NO) (19)	3 (15.7%)-16		1 (12.5%)-7		2 (18.1%)-9		1
Echocardiographic characteristics							
LV EF (19)	62.80	8.68	65.40	8.62	60.90	8.61	0.177
LV mass g (18)	153.83	115.04	154.54	106.86	153.38	125.08	0.928
Mean aortic gradient mmHg (19)	44.68	13.06	43.88	10.43	45.27	15.17	0.804
Functional AVA cm2 (14)	0.73	0.22	0.74	0.35	0.72	0.12	0.787
Mitral regurgitation (>3+ YES-NO) (19)	2 (10.5%)-17		1 (12.5%)-7		1 (9%)-10		1
Tricuspid regurgitation (>3+ YES-NO) (18)	-18 (100%)		-8 (100%)		-10 (100%)		NaN
Aortic regurgitation (>3+ YES-NO) (19)	-19 (100%)		-8 (100%)		-11 (100%)		NaN
Laboratory							
White blood count (19)	7.78	1.81	6.88	1.62	8.44	1.71	0.052
Neutrophils (19)	5.40	1.68	4.51	1.70	6.05	1.41	0.090
Lymphocytes (19)	1.59	0.48	1.64	0.35	1.55	0.56	0.707
Monocytes (19)	0.59	0.17	0.56	0.22	0.61	0.14	0.401
Eosinophils (19)	0.17	0.12	0.13	0.05	0.21	0.14	0.089
Basophils (19)	0.05	0.05	0.05	0.05	0.05	0.05	0.623
Hemoglobin g dl (19)	12.81	1.20	13.01	1.53	12.65	0.94	0.649
Platelets (19)	230.47	54.29	240.13	57.13	223.45	53.78	0.741
Creatinine mg dl (19)	0.91	0.33	0.79	0.24	1.01	0.36	0.152
Crockoft-gault eGFR ml min (>60 YES-NO) (19)	12 (63%)-7		6 (75%)-2		6 (54.5%)-5		0.667
Total cholesterol mg dl (19)	169.53	165.55	175.00	20.89	165.55	26.86	0.492
Triglycerides mg dl (19)	100.21	104.45	94.38	35.86	104.45	23.51	0.492
HDL mg dl (19)	53.11	51.00	56.00	10.54	51.00	16.91	0.247
Albumin g dl (17)	4.19	4.11	4.30	0.12	4.11	0.19	**0.042**
LDL (19)	96.38	93.65	100.13	23.20	93.65	18.37	0.442

Supplementary Table 4: Baseline characteristics, echocardiographic and laboratory parameters in patients with and without CHIP for RNA-Seq analysis. Each column displays the mean or the

standard deviation (SD) for the continuous variables of both groups (Total), the No-CHIP or the CHIP samples. For dichotomous variables, the total number of each variable and the percentage of the first one are reported. In the last column, the resulting p-value for each No-CHIP vs CHIP test is shown and the significant ones are written in bold.

Supplementary Table 5: Differentially Expressed Genes in No-CHIP vs Control contrast							
Genes	**baseMean**	**log2FoldChange**	**lfcSE**	**stat**	**pvalue**	**padj**	**FoldChange**
ISG15	172.46	0.97	0.26	3.70	0.00021	0.01002	1.96
AGRN	228.09	0.60	0.20	3.10	0.00192	0.03996	1.52
FNDC10	13.67	1.48	0.40	3.75	0.00018	0.00914	2.79
KCNAB2	138.62	1.02	0.25	4.12	3.75E-05	0.00321	2.03
SLC2A5	31.71	2.67	0.49	5.42	5.85E-08	3.13E-05	6.36
PDPN	83.54	1.85	0.40	4.66	3.18E-06	0.00058	3.62
TMEM51	31.71	0.86	0.28	3.08	0.00205	0.04114	1.81
PLA2G2D	11.20	5.09	1.39	3.66	0.00025	0.01123	34.16
C1QA	1673.90	0.87	0.24	3.62	0.00029	0.01191	1.83
C1QC	1087.01	0.94	0.28	3.37	0.00076	0.02278	1.92
C1QB	1534.44	0.85	0.25	3.37	0.00074	0.02227	1.81
MYOM3	65.13	0.85	0.26	3.31	0.00092	0.02562	1.81
RUNX3	16.45	1.64	0.54	3.01	0.0026	0.04841	3.11
CD52	42.60	1.67	0.52	3.25	0.00115	0.0294	3.19
RPS6KA1	100.06	0.83	0.28	3.00	0.00272	0.04949	1.78
IFI6	385.85	1.12	0.26	4.24	2.22E-05	0.00224	2.18
PTAFR	112.13	1.06	0.25	4.24	2.27E-05	0.00225	2.08
LAPTM5	883.56	1.37	0.32	4.23	2.30E-05	0.00227	2.58
LCK	30.72	1.79	0.52	3.43	0.00061	0.01963	3.46
COL8A2	594.11	0.68	0.19	3.56	0.00037	0.01387	1.61
BMP8A	27.62	1.85	0.60	3.08	0.00204	0.04105	3.61
HIVEP3	71.40	0.84	0.23	3.62	0.00029	0.01191	1.79
AL603840.1	9.44	-1.59	0.41	-3.90	9.60E-05	0.00612	-3.01
CACHD1	257.76	-0.72	0.15	-4.86	1.18E-06	0.00028	-1.65
IL12RB2	59.89	1.28	0.31	4.18	2.96E-05	0.00273	2.43
COL24A1	79.95	1.26	0.29	4.28	1.88E-05	0.00203	2.40
LMO4	564.34	-0.73	0.17	-4.31	1.67E-05	0.00192	-1.66
GBP5	82.45	1.64	0.37	4.41	1.03E-05	0.0014	3.12
TGFBR3	584.39	-0.77	0.11	-6.91	4.69E-12	1.25E-08	-1.71
F3	70.17	2.02	0.41	4.98	6.49E-07	0.00018	4.05
SLC44A3-AS1	38.35	1.95	0.36	5.38	7.27E-08	3.41E-05	3.86
SLC44A3	24.97	2.05	0.32	6.30	2.94E-10	4.64E-07	4.13
TLCD4	281.99	-1.27	0.34	-3.74	0.00018	0.00922	-2.42
GPR88	36.87	2.19	0.40	5.46	4.74E-08	2.68E-05	4.57

VCAM1	820.58	2.08	0.31	6.71	2.01E-11	3.87E-08	4.23
COL11A1	215.25	6.18	0.90	6.87	6.49E-12	1.39E-08	72.59
CSF1	469.49	0.59	0.19	3.05	0.0023	0.04451	1.50
KCNA2	20.82	-1.17	0.37	-3.13	0.00176	0.03826	-2.25
CD53	266.38	0.90	0.24	3.68	0.00024	0.01076	1.87
C1orf162	99.39	0.77	0.26	2.99	0.00275	0.04983	1.70
TMIGD3	15.52	2.00	0.49	4.05	5.06E-05	0.00389	3.99
PTPN22	87.58	1.14	0.21	5.41	6.25E-08	3.16E-05	2.21
TSPAN2	48.70	1.28	0.24	5.35	8.71E-08	3.81E-05	2.42
CD2	38.94	1.37	0.42	3.22	0.00129	0.03148	2.58
TBX15	105.65	0.61	0.20	3.01	0.00263	0.0486	1.52
PHGDH	101.83	-0.96	0.22	-4.35	1.34E-05	0.00168	-1.94
FCGR1B	28.96	1.49	0.35	4.29	1.79E-05	0.00197	2.81
FCGR1CP	22.72	1.22	0.38	3.17	0.00153	0.03454	2.33
FCGR1A	102.24	1.99	0.42	4.71	2.48E-06	0.00049	3.96
SV2A	87.96	-0.65	0.18	-3.66	0.00026	0.01136	-1.56
CTSS	619.80	0.83	0.27	3.13	0.00174	0.03788	1.78
SELENBP1	316.39	-0.87	0.19	-4.49	6.97E-06	0.00107	-1.82
TCHH	7.18	1.66	0.54	3.06	0.00224	0.04384	3.16
SH2D2A	7.46	1.87	0.60	3.12	0.00183	0.03884	3.65
PYHIN1	11.08	1.91	0.59	3.24	0.00118	0.03003	3.76
FCRL6	3.66	3.92	1.06	3.70	0.00021	0.01005	15.14
SLAMF8	113.01	2.22	0.42	5.29	1.24E-07	4.95E-05	4.67
SLAMF6	20.15	1.99	0.50	3.98	6.82E-05	0.00486	3.98
CD84	389.53	1.10	0.23	4.84	1.31E-06	0.0003	2.14
SLAMF1	10.79	1.97	0.59	3.35	0.00081	0.02385	3.92
CD48	31.08	1.69	0.46	3.69	0.00023	0.01049	3.23
ARHGAP30	183.70	0.84	0.25	3.42	0.00062	0.01977	1.79
NECTIN4	17.84	1.32	0.39	3.38	0.00072	0.02177	2.49
FCGR2A	998.86	1.06	0.25	4.29	1.78E-05	0.00197	2.09
FCGR3A	576.91	1.47	0.37	3.92	8.98E-05	0.00586	2.76
OLFML2B	617.79	0.73	0.23	3.24	0.00118	0.03003	1.66
ILDR2	20.44	2.28	0.41	5.63	1.79E-08	1.11E-05	4.87
STYXL2	17.16	1.17	0.37	3.12	0.0018	0.03849	2.25
MYOC	124.51	-1.55	0.52	-3.01	0.00265	0.04866	-2.93
TNFSF18	5.59	3.43	0.83	4.13	3.70E-05	0.00319	10.81
TNN	8.53	2.46	0.61	4.02	5.77E-05	0.00424	5.51
TNR	20.12	2.77	0.54	5.17	2.31E-07	8.07E-05	6.83
AL365357.1	16.26	4.23	1.12	3.79	0.00015	0.00825	18.75
NPL	155.10	0.93	0.22	4.25	2.12E-05	0.0022	1.91
PRG4	679.76	3.35	0.35	9.54	1.47E-21	2.82E-17	10.19
PACERR	8.96	-1.12	0.34	-3.27	0.00109	0.02834	-2.17
PLA2G4A	219.25	-0.88	0.22	-4.04	5.37E-05	0.00408	-1.84
RGS13	6.81	2.74	0.61	4.49	7.01E-06	0.00107	6.68
PTPRC	677.15	0.78	0.25	3.18	0.00146	0.03384	1.72

PTPN7	29.21	1.75	0.51	3.42	0.00063	0.02007	3.37
BTG2	968.96	-0.83	0.25	-3.28	0.00103	0.02748	-1.78
LRRN2	12.51	2.23	0.53	4.18	2.95E-05	0.00273	4.69
RHEX	4.83	3.23	1.03	3.12	0.00181	0.03856	9.37
IKBKE	49.47	0.93	0.27	3.39	0.0007	0.02152	1.91
AL591846.1	12.81	5.04	1.46	3.45	0.00057	0.01874	32.98
FCMR	14.53	2.20	0.71	3.09	0.00198	0.04031	4.59
CR1	213.23	1.76	0.49	3.56	0.00038	0.01406	3.38
G0S2	81.50	-0.95	0.31	-3.04	0.00237	0.04561	-1.93
IRF6	186.81	-1.13	0.22	-5.21	1.90E-07	7.18E-05	-2.19
KCNK2	11.81	3.53	1.01	3.48	0.0005	0.01702	11.51
DNAH14	21.34	1.16	0.35	3.31	0.00092	0.02562	2.24
SIPA1L2	204.91	0.68	0.20	3.42	0.00064	0.02027	1.60
ACTN2	116.14	-0.68	0.22	-3.02	0.00256	0.04773	-1.60
RYR2	369.89	-0.86	0.28	-3.12	0.00179	0.03849	-1.82
MATN3	16.85	1.44	0.46	3.12	0.0018	0.03851	2.71
SDC1	42.23	2.27	0.65	3.51	0.00046	0.01615	4.83
CGREF1	90.99	1.06	0.29	3.71	0.00021	0.00995	2.08
PLB1	105.33	0.76	0.22	3.39	0.0007	0.02142	1.69
LBH	475.46	0.83	0.24	3.46	0.00054	0.01804	1.78
FSHR	10.37	-1.49	0.39	-3.77	0.00016	0.00852	-2.80
EFEMP1	8320.29	0.64	0.18	3.56	0.00037	0.014	1.55
AC092155.1	3.49	-2.50	0.69	-3.65	0.00027	0.01149	-5.66
PLEK	287.04	1.05	0.27	3.82	0.00014	0.00772	2.07
ARHGAP25	99.20	0.78	0.21	3.73	0.00019	0.00944	1.71
PAIP2B	77.77	-1.04	0.26	-3.92	8.76E-05	0.00579	-2.05
CAPG	330.58	1.49	0.34	4.36	1.32E-05	0.00167	2.81
ST3GAL5	195.32	-0.81	0.26	-3.14	0.00168	0.03693	-1.75
CD8A	17.63	2.18	0.62	3.49	0.00048	0.01679	4.54
IGKC	5923.50	3.58	1.10	3.26	0.00113	0.02889	11.94
IGKV1-5	194.32	4.09	1.32	3.10	0.00195	0.04015	17.01
IGKV3-11	340.37	4.48	1.34	3.34	0.00083	0.02405	22.32
IGKV3-15	55.92	4.95	1.65	3.01	0.00262	0.04848	31.01
IGKV1-16	12.67	5.67	1.57	3.62	0.00029	0.01193	51.04
FAHD2B	36.81	-0.70	0.21	-3.32	0.0009	0.0253	-1.62
ZAP70	35.17	1.59	0.45	3.51	0.00044	0.01583	3.00
SLC20A1	709.97	1.04	0.18	5.93	3.12E-09	2.86E-06	2.06
IL1RN	23.14	3.58	0.92	3.88	0.00011	0.00646	11.95
STEAP3	348.65	0.76	0.25	3.07	0.00216	0.04273	1.69
ARHGAP15	66.97	0.91	0.24	3.72	0.0002	0.00982	1.87
CACNB4	133.42	1.00	0.26	3.80	0.00014	0.00801	2.00
DPP4	41.60	1.88	0.43	4.41	1.03E-05	0.0014	3.69
FAP	603.10	1.12	0.31	3.61	0.0003	0.0122	2.18
GALNT3	33.51	3.03	0.52	5.79	7.06E-09	5.66E-06	8.17
SCN7A	238.79	-1.56	0.50	-3.13	0.00174	0.03788	-2.95

AC010680.1	8.64	-1.19	0.38	-3.12	0.0018	0.03849	-2.29
ITGA4	277.86	0.80	0.22	3.68	0.00023	0.01069	1.74
FAM171B	226.18	-0.63	0.20	-3.10	0.0019	0.03982	-1.55
GULP1	173.24	-0.73	0.20	-3.71	0.00021	0.00993	-1.66
COL5A2	3853.40	0.80	0.27	3.03	0.00246	0.04663	1.75
C2orf88	71.44	-1.13	0.35	-3.18	0.00148	0.03393	-2.18
STAT1	1131.03	0.63	0.17	3.65	0.00026	0.01142	1.55
SATB2	75.48	1.01	0.22	4.62	3.82E-06	0.00067	2.01
AOX1	262.80	-0.59	0.18	-3.32	0.00089	0.02512	-1.50
CD28	176.21	1.57	0.27	5.90	3.58E-09	3.13E-06	2.96
NRP2	571.68	0.71	0.17	4.10	4.22E-05	0.00353	1.64
ACADL	72.02	-0.64	0.19	-3.40	0.00068	0.0212	-1.56
FN1	102162.74	1.49	0.25	6.03	1.61E-09	1.72E-06	2.82
IGFBP2	489.70	2.42	0.47	5.14	2.68E-07	8.87E-05	5.35
IGFBP5	10402.36	-0.80	0.23	-3.45	0.00056	0.01866	-1.74
SLC11A1	117.04	1.69	0.56	3.02	0.00255	0.0476	3.22
PRKAG3	11.38	1.64	0.47	3.47	0.00052	0.01753	3.11
SGPP2	7.47	2.50	0.64	3.93	8.43E-05	0.00563	5.66
SCG2	305.64	1.94	0.36	5.44	5.23E-08	2.88E-05	3.84
DOCK10	302.32	0.88	0.26	3.39	0.00069	0.02122	1.85
IRS1	267.35	-0.65	0.15	-4.25	2.17E-05	0.00222	-1.57
SLC19A3	15.83	-1.11	0.31	-3.64	0.00027	0.01156	-2.17
NGEF	129.11	1.01	0.31	3.24	0.00119	0.03003	2.01
INPP5D	221.44	0.97	0.25	3.90	9.51E-05	0.00608	1.96
ARL4C	235.14	0.73	0.23	3.20	0.00136	0.0327	1.66
AC112721.2	3.23	3.63	1.14	3.20	0.00138	0.03302	12.39
RNPEPL1	220.57	0.59	0.19	3.19	0.00143	0.03358	1.51
KIF1A	36.94	-1.19	0.38	-3.14	0.00167	0.03683	-2.29
SNED1	976.69	0.80	0.22	3.55	0.00039	0.01434	1.74
LRRN1	30.33	0.90	0.27	3.35	0.00082	0.02394	1.87
LMCD1-AS1	15.79	-1.04	0.32	-3.29	0.00102	0.02716	-2.06
HRH1	214.21	0.71	0.19	3.73	0.00019	0.00944	1.64
ZNF385D	89.00	0.81	0.22	3.62	0.0003	0.01214	1.75
MYD88	110.12	0.97	0.32	3.07	0.00212	0.0422	1.96
VIPR1	105.02	-1.13	0.37	-3.01	0.00263	0.0486	-2.18
CDCP1	54.47	1.47	0.38	3.82	0.00013	0.00766	2.76
SLC6A20	17.17	-1.73	0.53	-3.29	0.00099	0.02672	-3.32
CCR1	169.22	1.30	0.29	4.46	8.25E-06	0.00118	2.46
STAB1	4669.38	0.71	0.21	3.37	0.00074	0.02227	1.63
ITIH3	52.07	1.49	0.47	3.17	0.00151	0.03426	2.80
PRKCD	92.03	0.69	0.20	3.52	0.00043	0.01545	1.62
AC115282.2	4.93	-2.41	0.78	-3.10	0.00194	0.04004	-5.32
CACNA2D3	28.87	-0.79	0.25	-3.18	0.00148	0.03393	-1.73
CFAP20DC	15.46	-0.99	0.32	-3.10	0.00192	0.03996	-1.98
CADM2	118.57	-1.38	0.36	-3.82	0.00014	0.00772	-2.60

COL8A1	2195.58	1.02	0.24	4.28	1.86E-05	0.00203	2.03
CD96	31.71	1.98	0.53	3.71	0.00021	0.00993	3.94
CCDC80	7267.24	0.98	0.26	3.81	0.00014	0.00774	1.97
AC026341.3	18.32	1.60	0.50	3.18	0.00146	0.03384	3.04
GAP43	239.80	0.93	0.29	3.16	0.00159	0.0357	1.90
CFAP91	35.57	-0.89	0.30	-2.99	0.00276	0.04992	-1.85
AC092910.3	15.09	-1.10	0.33	-3.29	0.00101	0.027	-2.15
STXBP5L	86.00	-1.50	0.34	-4.44	9.04E-06	0.00128	-2.83
CD86	95.83	0.99	0.27	3.71	0.0002	0.00989	1.99
PARP15	51.79	1.39	0.35	3.95	7.90E-05	0.00533	2.62
COL6A6	466.87	-1.47	0.48	-3.09	0.00203	0.04091	-2.77
TF	225.25	-1.69	0.51	-3.29	0.00099	0.02672	-3.22
AC010207.1	6.17	-1.76	0.55	-3.20	0.00139	0.03308	-3.38
RBP1	85.43	-1.00	0.22	-4.48	7.63E-06	0.00113	-2.00
CLSTN2	506.91	-1.70	0.33	-5.12	3.07E-07	9.54E-05	-3.25
CPA3	62.86	2.25	0.60	3.78	0.00016	0.0084	4.76
IGSF10	484.01	-1.66	0.42	-3.92	8.89E-05	0.00584	-3.15
SUCNR1	22.57	1.12	0.35	3.24	0.00121	0.03025	2.17
P2RY1	158.05	-0.86	0.22	-3.88	0.00011	0.00647	-1.81
PLCH1	130.11	-1.91	0.34	-5.57	2.58E-08	1.55E-05	-3.75
SHOX2	6.55	1.96	0.51	3.88	0.0001	0.00645	3.89
AC080013.1	85.68	-0.92	0.28	-3.31	0.00094	0.02592	-1.90
PPM1L	363.69	-0.63	0.15	-4.25	2.17E-05	0.00222	-1.55
CLDN11	328.08	-0.95	0.18	-5.35	8.58E-08	3.81E-05	-1.93
SLC7A14-AS1	29.85	-1.06	0.33	-3.26	0.0011	0.02855	-2.09
TNFSF10	327.91	0.73	0.22	3.26	0.00113	0.02903	1.66
NLGN1	41.98	-0.93	0.25	-3.73	0.00019	0.00944	-1.91
AC117453.1	23.29	2.48	0.54	4.58	4.56E-06	0.00075	5.57
KLHL6	78.65	1.23	0.33	3.66	0.00025	0.01117	2.34
AC007920.2	19.47	-1.18	0.26	-4.51	6.54E-06	0.00102	-2.27
BCL6	632.78	-0.72	0.16	-4.57	4.98E-06	0.00079	-1.65
TPRG1	165.27	-0.77	0.21	-3.61	0.00031	0.0123	-1.71
LRRC15	203.65	3.28	0.69	4.75	2.00E-06	0.00042	9.73
ZNF595	104.08	-0.63	0.20	-3.09	0.00203	0.04094	-1.54
LAP3	452.02	0.71	0.21	3.40	0.00068	0.0212	1.64
LGI2	121.67	0.68	0.22	3.06	0.00223	0.04374	1.60
DTHD1	4.68	2.87	0.89	3.23	0.00122	0.03043	7.32
ATP8A1	431.58	-1.19	0.25	-4.73	2.25E-06	0.00046	-2.28
LNX1	79.00	0.79	0.23	3.52	0.00043	0.0155	1.73
KIT	62.92	1.83	0.40	4.60	4.22E-06	0.00071	3.54
JCHAIN	649.09	3.44	1.10	3.12	0.00179	0.03849	10.89
CXCL5	24.13	5.63	1.20	4.71	2.49E-06	0.00049	49.65
CXCL3	5.66	2.02	0.64	3.16	0.00159	0.0357	4.06
BTC	37.68	-0.93	0.29	-3.24	0.0012	0.0301	-1.91
CXCL10	32.14	2.31	0.55	4.18	2.96E-05	0.00273	4.95

CXCL11	3.74	3.30	1.05	3.16	0.00159	0.03571	9.86
CXCL13	5.58	4.20	1.40	3.00	0.00268	0.04915	18.36
ANXA3	108.04	-0.75	0.24	-3.08	0.00209	0.04182	-1.68
LINC01094	74.22	1.01	0.27	3.71	0.00021	0.00993	2.01
LINC01088	158.32	-0.79	0.25	-3.20	0.0014	0.03313	-1.73
BMP3	7.30	6.34	1.65	3.84	0.00012	0.00732	80.85
PLAC8	8.30	2.23	0.68	3.26	0.0011	0.02854	4.70
PTPN13	1310.16	-0.62	0.15	-4.08	4.49E-05	0.00363	-1.53
DMP1	5.33	4.96	1.22	4.08	4.51E-05	0.00363	31.10
IBSP	78.16	5.52	1.05	5.27	1.38E-07	5.41E-05	45.78
SPP1	2847.46	4.66	0.91	5.13	2.82E-07	9.06E-05	25.28
GRID2	16.55	-1.96	0.54	-3.63	0.00028	0.01169	-3.89
UNC5C	697.87	-0.59	0.15	-3.96	7.62E-05	0.0052	-1.51
AC106881.1	21.50	-0.94	0.25	-3.73	0.00019	0.00944	-1.91
CFI	27.45	1.22	0.32	3.79	0.00015	0.00815	2.34
SMIM43	11.24	2.70	0.73	3.70	0.00021	0.01005	6.48
INTU	310.12	-0.60	0.17	-3.50	0.00046	0.01645	-1.52
NR3C2	198.39	-0.59	0.17	-3.48	0.00049	0.01702	-1.50
AC106865.1	23.47	1.93	0.63	3.05	0.00232	0.04485	3.82
TLR2	266.26	0.83	0.23	3.59	0.00034	0.01292	1.77
TDO2	17.48	4.48	1.04	4.31	1.64E-05	0.00191	22.28
GRIA2	6.48	-2.38	0.65	-3.67	0.00024	0.01079	-5.20
MARCHF1	220.13	0.77	0.22	3.49	0.00048	0.01676	1.71
APELA	7.70	4.90	1.14	4.29	1.79E-05	0.00197	29.83
HAND2	216.18	-0.75	0.25	-3.02	0.00254	0.04756	-1.68
TENM3	80.75	-1.11	0.27	-4.08	4.48E-05	0.00363	-2.16
STOX2	100.13	-0.66	0.17	-3.90	9.82E-05	0.00619	-1.58
TPPP	117.33	-1.01	0.33	-3.03	0.00241	0.04587	-2.02
ZDHHC11B	64.19	-2.10	0.42	-4.95	7.43E-07	0.0002	-4.29
ZDHHC11	33.29	-1.65	0.36	-4.60	4.17E-06	0.00071	-3.14
AC010343.3	6.26	4.87	1.07	4.55	5.36E-06	0.00084	29.15
GDNF	14.95	1.32	0.37	3.61	0.0003	0.01219	2.50
FYB1	262.75	1.14	0.23	4.97	6.77E-07	0.00019	2.20
DAB2	1695.15	0.61	0.16	3.90	9.81E-05	0.00619	1.53
FST	262.13	0.90	0.29	3.06	0.00223	0.04374	1.86
GZMK	19.95	2.31	0.64	3.61	0.00031	0.01227	4.96
GZMA	23.08	2.32	0.50	4.62	3.91E-06	0.00068	5.01
HTR1A	7.93	-1.97	0.63	-3.14	0.00167	0.03684	-3.91
NAIP	61.76	1.07	0.28	3.83	0.00013	0.00751	2.10
NR2F1-AS1	302.39	-0.77	0.26	-3.02	0.00251	0.0472	-1.71
NR2F1	66.67	-0.83	0.22	-3.76	0.00017	0.00876	-1.78
MCTP1	101.27	0.88	0.29	3.00	0.00266	0.04876	1.83
RHOBTB3	413.39	-0.67	0.21	-3.20	0.00137	0.03275	-1.59
HSPD1P11	14.71	-1.09	0.36	-3.00	0.00273	0.04961	-2.13
ST8SIA4	154.23	0.89	0.21	4.31	1.61E-05	0.0019	1.85

PRDM6	21.59	1.02	0.32	3.23	0.00123	0.03058	2.03
PDLIM4	42.94	1.05	0.35	3.04	0.0024	0.04587	2.07
MIR3936HG	43.47	-0.90	0.29	-3.12	0.00179	0.03849	-1.87
CXCL14	216.28	2.15	0.60	3.62	0.0003	0.01217	4.44
SPOCK1	304.63	1.54	0.33	4.67	2.95E-06	0.00056	2.90
CD14	1122.63	0.91	0.24	3.74	0.00019	0.00927	1.88
PCDHGB4	49.05	-0.65	0.21	-3.18	0.00146	0.03383	-1.57
PCDH1	204.66	1.03	0.30	3.40	0.00068	0.02109	2.04
PCDH12	235.58	0.82	0.27	3.03	0.00246	0.04663	1.77
STK32A	162.21	-0.66	0.20	-3.26	0.00111	0.02861	-1.58
CSF1R	1034.41	0.91	0.29	3.18	0.00149	0.03404	1.88
CD74	7848.91	1.14	0.27	4.26	2.00E-05	0.00214	2.20
GRIA1	6.25	5.61	1.28	4.38	1.21E-05	0.00153	48.99
SGCD	336.71	0.62	0.19	3.21	0.00133	0.03208	1.54
TIMD4	44.16	2.69	0.64	4.17	3.04E-05	0.00277	6.44
DOCK2	413.13	0.72	0.21	3.48	0.00049	0.01702	1.65
LCP2	193.07	1.21	0.27	4.47	7.99E-06	0.00116	2.32
SH3PXD2B	372.00	0.60	0.18	3.43	0.00061	0.01958	1.52
HRH2	45.76	1.01	0.31	3.22	0.00129	0.03148	2.01
HK3	79.65	1.29	0.36	3.57	0.00036	0.01355	2.44
RGS14	40.43	1.09	0.27	3.97	7.34E-05	0.00508	2.13
DOK3	58.13	1.47	0.36	4.06	4.93E-05	0.00386	2.77
TUBB2B	64.20	-1.31	0.32	-4.13	3.68E-05	0.00319	-2.47
F13A1	4679.05	0.96	0.29	3.34	0.00083	0.02411	1.95
LY86	37.25	1.20	0.38	3.13	0.00177	0.03836	2.30
ADTRP	9.81	1.42	0.41	3.45	0.00056	0.01856	2.68
PHACTR1	49.89	0.70	0.19	3.64	0.00027	0.01158	1.63
CASC15	257.11	-0.84	0.21	-3.95	7.84E-05	0.00531	-1.79
H1-3	98.12	0.98	0.29	3.42	0.00062	0.01977	1.97
H4C12	5.17	1.72	0.54	3.18	0.00149	0.03404	3.30
TNF	12.98	1.37	0.43	3.17	0.00151	0.03426	2.59
C2	121.80	0.90	0.21	4.30	1.73E-05	0.00195	1.87
CFB	52.76	0.70	0.20	3.49	0.00049	0.01698	1.62
C4A	91.56	0.99	0.32	3.12	0.00183	0.03876	1.98
GPSM3	84.22	0.90	0.27	3.30	0.00096	0.02607	1.87
HLA-DRA	3926.94	0.99	0.28	3.55	0.00039	0.01434	1.99
HLA-DRB1	2439.55	1.09	0.27	3.98	6.99E-05	0.00493	2.13
HLA-DQA1	626.13	1.76	0.33	5.40	6.74E-08	3.24E-05	3.40
HLA-DQB1	747.23	2.17	0.49	4.42	1.00E-05	0.00138	4.50
HLA-DMB	285.37	0.83	0.23	3.54	0.0004	0.0148	1.78
HLA-DMA	350.71	0.79	0.21	3.74	0.00019	0.00927	1.73
HLA-DPA1	2276.01	0.96	0.25	3.92	9.03E-05	0.00586	1.94
HLA-DPB1	1242.87	0.85	0.25	3.41	0.00066	0.02075	1.80
SCUBE3	28.66	2.29	0.48	4.76	1.97E-06	0.00042	4.89
MAPK13	43.00	2.06	0.33	6.20	5.50E-10	6.61E-07	4.17

KCNK17	133.94	-0.93	0.20	-4.73	2.29E-06	0.00046	-1.90
TREM2	67.28	1.41	0.37	3.83	0.00013	0.00754	2.66
TREM1	61.33	2.22	0.67	3.30	0.00096	0.02607	4.67
HMGCLL1	55.23	-1.41	0.34	-4.18	2.94E-05	0.00273	-2.66
AL391807.1	13.40	-1.23	0.41	-3.00	0.00272	0.04944	-2.35
COL12A1	5250.82	0.85	0.19	4.40	1.07E-05	0.00141	1.80
IRAK1BP1	90.06	-0.62	0.17	-3.70	0.00021	0.01002	-1.54
TBX18	357.80	-0.78	0.26	-3.02	0.00255	0.04764	-1.72
CNR1	130.37	-0.97	0.24	-3.98	7.02E-05	0.00493	-1.96
EPHA7	59.65	-0.98	0.32	-3.03	0.00242	0.04598	-1.98
CRYBG1	208.99	1.09	0.25	4.41	1.05E-05	0.0014	2.14
SLC22A16	2.96	2.68	0.89	3.01	0.00263	0.0486	6.40
SLC16A10	83.12	1.72	0.44	3.92	8.85E-05	0.00583	3.30
COL10A1	126.01	2.85	0.85	3.34	0.00083	0.02404	7.23
ROS1	5.71	5.06	1.26	4.03	5.62E-05	0.00418	33.42
TRDN	12.71	-2.05	0.47	-4.33	1.50E-05	0.00183	-4.15
TRDN-AS1	6.82	-3.86	0.75	-5.13	2.95E-07	9.29E-05	-14.49
NKAIN2	18.71	-2.12	0.46	-4.66	3.20E-06	0.00058	-4.36
AL365259.1	20.91	-0.97	0.32	-3.04	0.00233	0.04495	-1.95
HEY2	218.88	-0.67	0.17	-4.08	4.46E-05	0.00363	-1.60
AL356124.1	45.61	0.91	0.23	3.85	0.00012	0.00694	1.87
AL356124.2	3.17	2.26	0.70	3.21	0.00132	0.03191	4.79
ARHGAP18	433.86	0.64	0.19	3.43	0.00061	0.01961	1.55
TMEM200A	52.72	1.61	0.40	4.07	4.63E-05	0.00367	3.06
ENPP1	399.37	2.17	0.31	6.99	2.70E-12	1.25E-08	4.49
CCN2	4197.71	0.88	0.23	3.88	0.0001	0.00645	1.84
MOXD1	36.34	1.77	0.47	3.73	0.00019	0.00944	3.40
AL121933.2	10.82	1.22	0.38	3.18	0.00147	0.03392	2.32
PLAGL1	255.41	0.72	0.16	4.49	7.26E-06	0.00109	1.65
UST	233.96	-0.71	0.20	-3.60	0.00032	0.0124	-1.64
AKAP12	2065.26	-0.60	0.14	-4.14	3.42E-05	0.003	-1.52
FNDC1	550.50	1.81	0.43	4.22	2.48E-05	0.00241	3.50
LPAL2	10.62	1.34	0.40	3.37	0.00074	0.02235	2.54
SMOC2	291.53	1.71	0.28	6.11	1.02E-09	1.16E-06	3.28
THBS2	6911.45	1.12	0.27	4.16	3.17E-05	0.00286	2.17
AC215522.2	3.68	2.39	0.75	3.18	0.00146	0.03384	5.26
FAM20C	258.79	0.83	0.22	3.81	0.00014	0.00786	1.78
TTYH3	338.36	0.86	0.27	3.13	0.00175	0.03812	1.81
CARD11	30.23	1.25	0.38	3.26	0.00111	0.02857	2.39
MPP6	384.45	-0.97	0.21	-4.59	4.52E-06	0.00075	-1.96
SNX10	54.03	1.28	0.30	4.29	1.79E-05	0.00197	2.43
CPVL	292.55	0.97	0.27	3.60	0.00031	0.01239	1.96
MTURN	437.35	-0.60	0.14	-4.43	9.64E-06	0.00133	-1.52
INMT	1587.48	-0.80	0.17	-4.68	2.83E-06	0.00055	-1.74
AOAH	86.47	1.09	0.31	3.53	0.00041	0.01501	2.12

TRG-AS1	10.25	2.08	0.60	3.46	0.00054	0.01809	4.22
POU6F2	7.80	2.59	0.74	3.48	0.0005	0.01702	6.00
MYO1G	80.30	1.48	0.41	3.61	0.0003	0.01219	2.78
IGFBP1	4.96	3.66	0.98	3.73	0.00019	0.00944	12.68
IKZF1	142.19	1.29	0.30	4.21	2.50E-05	0.00241	2.44
LIMK1	155.00	0.61	0.19	3.21	0.00135	0.03247	1.52
LAT2	73.34	1.13	0.29	3.88	0.0001	0.00645	2.19
PHTF2	265.14	0.84	0.16	5.16	2.52E-07	8.50E-05	1.79
SEMA3A	300.03	-0.98	0.26	-3.80	0.00015	0.00814	-1.97
AC005076.2	4.26	-1.63	0.50	-3.27	0.00106	0.02802	-3.08
STEAP1	102.10	1.47	0.23	6.46	1.06E-10	1.86E-07	2.78
STEAP2	338.22	0.78	0.19	4.11	3.91E-05	0.00331	1.72
PPP1R9A	39.86	-1.13	0.27	-4.15	3.37E-05	0.00297	-2.19
DLX5	4.80	5.31	1.32	4.02	5.73E-05	0.00422	39.64
PILRA	76.52	1.13	0.25	4.43	9.60E-06	0.00133	2.19
LRRC17	367.65	0.87	0.23	3.75	0.00018	0.00914	1.83
PIK3CG	172.27	0.86	0.22	3.96	7.36E-05	0.00508	1.82
PRKAR2B	110.84	-0.62	0.20	-3.08	0.00208	0.04162	-1.54
LEP	24.76	1.88	0.59	3.18	0.00148	0.03393	3.69
ATP6V1F	142.78	0.60	0.18	3.29	0.00101	0.027	1.52
TSPAN33	116.34	0.90	0.22	4.15	3.28E-05	0.00292	1.87
STRIP2	11.03	1.26	0.41	3.10	0.00194	0.04004	2.40
DGKI	206.09	1.04	0.23	4.56	5.11E-06	0.00081	2.05
DENND2A	166.29	-0.60	0.19	-3.17	0.00153	0.03443	-1.52
TRBC1	21.34	1.90	0.57	3.35	0.00082	0.02395	3.74
TRBC2	38.94	2.10	0.55	3.79	0.00015	0.00815	4.28
EPHB6	114.41	-0.77	0.25	-3.13	0.00173	0.03771	-1.70
GIMAP1	51.00	0.79	0.25	3.21	0.00134	0.03221	1.73
MSR1	932.46	1.00	0.28	3.63	0.00028	0.01169	2.00
SLC7A2	165.42	1.73	0.34	5.03	4.98E-07	0.00015	3.31
PDGFRL	27.24	1.20	0.37	3.23	0.00125	0.03094	2.30
AC100849.1	10.73	1.38	0.44	3.11	0.00184	0.03892	2.60
HR	65.84	-0.99	0.22	-4.46	8.08E-06	0.00116	-1.98
SLC39A14	602.39	0.67	0.20	3.32	0.00089	0.02512	1.59
ADAM28	119.56	0.94	0.27	3.54	0.0004	0.0146	1.92
EBF2	10.21	2.53	0.63	4.02	5.89E-05	0.00429	5.76
EPHX2	111.70	-0.63	0.18	-3.53	0.00042	0.01527	-1.55
SCARA5	736.43	-1.00	0.31	-3.22	0.00127	0.03141	-2.00
ZNF395	247.48	-0.68	0.13	-5.16	2.49E-07	8.50E-05	-1.61
IDO1	6.18	3.53	0.91	3.88	0.0001	0.00645	11.52
LYN	220.85	0.65	0.19	3.47	0.00051	0.01744	1.57
AC104051.2	27.66	-1.77	0.57	-3.13	0.00176	0.0382	-3.42
FAM110B	149.26	-0.70	0.20	-3.49	0.00048	0.01676	-1.62
PKIA	49.31	-0.99	0.26	-3.80	0.00014	0.00793	-1.98
STMN2	78.27	3.95	0.56	7.07	1.53E-12	9.84E-09	15.42

MATN2	2205.57	-0.91	0.22	-4.09	4.24E-05	0.00353	-1.88
BAALC	5.40	2.41	0.71	3.41	0.00065	0.02057	5.32
BAALC-AS1	53.30	0.71	0.23	3.12	0.00183	0.03876	1.63
CTHRC1	241.05	1.33	0.36	3.68	0.00023	0.0106	2.51
RSPO2	63.73	1.34	0.38	3.49	0.00049	0.01698	2.53
SAMD12	32.03	-0.96	0.31	-3.06	0.00222	0.04359	-1.94
TNFRSF11B	779.98	1.84	0.27	6.90	5.20E-12	1.25E-08	3.57
CCN3	547.01	1.15	0.28	4.08	4.54E-05	0.00363	2.22
COL14A1	9092.95	0.63	0.15	4.28	1.84E-05	0.00201	1.54
AC100858.2	8.87	1.24	0.41	3.03	0.00241	0.04587	2.36
LINC00861	14.87	3.11	0.76	4.09	4.38E-05	0.0036	8.62
LRATD2	214.62	-0.60	0.20	-3.03	0.00241	0.04587	-1.52
ASAP1	486.13	0.75	0.13	5.74	9.75E-09	7.21E-06	1.68
TG	15.73	1.52	0.44	3.41	0.00064	0.02032	2.86
CCN4	362.57	1.84	0.34	5.41	6.43E-08	3.17E-05	3.57
LY6E	340.31	0.60	0.20	3.01	0.00265	0.04866	1.52
EPPK1	14.35	1.39	0.42	3.34	0.00083	0.02413	2.62
DOCK8	337.38	0.84	0.22	3.75	0.00018	0.00914	1.79
JAK2	530.90	0.72	0.12	6.01	1.82E-09	1.84E-06	1.65
MTCO1P11	8.52	1.70	0.46	3.69	0.00023	0.01049	3.25
MTCO3P11	6.83	1.99	0.56	3.58	0.00034	0.01301	3.97
CD72	28.19	1.29	0.30	4.31	1.66E-05	0.00192	2.45
ALDH1B1	137.34	0.68	0.21	3.22	0.00128	0.03143	1.61
PGM5P2	13.59	-1.33	0.35	-3.81	0.00014	0.0078	-2.51
FP325317.1	4.45	-2.40	0.68	-3.52	0.00044	0.01583	-5.29
FAM189A2	65.95	-0.71	0.20	-3.61	0.0003	0.01219	-1.64
ALDH1A1	432.09	-1.19	0.29	-4.10	4.09E-05	0.00344	-2.28
GCNT1	157.36	0.69	0.22	3.12	0.00178	0.03849	1.61
PSAT1	44.14	-0.97	0.29	-3.36	0.00077	0.02304	-1.96
GKAP1	34.74	-0.83	0.22	-3.82	0.00014	0.00772	-1.78
SLC28A3	5.18	3.37	0.99	3.42	0.00063	0.02008	10.32
SEMA4D	114.51	0.99	0.31	3.20	0.00139	0.03308	1.99
ROR2	53.41	1.23	0.33	3.73	0.00019	0.00944	2.34
OGN	592.76	1.48	0.21	6.94	3.98E-12	1.25E-08	2.79
OMD	807.47	0.84	0.25	3.40	0.00067	0.02104	1.78
ASPN	2044.13	1.17	0.27	4.32	1.55E-05	0.00185	2.25
FGD3	73.09	0.89	0.28	3.19	0.00141	0.03334	1.86
FBP1	22.44	1.38	0.45	3.07	0.00212	0.04225	2.59
TRIM14	104.11	0.80	0.24	3.35	0.0008	0.0237	1.74
TBC1D2	81.84	0.88	0.20	4.39	1.14E-05	0.00147	1.85
COL15A1	2796.40	0.77	0.24	3.22	0.00128	0.03143	1.71
EPB41L4B	30.50	-1.86	0.49	-3.80	0.00014	0.00793	-3.63
SLC31A2	96.18	0.73	0.23	3.15	0.00164	0.0364	1.66
TNC	6181.37	2.56	0.35	7.26	3.89E-13	3.74E-09	5.90
NEK6	392.33	0.64	0.16	4.05	5.13E-05	0.00393	1.56

ANGPTL2	693.38	1.06	0.31	3.45	0.00057	0.01868	2.08
CERCAM	553.09	0.66	0.17	3.97	7.10E-05	0.00496	1.58
LINC01503	29.15	0.90	0.24	3.66	0.00025	0.01117	1.86
LAMC3	372.23	-1.10	0.33	-3.33	0.00087	0.02484	-2.15
RAPGEF1	363.71	0.63	0.18	3.44	0.00058	0.01906	1.55
AKR1C1	1070.76	-0.74	0.21	-3.53	0.00042	0.01535	-1.67
CUBN	166.48	-0.64	0.16	-3.96	7.55E-05	0.00519	-1.56
TMEM236	23.79	1.26	0.28	4.57	4.97E-06	0.00079	2.39
KIAA1217	104.45	1.66	0.34	4.92	8.77E-07	0.00023	3.15
PRTFDC1	258.47	-0.64	0.21	-3.04	0.00238	0.04571	-1.56
APBB1IP	61.58	1.03	0.30	3.44	0.00058	0.01906	2.04
BAMBI	75.46	-0.67	0.20	-3.39	0.0007	0.02138	-1.60
LINC00841	4.94	2.33	0.72	3.23	0.00125	0.03101	5.03
CXCL12	1856.22	0.66	0.21	3.21	0.00131	0.03191	1.58
DEPP1	2187.25	-0.85	0.24	-3.57	0.00036	0.01353	-1.80
ALOX5	200.45	1.10	0.24	4.66	3.10E-06	0.00058	2.14
WDFY4	197.17	0.82	0.26	3.13	0.00174	0.03788	1.77
SLC16A9	74.08	-1.13	0.33	-3.44	0.00058	0.01891	-2.19
LINC01515	40.44	-2.03	0.42	-4.80	1.62E-06	0.00035	-4.07
TSPAN15	79.12	1.08	0.26	4.25	2.18E-05	0.00222	2.12
NPFFR1	14.55	-1.50	0.44	-3.39	0.00069	0.0212	-2.82
PRF1	19.78	2.20	0.57	3.87	0.00011	0.00658	4.58
MYOZ1	11.68	2.64	0.68	3.90	9.78E-05	0.00619	6.21
PLAU	332.80	1.29	0.31	4.23	2.34E-05	0.00229	2.45
MAT1A	11.01	4.95	1.28	3.88	0.00011	0.00648	30.88
SLC16A12	104.22	-1.11	0.32	-3.49	0.00048	0.01679	-2.15
PIK3AP1	285.03	0.83	0.23	3.61	0.0003	0.01219	1.78
CRTAC1	1520.41	1.46	0.24	5.98	2.22E-09	2.13E-06	2.74
SH3PXD2A	719.44	0.67	0.17	3.98	6.93E-05	0.0049	1.60
ADRA2A	70.80	3.39	0.63	5.35	8.91E-08	3.81E-05	10.45
PLEKHS1	20.06	5.88	0.93	6.29	3.19E-10	4.64E-07	58.70
NANOS1	121.50	-1.28	0.34	-3.73	0.00019	0.0095	-2.43
HTRA1	1684.03	0.85	0.18	4.68	2.91E-06	0.00055	1.81
ADAM12	59.65	1.48	0.47	3.12	0.00179	0.03849	2.79
PTPRE	250.59	0.62	0.19	3.30	0.00096	0.02611	1.54
ADAM8	60.41	1.67	0.49	3.45	0.00056	0.01866	3.19
IFITM10	35.73	1.35	0.40	3.34	0.00084	0.02418	2.54
AC068580.4	55.02	1.67	0.39	4.24	2.19E-05	0.00222	3.18
LSP1	344.59	1.15	0.29	4.04	5.45E-05	0.00412	2.22
KCNQ1	53.71	0.88	0.25	3.56	0.00037	0.014	1.85
HBB	905.12	2.39	0.77	3.12	0.00179	0.03849	5.25
TPP1	368.66	0.84	0.23	3.64	0.00027	0.01158	1.79
AMPD3	77.12	1.03	0.30	3.46	0.00053	0.01788	2.04
PDE3B	366.37	-0.65	0.21	-3.03	0.00241	0.04587	-1.57
INSC	4.83	5.07	1.43	3.55	0.00038	0.01426	33.49

ABCC8	5.63	-3.71	0.90	-4.14	3.51E-05	0.00307	-13.10
LDHA	1566.71	0.59	0.18	3.27	0.00106	0.02793	1.50
CD44	1867.04	0.67	0.19	3.61	0.00031	0.01232	1.59
TP53I11	95.67	1.50	0.35	4.22	2.40E-05	0.00234	2.82
SLC35C1	74.37	0.61	0.20	3.09	0.00201	0.04076	1.53
SPI1	134.47	0.96	0.28	3.40	0.00066	0.02093	1.94
MS4A2	19.34	1.94	0.61	3.19	0.00142	0.0334	3.85
MS4A6A	677.48	0.73	0.19	3.89	0.0001	0.0064	1.66
CD5	15.03	2.19	0.62	3.52	0.00043	0.01562	4.57
PLAAT4	126.86	0.63	0.19	3.27	0.00106	0.02793	1.55
TM7SF2	42.40	-1.62	0.41	-3.95	7.96E-05	0.00535	-3.07
SYT12	205.96	1.79	0.39	4.66	3.23E-06	0.00058	3.47
RHOD	50.51	0.84	0.19	4.41	1.04E-05	0.0014	1.79
P2RY6	58.58	1.13	0.30	3.79	0.00015	0.00815	2.19
UCP2	72.19	1.08	0.28	3.79	0.00015	0.00815	2.11
P4HA3	46.15	0.98	0.30	3.22	0.00128	0.03143	1.98
CHRDL2	28.92	2.92	0.72	4.04	5.30E-05	0.00405	7.57
SLCO2B1	1294.51	0.84	0.25	3.34	0.00083	0.02405	1.79
TENM4	118.55	1.19	0.34	3.51	0.00045	0.01598	2.28
DLG2	184.44	1.10	0.27	4.07	4.72E-05	0.00372	2.14
CTSC	1006.34	0.83	0.26	3.18	0.00146	0.03383	1.77
CFAP300	34.53	-0.77	0.20	-3.81	0.00014	0.00779	-1.71
MMP7	10.39	4.20	1.21	3.47	0.00051	0.01734	18.43
MMP1	7.81	5.05	1.16	4.35	1.37E-05	0.0017	33.12
MMP12	18.29	4.29	1.03	4.18	2.92E-05	0.00273	19.54
MMP13	35.80	6.84	1.53	4.48	7.54E-06	0.00112	114.48
IL18	35.98	0.93	0.28	3.31	0.00095	0.02592	1.90
IL10RA	430.53	0.68	0.21	3.31	0.00093	0.02577	1.60
CD3E	17.56	2.01	0.59	3.39	0.00071	0.02153	4.02
TLCD5	87.00	-0.64	0.18	-3.55	0.00038	0.01415	-1.55
ADAMTS15	130.17	-0.82	0.24	-3.45	0.00056	0.01864	-1.77
WNT5B	37.62	1.36	0.37	3.64	0.00027	0.01158	2.57
CACNA2D4	34.39	1.15	0.31	3.65	0.00026	0.01142	2.22
LPAR5	37.70	0.89	0.27	3.27	0.00107	0.02802	1.85
CD4	528.87	0.87	0.22	4.02	5.72E-05	0.00422	1.82
PTPN6	149.49	0.89	0.29	3.06	0.00218	0.04297	1.86
CD163L1	287.34	1.05	0.34	3.10	0.00194	0.04004	2.08
C3AR1	265.14	0.83	0.24	3.43	0.0006	0.01945	1.78
CLEC4D	3.37	3.90	1.18	3.30	0.00097	0.02626	14.88
MFAP5	104.51	1.95	0.62	3.14	0.00168	0.03693	3.88
A2M	5817.86	0.83	0.19	4.41	1.06E-05	0.0014	1.78
ARHGDIB	766.19	0.59	0.15	3.93	8.54E-05	0.00567	1.51
RERG	311.76	-0.70	0.17	-3.98	6.87E-05	0.00487	-1.62
LMO3	216.61	-0.90	0.29	-3.11	0.0019	0.03982	-1.87
TSPAN11	121.41	1.48	0.41	3.59	0.00033	0.01267	2.80

KIF21A	226.15	-0.70	0.19	-3.70	0.00021	0.01002	-1.62
NELL2	32.95	3.13	0.86	3.64	0.00027	0.01156	8.77
PCED1B-AS1	32.93	1.24	0.33	3.77	0.00016	0.00858	2.37
VDR	82.90	1.68	0.31	5.37	7.82E-08	3.58E-05	3.21
COL2A1	13.38	2.87	0.80	3.60	0.00032	0.0124	7.33
BIN2	77.25	1.15	0.27	4.24	2.27E-05	0.00225	2.22
GALNT6	46.21	1.15	0.30	3.79	0.00015	0.00815	2.22
ITGB7	29.54	1.29	0.36	3.64	0.00027	0.01158	2.45
ESPL1	11.40	1.22	0.41	3.00	0.00269	0.04918	2.33
SP7	8.98	6.16	1.27	4.86	1.15E-06	0.00028	71.32
NCKAP1L	511.65	0.72	0.20	3.65	0.00026	0.01142	1.64
LRP1	14866.26	0.65	0.18	3.51	0.00045	0.01607	1.57
ARHGAP9	76.02	1.04	0.29	3.55	0.00038	0.01415	2.06
AGAP2	31.84	1.18	0.34	3.49	0.00048	0.01679	2.27
CYP27B1	3.36	3.44	0.90	3.82	0.00013	0.00766	10.86
AVIL	96.34	1.14	0.24	4.76	1.95E-06	0.00042	2.21
LYZ	486.43	1.50	0.44	3.39	0.00071	0.02156	2.83
TSPAN8	154.50	-1.10	0.34	-3.24	0.0012	0.03009	-2.14
TRHDE	155.63	-1.23	0.25	-4.83	1.40E-06	0.00031	-2.34
TRHDE-AS1	89.98	-1.44	0.39	-3.69	0.00023	0.01049	-2.72
CAPS2	101.30	-0.70	0.23	-3.11	0.00186	0.03928	-1.63
PTPRQ	14.52	-1.55	0.48	-3.22	0.00128	0.03143	-2.94
LIN7A	155.19	-0.89	0.25	-3.60	0.00031	0.01236	-1.85
MGAT4C	10.19	2.00	0.64	3.11	0.0019	0.03982	4.00
LUM	12067.03	1.11	0.28	3.89	9.94E-05	0.00625	2.16
PLXNC1	250.61	0.74	0.20	3.70	0.00021	0.01002	1.67
USP44	10.78	-1.15	0.37	-3.15	0.00163	0.03628	-2.23
BTBD11	31.78	1.06	0.28	3.83	0.00013	0.00748	2.08
WSCD2	38.45	1.71	0.38	4.49	7.23E-06	0.00109	3.28
CMKLR1	722.13	1.01	0.18	5.67	1.42E-08	9.40E-06	2.01
TMEM119	177.38	1.20	0.28	4.25	2.09E-05	0.00219	2.29
SELPLG	138.72	0.95	0.26	3.64	0.00028	0.01159	1.93
TRPV4	26.55	1.39	0.29	4.75	1.99E-06	0.00042	2.62
SH2B3	441.40	0.62	0.17	3.64	0.00027	0.01156	1.54
ALDH2	460.73	-0.99	0.24	-4.08	4.56E-05	0.00363	-1.98
OAS3	364.87	0.73	0.23	3.20	0.00138	0.03284	1.66
OAS2	313.51	0.73	0.21	3.50	0.00047	0.01645	1.65
SPRING1	166.95	0.63	0.16	4.03	5.49E-05	0.00413	1.55
BICDL1	7.08	3.20	0.76	4.19	2.84E-05	0.00268	9.17
OASL	17.73	1.61	0.45	3.56	0.00038	0.01406	3.05
RHOF	35.30	0.84	0.26	3.29	0.00102	0.02716	1.79
LINC00944	4.48	2.24	0.70	3.18	0.00148	0.03393	4.72
TMEM132C	85.71	-1.29	0.41	-3.19	0.00141	0.03327	-2.45
FZD10-AS1	107.19	-0.92	0.25	-3.62	0.0003	0.01217	-1.89
GJA3	3.02	3.51	1.05	3.34	0.00082	0.02401	11.38

TNFRSF19	446.74	-0.88	0.23	-3.88	0.0001	0.00645	-1.84
BRCA2	78.66	0.65	0.21	3.07	0.00217	0.04288	1.57
RGCC	86.43	1.00	0.27	3.64	0.00027	0.01156	2.00
TNFSF11	11.01	3.97	0.77	5.14	2.74E-07	8.95E-05	15.69
EPSTI1	96.38	1.04	0.27	3.91	9.11E-05	0.00586	2.06
LCP1	831.23	0.89	0.28	3.12	0.00183	0.03876	1.85
CYSLTR2	240.65	-0.68	0.21	-3.20	0.0014	0.03313	-1.60
ARL11	19.18	1.07	0.30	3.58	0.00034	0.01299	2.10
SLAIN1	52.69	-0.92	0.21	-4.32	1.58E-05	0.00187	-1.90
SLITRK5	30.10	-1.78	0.39	-4.63	3.71E-06	0.00065	-3.44
F10	144.47	-0.75	0.23	-3.27	0.00108	0.02825	-1.68
TMEM255B	28.03	0.94	0.27	3.48	0.0005	0.01705	1.91
LINC00565	8.46	1.38	0.43	3.22	0.00127	0.03141	2.60
NDRG2	612.51	-0.95	0.24	-4.03	5.60E-05	0.00417	-1.93
SLC7A8	100.07	0.90	0.24	3.81	0.00014	0.00781	1.86
RIPK3	38.89	0.89	0.26	3.47	0.00052	0.01753	1.85
CMA1	7.89	4.30	1.04	4.12	3.87E-05	0.00329	19.63
CTSG	20.28	2.98	0.63	4.75	2.08E-06	0.00043	7.87
GZMH	5.92	1.86	0.62	3.02	0.00254	0.04756	3.64
AL121821.2	17.65	-1.26	0.30	-4.16	3.19E-05	0.00287	-2.39
LRFN5	48.57	-1.35	0.29	-4.57	4.84E-06	0.00078	-2.55
RN7SL1	21965.85	0.97	0.32	3.05	0.0023	0.04451	1.96
GCH1	36.64	0.95	0.27	3.44	0.00057	0.01879	1.93
HIF1A	979.01	0.82	0.26	3.09	0.00197	0.0403	1.76
SUSD6	373.81	0.70	0.19	3.65	0.00026	0.01144	1.62
SMOC1	182.92	1.23	0.37	3.35	0.00082	0.02394	2.35
SLC8A3	4.06	3.28	1.00	3.28	0.00104	0.02761	9.73
NPC2	937.43	0.70	0.18	3.93	8.49E-05	0.00565	1.63
PGF	117.81	1.26	0.35	3.64	0.00028	0.01159	2.40
BATF	19.52	1.07	0.34	3.10	0.00196	0.04015	2.10
FLVCR2	47.88	0.81	0.26	3.15	0.00162	0.03624	1.75
LINC02289	7.10	-1.70	0.47	-3.63	0.00028	0.01166	-3.25
GPR65	52.27	0.82	0.27	3.07	0.00212	0.04227	1.76
GPR68	56.18	2.66	0.47	5.71	1.11E-08	7.88E-06	6.34
AL135818.1	3.43	3.03	0.98	3.09	0.00197	0.0403	8.18
TC2N	364.68	-0.82	0.20	-4.08	4.52E-05	0.00363	-1.77
PRIMA1	40.15	-1.00	0.33	-3.05	0.00228	0.04433	-2.00
CLMN	148.40	0.72	0.20	3.55	0.00038	0.01415	1.65
BCL11B	21.11	2.11	0.58	3.66	0.00025	0.01128	4.31
AHNAK2	1541.78	0.74	0.20	3.72	0.0002	0.00982	1.67
IGHG4	483.40	8.92	1.84	4.85	1.23E-06	0.00029	483.02
IGHG2	2277.83	4.22	1.29	3.27	0.00106	0.02802	18.64
IGHA1	1032.46	3.81	1.10	3.46	0.00053	0.01788	14.07
IGHG1	3712.26	3.72	1.18	3.14	0.0017	0.0373	13.13
IGHV1-2	16.79	5.23	1.56	3.36	0.00079	0.02342	37.43

IGHV4-34	18.02	6.23	1.79	3.48	0.00049	0.01702	75.00
FAM189A1	38.45	-0.98	0.26	-3.74	0.00018	0.00914	-1.98
GREM1	38.20	3.45	1.03	3.33	0.00085	0.02456	10.92
MEIS2	482.60	-0.67	0.17	-3.86	0.00011	0.00683	-1.60
LINC02345	6.48	2.68	0.76	3.52	0.00044	0.01574	6.40
RASGRP1	30.80	1.91	0.47	4.08	4.42E-05	0.00362	3.76
PLCB2	165.19	0.87	0.26	3.32	0.00089	0.02521	1.83
SEMA6D	167.53	-0.86	0.15	-5.85	5.06E-09	4.24E-06	-1.81
FGF7	766.17	1.54	0.31	4.96	6.91E-07	0.00019	2.92
HDC	18.40	2.70	0.60	4.47	7.68E-06	0.00113	6.51
CYP19A1	10.97	1.37	0.39	3.50	0.00047	0.01646	2.59
TEX9	99.16	1.02	0.25	4.16	3.13E-05	0.00284	2.03
CA12	84.21	2.28	0.41	5.50	3.87E-08	2.25E-05	4.86
CORO2B	120.39	-0.70	0.20	-3.45	0.00056	0.01856	-1.62
THSD4	278.53	-0.97	0.27	-3.66	0.00026	0.01136	-1.96
STRA6	77.14	-0.98	0.29	-3.38	0.00072	0.02183	-1.98
SEMA7A	41.19	1.39	0.43	3.23	0.00123	0.03058	2.63
CRABP1	7.29	2.31	0.68	3.40	0.00069	0.0212	4.95
CTSH	333.66	0.90	0.25	3.66	0.00025	0.01132	1.87
CEMIP	497.06	2.23	0.47	4.70	2.57E-06	0.0005	4.69
TM6SF1	76.22	0.64	0.21	3.02	0.00254	0.04756	1.56
LINC00933	8.55	-1.09	0.35	-3.12	0.00183	0.03876	-2.12
ALPK3	169.17	0.70	0.17	4.01	6.16E-05	0.00447	1.63
ACAN	596.23	2.86	0.54	5.29	1.23E-07	4.95E-05	7.28
HAPLN3	123.93	1.49	0.32	4.66	3.20E-06	0.00058	2.80
ANPEP	265.77	1.58	0.28	5.65	1.64E-08	1.05E-05	2.99
SLCO3A1	186.16	0.60	0.13	4.64	3.46E-06	0.00062	1.52
MCTP2	56.13	1.30	0.27	4.88	1.04E-06	0.00026	2.46
HBA2	212.30	2.37	0.73	3.23	0.00122	0.03049	5.16
HBA1	48.97	2.44	0.73	3.33	0.00086	0.0247	5.44
TPSB2	31.41	3.57	0.74	4.81	1.52E-06	0.00034	11.88
TPSAB1	31.42	2.56	0.60	4.25	2.18E-05	0.00222	5.90
TPSD1	3.52	3.60	1.17	3.07	0.00211	0.0422	12.14
MEFV	18.53	1.56	0.47	3.32	0.0009	0.0253	2.94
NLRC3	36.45	1.50	0.48	3.10	0.00194	0.04004	2.83
AC099489.1	23.91	0.93	0.28	3.34	0.00084	0.02421	1.91
XYLT1	352.73	0.78	0.15	5.20	1.99E-07	7.36E-05	1.72
IL21R	35.49	2.46	0.57	4.30	1.68E-05	0.00193	5.50
CORO1A	167.04	0.92	0.30	3.09	0.00201	0.04065	1.89
ITGAM	328.85	0.70	0.18	3.97	7.31E-05	0.00508	1.63
ITGAX	128.65	1.89	0.61	3.12	0.00181	0.03865	3.71
MYLK3	11.92	-1.84	0.41	-4.47	7.92E-06	0.00115	-3.59
NETO2	58.19	-0.91	0.29	-3.11	0.00188	0.03961	-1.88
SNX20	39.40	1.29	0.31	4.21	2.51E-05	0.00241	2.44
NOD2	32.62	0.92	0.30	3.09	0.00198	0.04032	1.89

MMP2	3712.52	0.79	0.21	3.78	0.00016	0.00832	1.73
LPCAT2	206.34	0.66	0.16	4.13	3.69E-05	0.00319	1.58
NUDT7	26.40	-0.82	0.25	-3.32	0.00091	0.02542	-1.77
CLEC3A	5.66	4.62	1.21	3.83	0.00013	0.00748	24.57
PKD1L2	5.57	-1.71	0.53	-3.26	0.0011	0.02855	-3.28
PLCG2	113.38	0.95	0.31	3.09	0.00197	0.0403	1.93
WFDC1	54.45	1.14	0.34	3.32	0.00089	0.02512	2.21
IRF8	97.47	0.61	0.20	3.01	0.00264	0.04866	1.53
CYBA	425.28	0.67	0.20	3.32	0.00089	0.02512	1.59
CPNE7	4.69	3.19	1.05	3.03	0.00241	0.04587	9.15
CXCL16	215.73	1.10	0.29	3.83	0.00013	0.00754	2.15
VMO1	35.58	1.37	0.40	3.44	0.00059	0.01925	2.59
ACAP1	41.31	1.51	0.47	3.19	0.00141	0.03327	2.86
PIK3R5	139.85	0.76	0.24	3.21	0.00132	0.03203	1.70
HS3ST3B1	20.41	1.46	0.47	3.10	0.00195	0.04015	2.74
MEIS3P1	65.83	-0.66	0.18	-3.73	0.00019	0.00952	-1.58
LGALS9	95.13	0.83	0.25	3.40	0.00067	0.02104	1.78
EVI2B	42.54	1.08	0.31	3.49	0.00049	0.01699	2.11
MYO1D	2236.15	0.99	0.26	3.82	0.00013	0.00766	1.99
CCL11	4.86	3.20	0.99	3.25	0.00117	0.02988	9.21
CCL8	32.51	2.77	0.44	6.24	4.38E-10	5.62E-07	6.81
CCL5	69.25	2.13	0.53	4.00	6.40E-05	0.00461	4.39
CCL3	28.08	1.97	0.55	3.60	0.00032	0.0124	3.93
CCL4	17.72	1.76	0.52	3.36	0.00079	0.02342	3.38
AC243829.1	6.96	1.96	0.64	3.08	0.00208	0.04162	3.90
CCL4L2	10.22	2.64	0.70	3.75	0.00018	0.00901	6.24
STAC2	10.56	1.80	0.53	3.39	0.00069	0.0212	3.49
IKZF3	68.38	2.05	0.64	3.19	0.00145	0.0338	4.14
KRT16	12.30	3.10	0.63	4.90	9.57E-07	0.00024	8.58
KRT17	58.25	1.56	0.38	4.06	5.00E-05	0.00389	2.94
AOC2	14.06	1.02	0.34	2.99	0.00278	0.04996	2.03
RND2	32.55	-0.85	0.26	-3.24	0.0012	0.03009	-1.80
FMNL1	131.66	1.07	0.32	3.31	0.00095	0.02592	2.10
MAPT	108.66	-1.35	0.28	-4.90	9.48E-07	0.00024	-2.55
RPRML	3.28	3.31	1.05	3.15	0.00162	0.03619	9.95
TBX21	3.48	2.73	0.87	3.12	0.00182	0.03876	6.61
SKAP1	7.73	2.52	0.65	3.87	0.00011	0.00666	5.74
HOXB6	12.60	1.59	0.37	4.30	1.69E-05	0.00193	3.01
DLX3	5.63	2.33	0.60	3.92	9.01E-05	0.00586	5.03
ABCC3	280.62	0.87	0.26	3.37	0.00076	0.02282	1.82
TMEM100	139.14	-1.10	0.33	-3.30	0.00098	0.02653	-2.15
ACE	19.88	1.86	0.43	4.38	1.20E-05	0.00153	3.64
LIMD2	103.33	0.80	0.26	3.08	0.0021	0.04199	1.74
MILR1	95.13	0.71	0.22	3.19	0.00142	0.03337	1.64
RGS9	34.34	-0.81	0.25	-3.21	0.00131	0.03182	-1.75

AXIN2	145.66	-1.11	0.18	-6.28	3.38E-10	4.64E-07	-2.16
SLC16A6	8.82	2.03	0.52	3.91	9.08E-05	0.00586	4.07
FAM20A	190.76	1.63	0.28	5.74	9.57E-09	7.21E-06	3.10
ABCA8	2669.63	-1.02	0.31	-3.26	0.0011	0.02847	-2.02
ABCA9	955.99	-0.85	0.17	-4.92	8.82E-07	0.00023	-1.80
ABCA6	1923.80	-0.73	0.20	-3.65	0.00026	0.01142	-1.66
ABCA5	244.15	-0.63	0.20	-3.20	0.00138	0.03284	-1.55
MAP2K6	147.62	-1.03	0.21	-4.84	1.28E-06	0.0003	-2.04
CD300C	23.65	1.32	0.37	3.61	0.0003	0.01219	2.50
RHBDF2	159.18	0.91	0.26	3.54	0.00039	0.01453	1.87
PRCD	77.60	-1.07	0.36	-3.01	0.00262	0.04848	-2.10
SYNGR2	202.57	0.81	0.19	4.24	2.27E-05	0.00225	1.75
PYCR1	122.05	1.07	0.27	3.95	7.73E-05	0.00525	2.10
SLC16A3	155.03	1.30	0.38	3.40	0.00067	0.02104	2.46
CD7	7.00	2.51	0.69	3.63	0.00028	0.01164	5.70
SECTM1	44.10	1.25	0.34	3.64	0.00027	0.01158	2.38
METRNL	225.75	0.63	0.20	3.14	0.00167	0.03689	1.55
ADCYAP1	6.41	4.44	1.22	3.64	0.00027	0.01156	21.77
GAPLINC	8.90	1.51	0.41	3.69	0.00023	0.01049	2.85
APCDD1	1368.49	-1.26	0.25	-5.11	3.25E-07	9.94E-05	-2.39
GREB1L	4.14	-2.41	0.58	-4.17	3.03E-05	0.00277	-5.32
GATA6-AS1	33.24	-0.82	0.24	-3.36	0.00077	0.02296	-1.77
ASXL3	72.72	-1.14	0.28	-4.09	4.33E-05	0.00357	-2.20
FHOD3	65.31	0.97	0.32	3.07	0.00217	0.04288	1.95
SIGLEC15	6.51	2.40	0.79	3.05	0.00227	0.04418	5.29
MYO5B	22.54	1.18	0.33	3.58	0.00035	0.01327	2.27
RAB27B	13.73	2.30	0.54	4.30	1.73E-05	0.00195	4.93
DOK6	136.54	-0.97	0.23	-4.26	2.04E-05	0.00216	-1.96
CD226	36.17	1.13	0.32	3.48	0.0005	0.01719	2.19
AC016588.2	4.08	-2.08	0.69	-3.02	0.00251	0.0472	-4.24
ARID3A	45.25	0.73	0.21	3.38	0.00071	0.02163	1.65
ARHGAP45	205.95	0.83	0.27	3.05	0.0023	0.04451	1.78
DIRAS1	22.44	1.43	0.36	3.96	7.61E-05	0.0052	2.69
MFSD12	200.99	0.78	0.18	4.43	9.40E-06	0.00132	1.71
MATK	20.49	2.25	0.56	4.05	5.04E-05	0.00389	4.77
SEMA6B	30.10	2.25	0.67	3.33	0.00086	0.02457	4.74
VAV1	102.46	0.72	0.22	3.32	0.0009	0.02528	1.65
ADGRE4P	6.40	3.12	0.90	3.45	0.00055	0.01839	8.69
STXBP2	27.28	1.21	0.35	3.42	0.00062	0.01994	2.31
CD209	126.86	1.77	0.48	3.72	0.0002	0.00961	3.41
MYO1F	181.46	1.09	0.29	3.76	0.00017	0.00885	2.13
COL5A3	260.65	-0.71	0.21	-3.48	0.0005	0.01702	-1.64
ACP5	198.33	1.68	0.46	3.67	0.00025	0.01107	3.20
ADGRE2	62.39	2.17	0.60	3.60	0.00032	0.01251	4.52
RASAL3	40.15	1.50	0.39	3.81	0.00014	0.0079	2.83

CYP4F12	55.29	-1.09	0.30	-3.63	0.00028	0.01169	-2.13
HSH2D	9.11	2.42	0.80	3.03	0.00246	0.04663	5.36
TMEM38A	29.72	-1.04	0.29	-3.57	0.00036	0.01368	-2.06
NWD1	59.39	-1.14	0.36	-3.20	0.00136	0.03256	-2.21
JAK3	170.42	1.21	0.32	3.72	0.0002	0.00961	2.31
IL12RB1	22.13	1.13	0.34	3.33	0.00088	0.02511	2.19
CRLF1	370.18	1.52	0.28	5.42	6.06E-08	3.15E-05	2.87
COMP	2826.05	1.84	0.36	5.10	3.34E-07	0.0001	3.57
CILP2	77.81	2.27	0.47	4.86	1.17E-06	0.00028	4.84
GMIP	84.74	0.76	0.24	3.09	0.00197	0.0403	1.69
HCST	53.16	1.11	0.29	3.77	0.00016	0.00857	2.15
TYROBP	343.38	1.10	0.27	4.04	5.46E-05	0.00412	2.15
SPINT2	65.05	0.69	0.19	3.59	0.00033	0.01292	1.62
FCGBP	1969.37	1.79	0.47	3.83	0.00013	0.00754	3.47
POU2F2	42.55	1.13	0.33	3.38	0.00073	0.02208	2.18
ETHE1	61.98	0.74	0.20	3.61	0.00031	0.01236	1.67
KCNN4	68.25	2.05	0.36	5.69	1.29E-08	8.89E-06	4.15
C5AR2	68.52	0.85	0.22	3.94	8.17E-05	0.00548	1.80
CD37	52.88	1.12	0.33	3.39	0.00071	0.02156	2.18
IL4I1	8.78	2.52	0.66	3.84	0.00012	0.00733	5.72
CD33	69.22	0.83	0.25	3.31	0.00093	0.02569	1.78
NKG7	10.55	1.72	0.54	3.21	0.00132	0.03198	3.30
LILRB3	42.98	1.25	0.40	3.10	0.00194	0.04004	2.38
LAIR1	309.37	1.08	0.25	4.31	1.64E-05	0.00191	2.11
LILRB1	51.80	1.40	0.43	3.29	0.001	0.02699	2.65
LILRB4	124.37	1.24	0.34	3.60	0.00032	0.01245	2.35
IL11	9.69	3.10	0.85	3.65	0.00026	0.01138	8.55
SLC4A11	5.40	2.31	0.63	3.64	0.00028	0.01159	4.95
SIGLEC1	470.81	1.07	0.31	3.41	0.00066	0.02083	2.10
ISM1	36.13	2.37	0.50	4.73	2.24E-06	0.00046	5.17
CD93	1269.85	1.43	0.29	5.01	5.54E-07	0.00016	2.70
SYNDIG1	46.38	1.39	0.43	3.24	0.00119	0.03003	2.62
CST7	11.70	2.24	0.61	3.65	0.00026	0.01137	4.73
MAFB	294.99	0.77	0.25	3.12	0.0018	0.03849	1.71
EMILIN3	124.39	-1.16	0.32	-3.68	0.00023	0.01069	-2.24
RIMS4	101.17	-0.94	0.25	-3.71	0.00021	0.00993	-1.92
SLPI	96.09	2.91	0.42	6.92	4.53E-12	1.25E-08	7.53
MATN4	23.11	1.84	0.59	3.14	0.0017	0.03724	3.58
NEURL2	30.83	1.13	0.37	3.02	0.0025	0.04716	2.19
AL008726.1	25.38	1.74	0.58	2.99	0.00275	0.04983	3.34
PLTP	2444.23	1.21	0.30	3.98	6.79E-05	0.00486	2.31
MMP9	229.46	4.72	0.98	4.84	1.31E-06	0.0003	26.32
KCNG1	16.08	-0.83	0.26	-3.17	0.00151	0.03426	-1.78
CBLN4	6.64	4.52	1.23	3.68	0.00023	0.01069	22.99
PCK1	5.39	-3.11	0.62	-5.04	4.78E-07	0.00014	-8.65

APCDD1L	33.18	1.77	0.56	3.18	0.00146	0.03383	3.40
CTSZ	1493.52	0.70	0.18	3.86	0.00012	0.00694	1.62
ZNF831	18.38	2.35	0.59	3.97	7.11E-05	0.00496	5.11
RGS19	70.19	0.84	0.23	3.58	0.00035	0.01333	1.79
CHODL	8.28	-1.67	0.46	-3.64	0.00027	0.01156	-3.17
RUNX1	768.24	1.04	0.19	5.34	9.37E-08	3.92E-05	2.06
KCNJ6	13.49	6.02	1.15	5.22	1.78E-07	6.85E-05	64.72
KCNJ15	23.43	1.93	0.47	4.09	4.27E-05	0.00354	3.82
SPATA20P1	4.02	5.17	1.17	4.40	1.08E-05	0.00142	35.89
UBASH3A	9.96	1.97	0.64	3.08	0.00209	0.04188	3.92
CSTB	197.39	0.71	0.19	3.65	0.00026	0.01137	1.64
TRPM2	111.84	1.30	0.27	4.88	1.05E-06	0.00026	2.46
ITGB2	564.34	1.41	0.31	4.58	4.67E-06	0.00076	2.66
S100B	257.25	-0.90	0.28	-3.23	0.00124	0.03078	-1.86
TMEM121B	6.38	1.93	0.54	3.59	0.00034	0.01295	3.80
BID	56.47	0.73	0.25	2.99	0.00277	0.04992	1.66
IGLV1-40	68.99	4.82	1.56	3.09	0.00197	0.0403	28.30
IGLV3-25	51.58	6.16	1.98	3.11	0.00187	0.03943	71.67
IGLV2-11	37.35	4.55	1.39	3.28	0.00103	0.02748	23.49
IGLC3	270.79	5.70	1.41	4.03	5.55E-05	0.00416	51.85
SGSM1	111.48	-0.85	0.24	-3.51	0.00045	0.01598	-1.80
EMID1	60.18	0.82	0.27	3.02	0.00253	0.04746	1.76
AP1B1	601.54	0.59	0.19	3.10	0.00193	0.03998	1.51
HMOX1	297.52	1.94	0.54	3.60	0.00031	0.01236	3.84
APOL1	234.13	0.66	0.16	4.20	2.62E-05	0.00251	1.58
NCF4	144.31	0.71	0.22	3.20	0.00136	0.03257	1.63
IL2RB	24.23	1.63	0.53	3.09	0.00198	0.04032	3.10
RAC2	73.25	1.24	0.37	3.36	0.00079	0.02342	2.37
CYTH4	428.51	1.02	0.20	5.19	2.13E-07	7.72E-05	2.03
KDELR3	235.31	0.84	0.23	3.66	0.00025	0.01132	1.79
LINC01315	9.57	-1.23	0.32	-3.83	0.00013	0.00751	-2.35
NFAM1	89.19	1.15	0.33	3.47	0.00052	0.01766	2.22
SCUBE1	6.04	3.95	0.96	4.12	3.71E-05	0.00319	15.50
LINC00899	57.48	-0.86	0.27	-3.18	0.00146	0.03383	-1.82
TYMP	331.98	0.80	0.26	3.06	0.0022	0.04319	1.75
MXRA5	4057.20	0.92	0.24	3.85	0.00012	0.00715	1.89
TLR7	123.99	1.07	0.24	4.39	1.11E-05	0.00144	2.10
TLR8	67.26	1.34	0.31	4.33	1.52E-05	0.00184	2.54
FANCB	16.27	-0.79	0.26	-2.99	0.00276	0.04992	-1.73
PIR	100.51	-0.62	0.20	-3.04	0.00238	0.04572	-1.53
SH3KBP1	201.25	0.87	0.18	4.96	7.09E-07	0.00019	1.83
MIR222HG	30.55	0.85	0.26	3.33	0.00086	0.02475	1.80
TIMP1	5581.74	1.10	0.29	3.77	0.00016	0.00848	2.15
WAS	53.08	1.18	0.35	3.40	0.00067	0.02104	2.26
VSIG4	668.59	0.71	0.22	3.18	0.00149	0.03404	1.64

AR	330.80	-0.62	0.15	-4.02	5.83E-05	0.00426	-1.54
ITGB1BP2	8.04	1.41	0.47	3.02	0.00256	0.04774	2.65
NHSL2	272.96	0.67	0.17	3.91	9.04E-05	0.00586	1.60
GPR174	18.18	1.98	0.60	3.30	0.00097	0.02632	3.93
ZNF711	56.63	-0.85	0.20	-4.26	2.00E-05	0.00214	-1.81
SYTL4	99.17	-0.77	0.15	-5.17	2.28E-07	8.07E-05	-1.70
BTK	70.33	0.92	0.21	4.38	1.18E-05	0.00151	1.90
RADX	29.04	-0.85	0.28	-3.03	0.00241	0.04587	-1.80
LONRF3	91.94	-0.94	0.27	-3.54	0.00039	0.01455	-1.92
ELF4	82.36	0.82	0.26	3.17	0.0015	0.03416	1.76
GPC4	160.04	0.66	0.18	3.64	0.00028	0.01159	1.58
SMIM10L2A	27.77	-0.86	0.24	-3.60	0.00031	0.01236	-1.81
BGN	6189.20	0.89	0.29	3.10	0.00194	0.04006	1.85
ARHGAP4	202.23	0.72	0.23	3.19	0.00142	0.0334	1.65
MT-CO2	1658.01	0.60	0.19	3.23	0.00125	0.03094	1.52

Supplementary Table 5: Differentially Expressed Genes in No-CHIP vs Control contrast. Only the genes with a p-value adjusted < 0.05 and a Fold Change < -1.5 and > 1.5 are shown.

Supplementary Table 6: Differentially Expressed Genes in CHIP vs Control							
Genes	**baseMean**	**log2FoldChange**	**lfcSE**	**stat**	**pvalue**	**padj**	**FoldChange**
SLC2A5	31.71	2.02	0.47	4.26	2.00E-05	0.004043	4.06
SLC9A1	96.46	0.79	0.22	3.65	0.000258	0.023634	1.73
HIVEP3	71.40	0.88	0.22	3.95	7.92E-05	0.011042	1.83
NFIA-AS2	40.32	-0.98	0.26	-3.76	0.000169	0.017803	-1.97
LEPR	416.78	-0.82	0.22	-3.67	0.000247	0.02281	-1.76
NEXN	154.44	1.14	0.28	4.15	3.40E-05	0.005831	2.21
GBP1P1	52.36	-0.59	0.17	-3.42	0.000619	0.041724	-1.50
F3	70.17	1.73	0.39	4.48	7.59E-06	0.002133	3.32
SLC44A3-AS1	38.35	1.55	0.35	4.46	8.31E-06	0.002233	2.93
SLC44A3	24.97	1.43	0.32	4.49	7.03E-06	0.002005	2.70
VCAM1	820.58	1.05	0.29	3.56	0.000365	0.029788	2.07
COL11A1	215.25	5.58	0.86	6.51	7.38E-11	2.72E-07	47.93
TCHH	7.18	2.02	0.52	3.86	0.000112	0.013834	4.05
FCRL5	31.89	6.04	1.42	4.25	2.09E-05	0.004043	65.78
SLAMF8	113.01	1.63	0.40	4.09	4.39E-05	0.007201	3.10
SLAMF6	20.15	1.66	0.48	3.44	0.000581	0.040514	3.15
SLAMF7	30.33	3.30	0.77	4.31	1.66E-05	0.003612	9.84
ITLN1	20.72	-1.90	0.50	-3.83	0.000127	0.015336	-3.72
ILDR2	20.44	1.40	0.40	3.51	0.00045	0.034037	2.63
PRG4	679.76	2.35	0.33	7.07	1.58E-12	1.47E-08	5.11
PLA2G4A	219.25	-0.86	0.21	-4.20	2.64E-05	0.004942	-1.82
LAX1	17.14	2.57	0.65	3.96	7.65E-05	0.010848	5.92

LRRN2	12.51	1.91	0.52	3.68	0.000232	0.022205	3.76
CR2	5.88	3.74	1.08	3.45	0.000555	0.039118	13.41
G0S2	81.50	-1.15	0.30	-3.88	0.000105	0.013443	-2.21
IRF6	186.81	-0.76	0.20	-3.70	0.000213	0.020478	-1.69
SDC1	42.23	2.48	0.62	4.03	5.66E-05	0.008747	5.58
LINC02580	79.58	0.73	0.20	3.71	0.00021	0.020439	1.66
ANKRD36BP2	49.53	6.76	1.28	5.27	1.38E-07	9.85E-05	108.59
IGKC	5923.50	7.45	1.04	7.17	7.45E-13	1.38E-08	175.18
IGKV4-1	217.88	4.93	1.21	4.06	4.93E-05	0.007892	30.48
IGKV1-5	194.32	7.96	1.26	6.34	2.35E-10	5.44E-07	249.56
IGKV1-9	62.88	6.90	1.57	4.39	1.14E-05	0.002709	119.53
IGKV3-11	340.37	7.85	1.27	6.17	6.74E-10	1.39E-06	231.34
IGKV1-12	44.61	7.86	1.53	5.13	2.83E-07	0.00017	232.90
IGKV3-15	55.92	7.54	1.58	4.78	1.74E-06	0.000674	185.81
IGKV1-16	12.67	6.89	1.51	4.58	4.74E-06	0.001568	118.76
IGKV3-20	527.93	7.71	1.19	6.49	8.79E-11	2.72E-07	209.67
IGKV1-27	30.92	6.38	1.81	3.53	0.000419	0.032543	83.31
IGKV1-39	52.69	8.74	1.89	4.62	3.75E-06	0.001265	427.94
IGKV1D-39	24.62	8.20	1.93	4.26	2.08E-05	0.004043	293.18
IGKV3D-11	4.06	4.87	1.40	3.47	0.000529	0.038429	29.16
IL1RL1	55.23	-1.32	0.35	-3.80	0.000146	0.016348	-2.49
SLC20A1	709.97	0.69	0.17	4.13	3.58E-05	0.006039	1.61
CACNB4	133.42	0.86	0.25	3.43	0.000599	0.041166	1.81
KCNH7	6.34	-2.27	0.65	-3.46	0.000537	0.038561	-4.81
GALNT3	33.51	2.37	0.50	4.71	2.47E-06	0.000916	5.19
CD28	176.21	0.92	0.25	3.65	0.000259	0.023634	1.90
ACADL	72.02	-0.69	0.18	-3.81	0.000139	0.016161	-1.61
FN1	102162.74	1.16	0.23	4.95	7.50E-07	0.000357	2.23
IGFBP2	489.70	1.73	0.45	3.89	0.000102	0.013263	3.32
SCG2	305.64	1.27	0.34	3.75	0.000174	0.01805	2.41
SLC19A3	15.83	-1.52	0.30	-5.10	3.41E-07	0.000198	-2.86
ITIH3	52.07	1.73	0.44	3.90	9.76E-05	0.01292	3.32
PRKCD	92.03	0.72	0.19	3.85	0.000118	0.014296	1.65
COL8A1	2195.58	0.83	0.23	3.68	0.000234	0.022205	1.78
PARP15	51.79	1.18	0.34	3.52	0.000424	0.03279	2.27
PLCH1	130.11	-1.16	0.32	-3.61	0.000307	0.026306	-2.24
AC117453.1	23.29	1.83	0.52	3.52	0.000433	0.033182	3.56
KLHL6	78.65	1.15	0.32	3.61	0.000304	0.026188	2.22
AC007920.2	19.47	-1.21	0.25	-4.85	1.23E-06	0.000531	-2.31
LRRC15	203.65	2.50	0.65	3.82	0.000135	0.015788	5.65
FGFR3	73.60	-0.92	0.27	-3.46	0.000535	0.038561	-1.90
ABLIM2	25.65	1.01	0.27	3.75	0.000176	0.018136	2.02
LGI2	121.67	0.71	0.21	3.36	0.000786	0.047912	1.64

ATP8A1	431.58	-0.87	0.24	-3.68	0.000235	0.02226	-1.83
KIT	62.92	1.43	0.38	3.78	0.00016	0.017383	2.69
JCHAIN	649.09	5.68	1.04	5.44	5.38E-08	4.99E-05	51.17
RASSF6	9.45	6.77	1.73	3.92	8.88E-05	0.011931	109.29
CXCL13	5.58	5.06	1.35	3.76	0.000173	0.018039	33.39
ANXA3	108.04	-1.02	0.23	-4.42	9.94E-06	0.002526	-2.03
IBSP	78.16	4.19	1.00	4.20	2.72E-05	0.005049	18.24
SPP1	2847.46	2.97	0.86	3.45	0.000554	0.039118	7.81
AC106881.1	21.50	-0.80	0.24	-3.40	0.000682	0.043904	-1.74
TDO2	17.48	3.66	1.00	3.65	0.000263	0.023634	12.62
APELA	7.70	4.22	1.12	3.77	0.000164	0.017383	18.66
ZDHHC11B	64.19	-1.86	0.40	-4.65	3.31E-06	0.001137	-3.64
ZDHHC11	33.29	-1.29	0.34	-3.83	0.000129	0.015478	-2.44
MYO10	155.82	1.01	0.30	3.40	0.000678	0.043792	2.02
AC010343.3	6.26	3.71	1.06	3.50	0.000466	0.034878	13.09
GDNF	14.95	1.18	0.35	3.34	0.000832	0.049752	2.27
FYB1	262.75	0.76	0.22	3.50	0.00046	0.034677	1.70
SPOCK1	304.63	1.26	0.31	4.06	4.89E-05	0.007892	2.40
MZB1	35.07	6.50	1.40	4.65	3.25E-06	0.001137	90.77
GRIA1	6.25	5.34	1.25	4.27	1.93E-05	0.004012	40.62
ATP10B	8.63	4.65	1.34	3.48	0.000493	0.036273	25.17
DOK3	58.13	1.20	0.35	3.47	0.000515	0.037777	2.30
IRF4	43.42	2.33	0.68	3.43	0.000597	0.041139	5.04
TUBB2B	64.20	-1.07	0.30	-3.58	0.000345	0.028571	-2.10
PHACTR1	49.89	0.84	0.18	4.57	4.85E-06	0.001578	1.79
C2	121.80	0.71	0.20	3.57	0.000363	0.029743	1.64
C4A	91.56	1.27	0.30	4.22	2.49E-05	0.004718	2.41
SCUBE3	28.66	1.70	0.46	3.67	0.000246	0.02281	3.25
MAPK13	43.00	1.68	0.32	5.24	1.63E-07	0.000108	3.20
PRDM1	57.98	1.41	0.32	4.46	8.26E-06	0.002233	2.65
CRYBG1	208.99	0.84	0.24	3.55	0.000388	0.030972	1.79
ROS1	5.71	5.50	1.22	4.51	6.55E-06	0.001898	45.32
TMEM200A	52.72	1.51	0.38	4.01	6.20E-05	0.009266	2.85
ENPP1	399.37	1.49	0.29	5.06	4.22E-07	0.000215	2.80
UST	233.96	-0.66	0.19	-3.49	0.000476	0.03517	-1.58
SMOC2	291.53	1.58	0.27	5.93	2.99E-09	4.26E-06	2.99
THBS2	6911.45	0.98	0.25	3.86	0.000114	0.013851	1.97
MPP6	384.45	-0.69	0.20	-3.46	0.000548	0.039095	-1.61
TRG-AS1	10.25	1.98	0.58	3.42	0.000634	0.042382	3.95
STEAP1	102.10	0.75	0.22	3.39	0.000689	0.044022	1.68
PDK4	852.63	-1.05	0.31	-3.42	0.000635	0.042382	-2.07
BHLHA15	8.99	5.46	1.60	3.42	0.000632	0.042382	44.02
AC018638.4	40.19	0.98	0.29	3.40	0.000677	0.043792	1.97

SLC7A2	165.42	1.65	0.33	5.06	4.09E-07	0.000215	3.14
EBF2	10.21	2.15	0.61	3.51	0.000443	0.033765	4.44
SLCO5A1	11.10	1.61	0.44	3.65	0.00026	0.023634	3.04
STMN2	78.27	2.93	0.53	5.48	4.14E-08	4.79E-05	7.62
TNFRSF11B	779.98	1.04	0.25	4.13	3.55E-05	0.006039	2.06
COLEC10	7.49	2.93	0.71	4.11	3.94E-05	0.006515	7.61
LINC00861	14.87	2.52	0.73	3.43	0.000607	0.041349	5.72
ASAP1	486.13	0.69	0.12	5.56	2.64E-08	3.26E-05	1.62
CCN4	362.57	1.27	0.32	3.94	8.32E-05	0.011508	2.41
PAX5	3.51	4.67	1.36	3.43	0.000603	0.041271	25.37
OGN	592.76	0.98	0.20	4.85	1.22E-06	0.000531	1.97
CTNNAL1	244.35	-0.65	0.18	-3.54	0.000403	0.031496	-1.57
TNC	6181.37	1.67	0.33	5.00	5.74E-07	0.00028	3.18
CERCAM	553.09	0.59	0.16	3.76	0.000171	0.017906	1.51
LINC01503	29.15	0.98	0.24	4.18	2.93E-05	0.005218	1.98
RAPGEF1	363.71	0.69	0.17	3.96	7.43E-05	0.010676	1.61
TMEM236	23.79	0.93	0.27	3.47	0.00052	0.037964	1.91
KIAA1217	104.45	1.24	0.32	3.86	0.000113	0.013851	2.36
LINC01515	40.44	-1.59	0.40	-4.00	6.26E-05	0.009289	-3.00
MYOZ1	11.68	2.89	0.65	4.42	9.76E-06	0.002514	7.40
CRTAC1	1520.41	0.96	0.23	4.19	2.84E-05	0.005164	1.95
SH3PXD2A	719.44	0.66	0.16	4.13	3.69E-05	0.006166	1.58
ADRA2A	70.80	2.57	0.60	4.26	2.07E-05	0.004043	5.94
PLEKHS1	20.06	5.06	0.92	5.47	4.39E-08	4.79E-05	33.25
NANOS1	121.50	-1.24	0.33	-3.80	0.000146	0.016348	-2.36
IFITM10	35.73	1.59	0.38	4.15	3.36E-05	0.005831	3.02
AC068580.4	55.02	1.90	0.37	5.09	3.65E-07	0.000205	3.74
TPH1	13.35	1.04	0.31	3.38	0.000728	0.045288	2.06
TP53I11	95.67	1.21	0.34	3.58	0.000338	0.028222	2.31
SYT12	205.96	1.71	0.37	4.66	3.09E-06	0.001122	3.26
CHRDL2	28.92	2.51	0.69	3.63	0.000279	0.024507	5.70
MMP1	7.81	4.41	1.14	3.88	0.000106	0.013514	21.32
POU2AF1	14.50	6.25	1.43	4.36	1.29E-05	0.002943	76.13
CD27	11.60	3.12	0.83	3.77	0.000162	0.017383	8.69
A2M	5817.86	0.81	0.18	4.52	6.31E-06	0.001857	1.75
PTHLH	99.35	-1.42	0.37	-3.82	0.000135	0.015788	-2.68
VDR	82.90	1.16	0.30	3.89	0.000102	0.013263	2.24
ITGB7	29.54	1.20	0.34	3.51	0.000445	0.033786	2.29
SP7	8.98	4.41	1.24	3.55	0.000386	0.03095	21.32
AVIL	96.34	1.01	0.23	4.39	1.13E-05	0.002709	2.01
IFNG-AS1	6.76	2.69	0.80	3.37	0.000757	0.046614	6.44
TRHDE	155.63	-1.03	0.24	-4.27	1.91E-05	0.004012	-2.04
ALDH1L2	282.45	0.59	0.15	4.05	5.11E-05	0.008101	1.51

WSCD2	38.45	1.24	0.37	3.38	0.000714	0.044902	2.36
CMKLR1	722.13	0.81	0.17	4.81	1.49E-06	0.000602	1.75
TMEM119	177.38	1.08	0.27	4.06	4.94E-05	0.007892	2.12
BICDL1	7.08	2.56	0.75	3.40	0.000674	0.043792	5.88
TNFSF11	11.01	2.62	0.76	3.44	0.000577	0.040383	6.16
SLAIN1	52.69	-0.75	0.20	-3.71	0.000211	0.020439	-1.68
TMEM255B	28.03	0.97	0.26	3.77	0.000162	0.017383	1.96
SLC7A8	100.07	0.93	0.22	4.15	3.31E-05	0.005831	1.91
LRFN5	48.57	-0.93	0.28	-3.38	0.000722	0.045126	-1.91
GPR68	56.18	2.02	0.45	4.53	5.89E-06	0.001833	4.06
TC2N	364.68	-0.70	0.19	-3.70	0.000213	0.020478	-1.63
CLMN	148.40	0.84	0.19	4.37	1.24E-05	0.002913	1.79
AHNAK2	1541.78	0.74	0.19	3.93	8.65E-05	0.011767	1.67
IGHG4	483.40	10.11	1.76	5.76	8.62E-09	1.14E-05	1102.67
IGHG2	2277.83	8.32	1.22	6.82	9.31E-12	4.31E-08	320.07
IGHGP	273.40	8.35	1.62	5.16	2.42E-07	0.00015	325.97
IGHA1	1032.46	7.30	1.04	7.00	2.53E-12	1.56E-08	157.87
IGHG1	3712.26	7.17	1.12	6.40	1.55E-10	4.09E-07	144.18
IGHG3	317.65	7.06	1.18	5.96	2.47E-09	3.82E-06	133.51
FAM30A	36.12	8.12	1.61	5.06	4.28E-07	0.000215	278.53
IGHV1-2	16.79	6.80	1.50	4.54	5.63E-06	0.0018	111.36
IGHV1-3	16.91	7.58	1.89	4.02	5.87E-05	0.008979	191.70
IGHV3-7	36.43	7.08	1.47	4.82	1.41E-06	0.000593	134.93
IGHV3-11	15.03	5.57	1.64	3.40	0.000685	0.043967	47.48
IGHV3-15	27.82	6.42	1.46	4.39	1.13E-05	0.002709	85.41
IGHV1-18	18.49	4.81	1.31	3.67	0.00024	0.022433	28.03
IGHV3-21	18.35	4.73	1.39	3.41	0.000655	0.043327	26.51
IGHV3-23	236.29	8.23	1.37	6.00	1.92E-09	3.24E-06	301.15
IGHV1-24	18.07	7.68	1.95	3.95	7.89E-05	0.011042	204.88
IGHV3-30	54.44	5.96	1.40	4.27	1.95E-05	0.004012	62.22
IGHV4-31	9.69	6.08	1.81	3.35	0.0008	0.048601	67.69
IGHV3-33	23.74	7.47	1.55	4.82	1.47E-06	0.000602	177.46
IGHV4-34	18.02	7.39	1.71	4.31	1.62E-05	0.003578	167.90
IGHV4-39	43.89	7.38	1.38	5.35	8.60E-08	6.93E-05	166.07
IGHV1-46	6.97	6.21	1.67	3.72	0.0002	0.019654	73.99
IGHV3-48	36.97	8.23	1.82	4.52	6.07E-06	0.001846	300.09
IGHV3-49	10.95	6.38	1.65	3.87	0.000111	0.013834	83.35
IGHV5-51	63.41	8.05	1.68	4.80	1.57E-06	0.000621	264.25
IGHV4-59	75.55	8.01	1.48	5.40	6.57E-08	5.80E-05	258.28
HERC2P3	73.51	1.48	0.40	3.73	0.000189	0.018893	2.79
HDC	18.40	1.97	0.58	3.38	0.000723	0.045126	3.93
CA12	84.21	1.55	0.40	3.92	9.03E-05	0.012044	2.93
ANPEP	265.77	1.34	0.27	5.06	4.25E-07	0.000215	2.54

MCTP2	56.13	0.93	0.26	3.65	0.000267	0.023759	1.91
AC104260.2	14.14	1.40	0.41	3.40	0.000677	0.043792	2.64
TPSB2	31.41	3.14	0.71	4.41	1.03E-05	0.002589	8.80
TPSAB1	31.42	2.16	0.58	3.74	0.000185	0.018782	4.46
AC099489.1	23.91	0.95	0.27	3.55	0.000391	0.030992	1.94
IL21R	35.49	2.05	0.55	3.75	0.00018	0.018441	4.13
NETO2	58.19	-1.19	0.28	-4.23	2.29E-05	0.004382	-2.27
WFDC1	54.45	1.18	0.33	3.61	0.000308	0.026306	2.26
SMTNL2	16.84	-1.77	0.52	-3.39	0.000699	0.044374	-3.40
DHRS13	24.75	-0.69	0.21	-3.35	0.000813	0.048922	-1.62
EVI2B	42.54	1.01	0.30	3.41	0.000647	0.042985	2.01
MYO1D	2236.15	0.85	0.25	3.46	0.000545	0.039014	1.80
CCL8	32.51	1.49	0.43	3.45	0.000566	0.039753	2.80
IKZF3	68.38	2.16	0.61	3.54	0.000395	0.031063	4.48
KRT16	12.30	2.59	0.62	4.19	2.78E-05	0.005111	6.03
AOC3	115.82	1.38	0.26	5.29	1.21E-07	9.37E-05	2.61
HOXB6	12.60	1.51	0.36	4.18	2.90E-05	0.005218	2.84
ABCC3	280.62	0.88	0.24	3.60	0.00032	0.027098	1.84
FAM20A	190.76	1.09	0.27	4.02	5.91E-05	0.008979	2.12
GREB1L	4.14	-1.97	0.52	-3.80	0.000144	0.016348	-3.92
DCC	12.17	7.17	1.47	4.88	1.09E-06	0.000504	143.89
ARID3A	45.25	0.87	0.20	4.26	2.06E-05	0.004043	1.83
DIRAS1	22.44	1.38	0.35	3.99	6.63E-05	0.009678	2.61
MFSD12	200.99	0.66	0.17	3.96	7.43E-05	0.010676	1.58
STXBP2	27.28	1.20	0.34	3.54	0.000395	0.031063	2.29
PDE4A	127.11	0.67	0.19	3.44	0.000585	0.040601	1.59
HSH2D	9.11	2.80	0.77	3.64	0.000274	0.024256	6.95
CRLF1	370.18	1.45	0.27	5.44	5.29E-08	4.99E-05	2.73
TMEM59L	35.25	0.91	0.23	4.01	6.12E-05	0.009227	1.88
COMP	2826.05	1.48	0.34	4.35	1.38E-05	0.003123	2.79
CILP2	77.81	1.69	0.45	3.80	0.000147	0.016359	3.23
FCGBP	1969.37	1.96	0.44	4.41	1.05E-05	0.0026	3.88
CD79A	21.43	4.69	1.09	4.29	1.81E-05	0.003849	25.88
POU2F2	42.55	1.36	0.32	4.29	1.76E-05	0.003804	2.57
KCNN4	68.25	1.64	0.35	4.76	1.89E-06	0.000716	3.13
LRRC4B	37.23	1.16	0.31	3.80	0.000142	0.016346	2.24
CD93	1269.85	0.93	0.27	3.42	0.000615	0.041724	1.90
SLPI	96.09	1.82	0.40	4.52	6.24E-06	0.001857	3.53
KCNG1	16.08	-0.85	0.25	-3.41	0.000657	0.043327	-1.80
CBLN4	6.64	4.19	1.20	3.50	0.000472	0.035099	18.25
PCK1	5.39	-3.74	0.62	-6.04	1.52E-09	2.81E-06	-13.35
RUNX1	768.24	0.74	0.18	4.00	6.38E-05	0.009389	1.67
KCNJ6	13.49	5.96	1.13	5.28	1.30E-07	9.62E-05	62.36

SPATA20P1	4.02	4.43	1.16	3.82	0.000132	0.015645	21.50
TRPM2	111.84	0.96	0.25	3.80	0.000146	0.016348	1.95
IGLV6-57	28.02	6.51	1.69	3.86	0.000112	0.013834	91.16
IGLV1-47	28.96	6.12	1.64	3.74	0.000186	0.018783	69.61
IGLV1-44	53.33	6.24	1.60	3.89	9.89E-05	0.013006	75.56
IGLV1-40	68.99	5.54	1.48	3.74	0.000183	0.018654	46.53
IGLV3-25	51.58	9.19	1.89	4.85	1.22E-06	0.000531	584.38
IGLV2-23	64.15	5.95	1.52	3.92	8.69E-05	0.011767	61.90
IGLV3-21	83.61	7.66	1.46	5.25	1.49E-07	0.000102	202.81
IGLV3-19	76.63	7.92	1.70	4.65	3.31E-06	0.001137	242.06
IGLV2-14	106.06	6.60	1.23	5.36	8.43E-08	6.93E-05	97.04
IGLV2-11	37.35	5.88	1.33	4.43	9.23E-06	0.00241	58.96
IGLV3-10	8.96	6.70	1.69	3.95	7.66E-05	0.010848	103.96
IGLV3-1	29.12	5.08	1.37	3.72	0.0002	0.019654	33.90
IGLL5	8.65	6.56	1.83	3.59	0.000333	0.02795	94.68
IGLC2	514.97	6.30	1.15	5.46	4.83E-08	4.98E-05	78.63
IGLC3	270.79	6.94	1.34	5.18	2.26E-07	0.000145	122.97
DERL3	24.23	3.95	0.90	4.37	1.26E-05	0.002928	15.42
MIF-AS1	11.75	2.08	0.59	3.52	0.000432	0.033182	4.23
C22orf46	60.54	0.69	0.19	3.73	0.00019	0.018905	1.62
SH3KBP1	201.25	0.70	0.17	4.15	3.37E-05	0.005831	1.62
TSPAN7	53.42	-1.16	0.33	-3.50	0.000473	0.035099	-2.24
PIM2	103.91	2.24	0.58	3.88	0.000104	0.013443	4.73
NHSL2	272.96	0.73	0.16	4.44	9.08E-06	0.002406	1.65
BGN	6189.20	0.93	0.27	3.42	0.000617	0.041724	1.90
MT-ATP8	58.48	0.97	0.25	3.86	0.000112	0.013834	1.97
MT-ATP6	757.32	0.82	0.24	3.40	0.00067	0.043792	1.77
MT-ND4	1535.88	0.80	0.24	3.35	0.000802	0.048601	1.74
AC233755.1	14.20	7.42	1.97	3.77	0.000164	0.017383	171.39

Supplementary Table 6: Differentially Expressed Genes in CHIP vs Control contrast. Only the genes with a p-value adjusted < 0.05 and a Fold Change < -1.5 and > 1.5 are shown.

Supplementary Table 7: Differentially Expressed Genes in CHIP vs No-CHIP contrast							
Genes	**baseMean**	**log2FoldChange**	**lfcSE**	**stat**	**pvalue**	**padj**	**FoldChange**
IGKC	5923.50	3.88	0.89	4.34	1.43E-05	0.03853	14.68
IGKV1-12	44.61	4.92	1.12	4.38	1.18E-05	0.03853	30.33
COL12A1	5250.82	-0.67	0.16	-4.25	2.16E-05	0.04205	-1.59
AXIN2	145.66	0.62	0.15	4.22	2.40E-05	0.04205	1.54
PCSK1N	9.50	-2.15	0.50	-4.33	1.47E-05	0.03853	-4.44

Supplementary Table 7: Differentially Expressed Genes in CHIP vs No-CHIP contrast. Only the genes with a p-value adjusted < 0.05 and a Fold Change < -1.5 and > 1.5 are shown.

7. REFERENCES

1. Otto, C.M., et al., *Characterization of the early lesion of 'degenerative' valvular aortic stenosis. Histological and immunohistochemical studies.* Circulation, 1994. **90**(2): p. 844-53.

2. Rajamannan, N.M., et al., *Calcific aortic valve disease: not simply a degenerative process: A review and agenda for research from the National Heart and Lung and Blood Institute Aortic Stenosis Working Group. Executive summary: Calcific aortic valve disease-2011 update.* Circulation, 2011. **124**(16): p. 1783-91.

3. Yadgir, S., et al., *Global, Regional, and National Burden of Calcific Aortic Valve and Degenerative Mitral Valve Diseases, 1990-2017.* Circulation, 2020. **141**(21): p. 1670-1680.

4. Dweck, M.R., N.A. Boon, and D.E. Newby, *Calcific aortic stenosis: a disease of the valve and the myocardium.* J Am Coll Cardiol, 2012. **60**(19): p. 1854-63.

5. Small, A., et al., *Biomarkers of Calcific Aortic Valve Disease.* Arterioscler Thromb Vasc Biol, 2017. **37**(4): p. 623-632.

6. Chan, K.L., et al., *Effect of Lipid lowering with rosuvastatin on progression of aortic stenosis: results of the aortic stenosis progression observation: measuring effects of rosuvastatin (ASTRONOMER) trial.* Circulation, 2010. **121**(2): p. 306-14.

7. Ngo, D.T., A.L. Sverdlov, and J.D. Horowitz, *Prevention of aortic valve stenosis: a realistic therapeutic target?* Pharmacol Ther, 2012. **135**(1): p. 78-93.

8. Stewart, B.F., et al., *Clinical factors associated with calcific aortic valve disease. Cardiovascular Health Study.* J Am Coll Cardiol, 1997. **29**(3): p. 630-4.

9. Thanassoulis, G., et al., *Genetic associations with valvular calcification and aortic stenosis.* N Engl J Med, 2013. **368**(6): p. 503-12.

10. Emdin, C.A., et al., *Phenotypic Characterization of Genetically Lowered Human Lipoprotein(a) Levels.* J Am Coll Cardiol, 2016. **68**(25): p. 2761-2772.

11. Garg, V., et al., *Mutations in NOTCH1 cause aortic valve disease.* Nature, 2005. **437**(7056): p. 270-4.

12. Theodoris, C.V., et al., *Human disease modeling reveals integrated transcriptional and epigenetic mechanisms of NOTCH1 haploinsufficiency.* Cell, 2015. **160**(6): p. 1072-86.

13. Zeng, Q., et al., *Notch1 promotes the pro-osteogenic response of human aortic valve interstitial cells via modulation of ERK1/2 and nuclear factor-κB activation.* Arterioscler Thromb Vasc Biol, 2013. **33**(7): p. 1580-90.

14. LaHaye, S., J. Lincoln, and V. Garg, *Genetics of valvular heart disease.* Curr Cardiol Rep, 2014. **16**(6): p. 487.

15. Huygens, S.A., et al., *How much does a heart valve implantation cost and what are the health care costs afterwards?* Open Heart, 2018. **5**(1): p. e000672.

16. Braunwald, E., *Aortic Stenosis: Then and Now.* Circulation, 2018. **137**(20): p. 2099-2100.

17. Miller, J.D., et al., *Dysregulation of antioxidant mechanisms contributes to increased oxidative stress in calcific aortic valvular stenosis in humans.* J Am Coll Cardiol, 2008. **52**(10): p. 843-50.

18. Kraler, S., et al., *Calcific aortic valve disease: from molecular and cellular mechanisms to medical therapy.* Eur Heart J, 2022. **43**(7): p. 683-697.

19. Ngo, D.T., et al., *Vitamin D(2) supplementation induces the development of aortic stenosis in rabbits: interactions with endothelial function and thioredoxin-interacting protein.* Eur J Pharmacol, 2008. **590**(1-3): p. 290-6.

20. Kopytek, M., et al., *NETosis is associated with the severity of aortic stenosis: Links with inflammation.* Int J Cardiol, 2019. **286**: p. 121-126.

21. Nagy, E., et al., *Upregulation of the 5-lipoxygenase pathway in human aortic valves correlates with severity of stenosis and leads to leukotriene-induced effects on valvular myofibroblasts.* Circulation, 2011. **123**(12): p. 1316-25.

22. Goody, P.R., et al., *Aortic Valve Stenosis: From Basic Mechanisms to Novel Therapeutic Targets.* Arterioscler Thromb Vasc Biol, 2020. **40**(4): p. 885-900.

23. Cho, K.I., et al., *Inflammatory and metabolic mechanisms underlying the calcific aortic valve disease.* Atherosclerosis, 2018. **277**: p. 60-65.

24. Chandrasekharan, N.V., et al., *COX-3, a cyclooxygenase-1 variant inhibited by acetaminophen and other analgesic/antipyretic drugs: cloning, structure, and expression.* Proc Natl Acad Sci U S A, 2002. **99**(21): p. 13926-31.

25. Ricciotti, E. and G.A. FitzGerald, *Prostaglandins and inflammation.* Arterioscler Thromb Vasc Biol, 2011. **31**(5): p. 986-1000.

26. Dubois, R.N., et al., *Cyclooxygenase in biology and disease.* FASEB J, 1998. **12**(12): p. 1063-73.

27. Katori, M. and M. Majima, *Cyclooxygenase-2: its rich diversity of roles and possible application of its selective inhibitors.* Inflamm Res, 2000. **49**(8): p. 367-92.

28. Vane, J.R., Y.S. Bakhle, and R.M. Botting, *Cyclooxygenases 1 and 2.* Annu Rev Pharmacol Toxicol, 1998. **38**: p. 97-120.

29. Adekeye, A., et al., *PTGES3 is a Putative Prognostic Marker in Breast Cancer.* J Surg Res, 2022. **271**: p. 154-162.

30. Sorokin, A., *Nitric Oxide Synthase and Cyclooxygenase Pathways: A Complex Interplay in Cellular Signaling.* Curr Med Chem, 2016. **23**(24): p. 2559-2578.

31. Kreke, M.R., et al., *Effect of intermittent shear stress on mechanotransductive signaling and osteoblastic differentiation of bone marrow stromal cells.* Tissue Eng Part A, 2008. **14**(4): p. 529-37.

32. Wirrig, E.E., et al., *COX2 inhibition reduces aortic valve calcification in vivo.* Arterioscler Thromb Vasc Biol, 2015. **35**(4): p. 938-47.

33. Bowler, M.A., et al., *Celecoxib Is Associated With Dystrophic Calcification and Aortic Valve Stenosis.* JACC Basic Transl Sci, 2019. **4**(2): p. 135-143.

34. Espinoza, I. and L. Miele, *Notch inhibitors for cancer treatment.* Pharmacol Ther, 2013. **139**(2): p. 95-110.

35. Kumar, R., L. Juillerat-Jeanneret, and D. Golshayan, *Notch Antagonists: Potential Modulators of Cancer and Inflammatory Diseases.* J Med Chem, 2016. **59**(17): p. 7719-37.

36. Ravindran, G. and H. Devaraj, *Aberrant expression of beta-catenin and its association with DeltaNp63, Notch-1, and clinicopathological factors in oral squamous cell carcinoma.* Clin Oral Investig, 2012. **16**(4): p. 1275-88.

37. Afshar, Y., et al., *The role of chorionic gonadotropin and Notch1 in implantation.* J Assist Reprod Genet, 2007. **24**(7): p. 296-302.

38. Shih, H.P., et al., *A Notch-dependent molecular circuitry initiates pancreatic endocrine and ductal cell differentiation.* Development, 2012. **139**(14): p. 2488-99.

39. Aquila, G., et al., *The Use of Nutraceuticals to Counteract Atherosclerosis: The Role of the Notch Pathway.* Oxid Med Cell Longev, 2019. **2019**: p. 5470470.

40. Benedito, R., et al., *The notch ligands Dll4 and Jagged1 have opposing effects on angiogenesis.* Cell, 2009. **137**(6): p. 1124-35.

41. Van de Walle, I., et al., *Specific Notch receptor-ligand interactions control human TCR-αβ/γδ development by inducing differential Notch signal strength.* J Exp Med, 2013. **210**(4): p. 683-97.

42. Boucher, J.M., et al., *The miR-143/145 cluster is a novel transcriptional target of Jagged-1/Notch signaling in vascular smooth muscle cells.* J Biol Chem, 2011. **286**(32): p. 28312-21.

43. Nakano, T., et al., *Delta-Like Ligand 4-Notch Signaling in Macrophage Activation.* Arterioscler Thromb Vasc Biol, 2016. **36**(10): p. 2038-47.

44. Fung, E., et al., *Delta-like 4 induces notch signaling in macrophages: implications for inflammation.* Circulation, 2007. **115**(23): p. 2948-56.

45. Aquila, G., et al., *Distinct gene expression profiles associated with Notch ligands Delta-like 4 and Jagged1 in plaque material from peripheral artery disease patients: a pilot study.* J Transl Med, 2017. **15**(1): p. 98.

46. Hofmann, J.J., et al., *Endothelial deletion of murine Jag1 leads to valve calcification and congenital heart defects associated with Alagille syndrome.* Development, 2012. **139**(23): p. 4449-60.

47. Rizzo, P., L. Miele, and R. Ferrari, *The Notch pathway: a crossroad between the life and death of the endothelium.* Eur Heart J, 2013. **34**(32): p. 2504-9.

48. Aquila, G., et al., *The Notch pathway: a novel therapeutic target for cardiovascular diseases?* Expert Opin Ther Targets, 2019. **23**(8): p. 695-710.

49. Fortini, F., et al., *Estrogen-mediated protection against coronary heart disease: The role of the Notch pathway.* J Steroid Biochem Mol Biol, 2019. **189**: p. 87-100.

50. Moore, G., et al., *Top Notch Targeting Strategies in Cancer: A Detailed Overview of Recent Insights and Current Perspectives.* Cells, 2020. **9**(6).

51. Rizzo, P., et al., *COVID-19 in the heart and the lungs: could we "Notch" the inflammatory storm?* Basic Res Cardiol, 2020. **115**(3): p. 31.

52. Kumari, M., et al., *DR-5 and DLL-4 mAb Functionalized SLNs of Gamma-Secretase Inhibitors- An Approach for TNBC Treatment.* Adv Pharm Bull, 2021. **11**(4): p. 618-623.

53. Zheng, H., et al., *Therapeutic Antibody Targeting Tumor- and Osteoblastic Niche-Derived Jagged1 Sensitizes Bone Metastasis to Chemotherapy.* Cancer Cell, 2017. **32**(6): p. 731-747.e6.

54. Danahay, H., et al., *Notch2 is required for inflammatory cytokine-driven goblet cell metaplasia in the lung.* Cell Rep, 2015. **10**(2): p. 239-52.

55. Park, J.S., et al., *Inhibition of notch signalling ameliorates experimental inflammatory arthritis.* Ann Rheum Dis, 2015. **74**(1): p. 267-74.

56. Fukuda, D., et al., *Notch ligand delta-like 4 blockade attenuates atherosclerosis and metabolic disorders.* Proc Natl Acad Sci U S A, 2012. **109**(27): p. E1868-77.

57. Nistri, S., C. Sassoli, and D. Bani, *Notch Signaling in Ischemic Damage and Fibrosis: Evidence and Clues from the Heart.* Front Pharmacol, 2017. **8**: p. 187.

58. Fortini, F., et al., *Estrogen receptor β-dependent Notch1 activation protects vascular endothelium against tumor necrosis factor α (TNFα)-induced apoptosis.* J Biol Chem, 2017. **292**(44): p. 18178-18191.

59. Ferrari, R. and P. Rizzo, *The Notch pathway: a novel target for myocardial remodelling therapy?* Eur Heart J, 2014. **35**(32): p. 2140-5.

60. Marracino, L., et al., *Adding a "Notch" to Cardiovascular Disease Therapeutics: A MicroRNA-Based Approach.* Front Cell Dev Biol, 2021. **9**: p. 695114.

61. Kostina, A., et al., *Different Notch signaling in cells from calcified bicuspid and tricuspid aortic valves.* J Mol Cell Cardiol, 2018. **114**: p. 211-219.

62. Hadji, F., et al., *Altered DNA Methylation of Long Noncoding RNA H19 in Calcific Aortic Valve Disease Promotes Mineralization by Silencing NOTCH1.* Circulation, 2016. **134**(23): p. 1848-1862.

63. Nigam, V. and D. Srivastava, *Notch1 represses osteogenic pathways in aortic valve cells.* J Mol Cell Cardiol, 2009. **47**(6): p. 828-34.

64. Acharya, A., et al., *Inhibitory role of Notch1 in calcific aortic valve disease.* PLoS One, 2011. **6**(11): p. e27743.

65. Butcher, J.T. and R.M. Nerem, *Valvular endothelial cells regulate the phenotype of interstitial cells in co-culture: effects of steady shear stress.* Tissue Eng, 2006. **12**(4): p. 905-15.

66. Richards, J., et al., *Side-specific endothelial-dependent regulation of aortic valve calcification: interplay of hemodynamics and nitric oxide signaling.* Am J Pathol, 2013. **182**(5): p. 1922-31.

67. Kostina, A., et al., *Human aortic endothelial cells have osteogenic Notch-dependent properties in co-culture with aortic smooth muscle cells.* Biochem Biophys Res Commun, 2019. **514**(2): p. 462-468.

68. Yu, L.X., et al., *The Notch1/cyclooxygenase-2/Snail/E-cadherin pathway is associated with hypoxia-induced hepatocellular carcinoma cell invasion and migration.* Oncol Rep, 2013. **29**(1): p. 362-70.

69. Ye, Y., et al., *COX-2 regulates Snail expression in gastric cancer via the Notch1 signaling pathway.* Int J Mol Med, 2017. **40**(2): p. 512-522.

70. Zhou, L., et al., *The down-regulation of Notch1 inhibits the invasion and migration of hepatocellular carcinoma cells by inactivating the cyclooxygenase-2/Snail/E-cadherin pathway in vitro.* Dig Dis Sci, 2013. **58**(4): p. 1016-25.

71. Clément, N., et al., *Notch3 and IL-1beta exert opposing effects on a vascular smooth muscle cell inflammatory pathway in which NF-kappaB drives crosstalk.* J Cell Sci, 2007. **120**(Pt 19): p. 3352-61.

72. Steensma, D.P., et al., *Clonal hematopoiesis of indeterminate potential and its distinction from myelodysplastic syndromes.* Blood, 2015. **126**(1): p. 9-16.

73. Jaiswal, S., et al., *Clonal Hematopoiesis and Risk of Atherosclerotic Cardiovascular Disease.* N Engl J Med, 2017. **377**(2): p. 111-121.

74. Genovese, G., et al., *Clonal hematopoiesis and blood-cancer risk inferred from blood DNA sequence.* N Engl J Med, 2014. **371**(26): p. 2477-87.

75. Jaiswal, S., et al., *Age-related clonal hematopoiesis associated with adverse outcomes.* N Engl J Med, 2014. **371**(26): p. 2488-98.

76. Papa, V., et al., *Translating Evidence from Clonal Hematopoiesis to Cardiovascular Disease: A Systematic Review.* J Clin Med, 2020. **9**(8).

77. Wolach, O., et al., *Increased neutrophil extracellular trap formation promotes thrombosis in myeloproliferative neoplasms.* Sci Transl Med, 2018. **10**(436).

78. Lamrani, L., et al., *Hemostatic disorders in a JAK2V617F-driven mouse model of myeloproliferative neoplasm.* Blood, 2014. **124**(7): p. 1136-45.

79. Yu, B., et al., *Supplemental Association of Clonal Hematopoiesis With Incident Heart Failure.* J Am Coll Cardiol, 2021. **78**(1): p. 42-52.

80. Dorsheimer, L., et al., *Association of Mutations Contributing to Clonal Hematopoiesis With Prognosis in Chronic Ischemic Heart Failure.* JAMA Cardiol, 2019. **4**(1): p. 25-33.

81. Wang, Y., et al., *Tet2-mediated clonal hematopoiesis in nonconditioned mice accelerates age-associated cardiac dysfunction.* JCI Insight, 2020. **5**(6).

82. Mas-Peiro, S., et al., *Clonal haematopoiesis in patients with degenerative aortic valve stenosis undergoing transcatheter aortic valve implantation.* Eur Heart J, 2020. **41**(8): p. 933-939.

83. Abplanalp, W.T., et al., *Association of Clonal Hematopoiesis of Indeterminate Potential With Inflammatory Gene Expression in Patients With Severe Degenerative Aortic Valve Stenosis or Chronic Postischemic Heart Failure.* JAMA Cardiol, 2020. **5**(10): p. 1170-1175.

84. Sano, S., et al., *Tet2-Mediated Clonal Hematopoiesis Accelerates Heart Failure Through a Mechanism Involving the IL-1β/NLRP3 Inflammasome.* J Am Coll Cardiol, 2018. **71**(8): p. 875-886.

85. Wang, W., et al., *Macrophage Inflammation, Erythrophagocytosis, and Accelerated Atherosclerosis in Jak2.* Circ Res, 2018. **123**(11): p. e35-e47.

86. Cook, E.K., et al., *Comorbid and inflammatory characteristics of genetic subtypes of clonal hematopoiesis.* Blood Adv, 2019. **3**(16): p. 2482-2486.

87. Sano, S., et al., *CRISPR-Mediated Gene Editing to Assess the Roles of Tet2 and Dnmt3a in Clonal Hematopoiesis and Cardiovascular Disease.* Circ Res, 2018. **123**(3): p. 335-341.

88. Fuster, J.J., et al., *Clonal hematopoiesis associated with TET2 deficiency accelerates atherosclerosis development in mice.* Science, 2017. **355**(6327): p. 842-847.

89. Pan, F., et al., *Tet2 loss leads to hypermutagenicity in haematopoietic stem/progenitor cells.* Nat Commun, 2017. **8**: p. 15102.

90. Chuang, S.M., et al., *Epigenetic regulation of COX-2 expression by DNA hypomethylation via NF-κB activation in ketamine-induced ulcerative cystitis.* Int J Mol Med, 2019. **44**(3): p. 797-812.

91. Kaasinen, E., et al., *Impact of constitutional TET2 haploinsufficiency on molecular and clinical phenotype in humans.* Nat Commun, 2019. **10**(1): p. 1252.

92. Cai, Z., et al., *Inhibition of Inflammatory Signaling in Tet2 Mutant Preleukemic Cells Mitigates Stress-Induced Abnormalities and Clonal Hematopoiesis.* Cell Stem Cell, 2018. **23**(6): p. 833-849.e5.

93. Eskandary, F., et al., *Clazakizumab in late antibody-mediated rejection: study protocol of a randomized controlled pilot trial.* Trials, 2019. **20**(1): p. 37.

94. Patel, A.M. and L.W. Moreland, *Interleukin-6 inhibition for treatment of rheumatoid arthritis: a review of tocilizumab therapy.* Drug Des Devel Ther, 2010. **4**: p. 263-78.

95. Ridker, P.M., et al., *Antiinflammatory Therapy with Canakinumab for Atherosclerotic Disease.* N Engl J Med, 2017. **377**(12): p. 1119-1131.

96. Yang, X., et al., *Inhibition of JAK2/STAT3/SOCS3 signaling attenuates atherosclerosis in rabbit.* BMC Cardiovasc Disord, 2020. **20**(1): p. 133.

97. Tang, Y., et al., *Inhibition of JAK2 Suppresses Myelopoiesis and Atherosclerosis in Apoe.* Cardiovasc Drugs Ther, 2020. **34**(2): p. 145-152.

98. Kostina, A.S., et al., *Notch-dependent EMT is attenuated in patients with aortic aneurysm and bicuspid aortic valve.* Biochim Biophys Acta, 2016. **1862**(4): p. 733-740.

99. Bolger, A.M., M. Lohse, and B. Usadel, *Trimmomatic: a flexible trimmer for Illumina sequence data.* Bioinformatics, 2014. **30**(15): p. 2114-20.

100. Smith, T., A. Heger, and I. Sudbery, *UMI-tools: modeling sequencing errors in Unique Molecular Identifiers to improve quantification accuracy.* Genome Res, 2017. **27**(3): p. 491-499.

101. Li, H., et al., *The Sequence Alignment/Map format and SAMtools.* Bioinformatics, 2009. **25**(16): p. 2078-9.

102. Van der Auwera, G.A., et al., *From FastQ data to high confidence variant calls: the Genome Analysis Toolkit best practices pipeline.* Curr Protoc Bioinformatics, 2013. **43**: p. 11.10.1-11.10.33.

103. Wang, K., M. Li, and H. Hakonarson, *ANNOVAR: functional annotation of genetic variants from high-throughput sequencing data.* Nucleic Acids Res, 2010. **38**(16): p. e164.

104. Kechin, A., et al., *cutPrimers: A New Tool for Accurate Cutting of Primers from Reads of Targeted Next Generation Sequencing.* J Comput Biol, 2017. **24**(11): p. 1138-1143.

105. Dobin, A., et al., *STAR: ultrafast universal RNA-seq aligner.* Bioinformatics, 2013. **29**(1): p. 15-21.

106. Liao, Y., G.K. Smyth, and W. Shi, *The R package Rsubread is easier, faster, cheaper and better for alignment and quantification of RNA sequencing reads.* Nucleic Acids Res, 2019. **47**(8): p. e47.

107. Love, M.I., W. Huber, and S. Anders, *Moderated estimation of fold change and dispersion for RNA-seq data with DESeq2.* Genome Biol, 2014. **15**(12): p. 550.

108. Krämer, A., et al., *Causal analysis approaches in Ingenuity Pathway Analysis.* Bioinformatics, 2014. **30**(4): p. 523-30.

109. Newman, A.M., et al., *Determining cell type abundance and expression from bulk tissues with digital cytometry.* Nat Biotechnol, 2019. **37**(7): p. 773-782.

110. Walker, G.A., et al., *Valvular myofibroblast activation by transforming growth factor-beta: implications for pathological extracellular matrix remodeling in heart valve disease.* Circ Res, 2004. **95**(3): p. 253-60.

111. Li, F., et al., *ADAMTS5 Deficiency in Calcified Aortic Valves Is Associated With Elevated Pro-Osteogenic Activity in Valvular Interstitial Cells.* Arterioscler Thromb Vasc Biol, 2017. **37**(7): p. 1339-1351.

112. Benton, J.A., et al., *Statins block calcific nodule formation of valvular interstitial cells by inhibiting alpha-smooth muscle actin expression.* Arterioscler Thromb Vasc Biol, 2009. **29**(11): p. 1950-7.

113. Kopanos, C., et al., *VarSome: the human genomic variant search engine.* Bioinformatics, 2019. **35**(11): p. 1978-1980.

114. Greene, C.L., et al., *Transcriptional Profiling of Normal, Stenotic, and Regurgitant Human Aortic Valves.* Genes (Basel), 2020. **11**(7).

115. Schlotter, F., et al., *Spatiotemporal Multi-Omics Mapping Generates a Molecular Atlas of the Aortic Valve and Reveals Networks Driving Disease.* Circulation, 2018. **138**(4): p. 377-393.

116. Rashdan, N.A., et al., *Osteocalcin Regulates Arterial Calcification Via Altered Wnt Signaling and Glucose Metabolism.* J Bone Miner Res, 2020. **35**(2): p. 357-367.

117. Izu, Y., et al., *Type XII collagen regulates osteoblast polarity and communication during bone formation.* J Cell Biol, 2011. **193**(6): p. 1115-30.

118. Natorska, J., et al., *Presence of B cells within aortic valves in patients with aortic stenosis: Relation to severity of the disease.* J Cardiol, 2016. **67**(1): p. 80-5.

119. Sorli, C.H., et al., *Basal expression of cyclooxygenase-2 and nuclear factor-interleukin 6 are dominant and coordinately regulated by interleukin 1 in the pancreatic islet.* Proc Natl Acad Sci U S A, 1998. **95**(4): p. 1788-93.

120. Varshney, R., et al., *Inactivation of platelet-derived TGF-β1 attenuates aortic stenosis progression in a robust murine model.* Blood Adv, 2019. **3**(5): p. 777-788.

121. Jian, B., et al., *Progression of aortic valve stenosis: TGF-beta1 is present in calcified aortic valve cusps and promotes aortic valve interstitial cell calcification via apoptosis.* Ann Thorac Surg, 2003. **75**(2): p. 457-65; discussion 465-6.

122. Zeng, Q., et al., *Cross-talk between the Toll-like receptor 4 and Notch1 pathways augments the inflammatory response in the interstitial cells of stenotic human aortic valves.* Circulation, 2012. **126**(11 Suppl 1): p. S222-30.

123. Tezuka, K., et al., *Stimulation of osteoblastic cell differentiation by Notch.* J Bone Miner Res, 2002. **17**(2): p. 231-9.

124. Nobta, M., et al., *Critical regulation of bone morphogenetic protein-induced osteoblastic differentiation by Delta1/Jagged1-activated Notch1 signaling.* J Biol Chem, 2005. **280**(16): p. 15842-8.

125. Raddatz, M.A., M.S. Madhur, and W.D. Merryman, *Adaptive immune cells in calcific aortic valve disease.* Am J Physiol Heart Circ Physiol, 2019. **317**(1): p. H141-H155.

126. Abplanalp, W.T., et al., *Clonal Hematopoiesis-Driver DNMT3A Mutations Alter Immune Cells in Heart Failure.* Circ Res, 2021. **128**(2): p. 216-228.

127. Venanzi, A., et al., *Dissecting Clonal Hematopoiesis in Tissues of Classical Hodgkin Lymphoma Patients.* Blood Cancer Discov, 2021. **2**(3): p. 216-225.

128. Steiner, I., et al., *Calcific aortic valve stenosis: Immunohistochemical analysis of inflammatory infiltrate.* Pathol Res Pract, 2012. **208**(4): p. 231-4.

129. Mazur, P., et al., *Lymphocyte and monocyte subpopulations in severe aortic stenosis at the time of surgical intervention.* Cardiovasc Pathol, 2018. **35**: p. 1-7.

130. Sun, C., et al., *Phenotypes of aortic valve disease according to detailed anatomical classification of patients who underwent aortic valve replacement surgery.* Cardiovasc Pathol, 2019. **41**: p. 1-7.

131. Delaney, J.A., et al., *Associations between aspirin and other non-steroidal anti-inflammatory drugs and aortic valve or coronary artery calcification: the Multi-Ethnic Study of Atherosclerosis and the Heinz Nixdorf Recall Study.* Atherosclerosis, 2013. **229**(2): p. 310-6.

132. Schurgers, L.J., E.C. Cranenburg, and C. Vermeer, *Matrix Gla-protein: the calcification inhibitor in need of vitamin K.* Thromb Haemost, 2008. **100**(4): p. 593-603.

133. Amaral, L.T.W., et al., *Gastrointestinal Bleeding and Aortic Stenosis: A Case of Heyde Syndrome.* Radiol Cardiothorac Imaging, 2021. **3**(3): p. e200615.

134. Lee, D.S.W., O.L. Rojas, and J.L. Gommerman, *B cell depletion therapies in autoimmune disease: advances and mechanistic insights.* Nat Rev Drug Discov, 2021. **20**(3): p. 179-199.

135. Bick, A.G., et al., *Inherited causes of clonal haematopoiesis in 97,691 whole genomes.* Nature, 2020. **586**(7831): p. 763-768.